2023

From calibration to implementation: stage-structured population forecasts for the vector of Lyme disease (ixodes scapularis) across the Eastern United States

BOSTON UNIVERSITY

GRADUATE SCHOOL OF ARTS AND SCIENCES

Dissertation

FROM CALIBRATION TO IMPLEMENTATION: STAGE-STRUCTURED POPULATION FORECASTS FOR THE VECTOR OF LYME DISEASE (*IXODES SCAPULARIS*) ACROSS THE EASTERN UNITED STATES

by

JOHN R. FOSTER, JR.

B.S., Colorado State University, 2012
M.S., Colorado State University, 2017

Submitted in partial fulfillment of the

requirements for the degree of

Doctor of Philosophy

2023

Approved by

First Reader

Michael Dietze, Ph.D.
Professor of Earth and Environment

Second Reader

Peter Buston, Ph.D.
Associate Professor of Biology

Third Reader

Shannon LaDeau, Ph.D.
Disease Ecologist
Cary Institute of Ecosystem Studies

Fourth Reader

Anne Short Gianotti, Ph.D.
Associate Professor of Earth and Environment

“The truth is, most of us discover where we are headed when we arrive.”

- *Bill Watterson*

DEDICATION

For Sarah, Liz, JR, Cody, and Cayenne.

ACKNOWLEDGMENTS

This work would not have been possible without the help of so many. First, I need to thank my partner, Sarah, for putting up with me these last few weeks! Your support has made this possible like no one else.

The science would not have happened without the guidance of my two advisors, Shannon LaDeau and Mike Dietze. Shannon, thank you for keeping me grounded in the theory and ecology and not just thinking about code. You also asked me "how are you doing?" more than any other, and for that I'm truly grateful. Mike, you continue to push me to think about the big picture, both from a systems perspective but also why ecological forecasting, and the methods we have developed, will matter to more than those of us in 457. The many skills (I'm not going to list because that would too long!) I have learned from you, technical and non-technical, will benefit me and my career in ways that I probably haven't fully grasped yet. I've learned and absorbed so much just from being in the lab, it has been great experience.

To my office mates Kathryn and Tess, what a ride it has been! There no two people who know what these past years have been like for me than you. Thanks for being there, for the impromptu therapy sessions, snack breaks, and just straight-up venting. It's been an honor to share in your accomplishments, I can't wait to see where you end up in your careers and in life!

My family has been there every step of the way, supporting me even if they don't really know what I do. The blind and unwavering support has given me some legs over the years, thanks for everything.

There is a long list of people who have aided my scientific career that helped me get to this point (and into graduate school). Kevin Crooks at Colorado State for my first independent study as an undergrad. Dan Tripp at Colorado Parks and Wildlife for hiring a guy to do field work who just broke his foot. That project was my first experience with disease ecology, who knew I'd end up here? I have to give a shoutout to the many crew members I worked alongside those summers (Dani, Cody, Austin, Marissa, Melissa, Sheri, and Elsa), what a time that was! Lastly to Brian Foy at Colorado State, who took a chance on someone to work in a lab who just walked out of the field. I also need to thank Andy Royle and Howie Ginsgerg at the USGS for advising me on Chapter four, who's help as been invaluable for wrangling and modeling such a large data set.

I know I've missed some people, but I would not be here without the community I've had over the years, this one's for you!

FROM CALIBRATION TO IMPLEMENTATION:

STAGE-STRUCTURED POPULATION FORECASTS FOR THE

VECTOR OF LYME DISEASE (*IXODES SCAPULARIS*) ACROSS

THE EASTERN UNITED STATES

JOHN R. FOSTER, JR.

Boston University Graduate School of Arts and Sciences, 2023

Major Professor: Michael Dietze, Professor of Earth and Environment

ABSTRACT

In the United States, the total confirmed and probable cases of Lyme disease have more than doubled in the past decade. The increase in human incidence has been attributed, in part, to the range expansion of the principal vector of the bacterial pathogen, the black-legged tick (*Ixodes scapularis*). The tick life cycle includes three distinct hematophagous stages, each with different temporal and spatial influence on tick infection and human exposure. Therefore, a model that accurately predicts the dynamics of all life stages would be more accurate in describing the risk of encountering a tick-borne disease (TBD).

To this end, I sought out to develop process-based models grounded in ecological theory and community ecology to make quantitative predictions of questing tick populations. Furthermore, the ultimate goal was to produce iterative, short (< 31 days) to intermediate (6 month - 1 year) forecasts on a daily basis in areas of the United States where Lyme disease is endemic.

In Chapter 1, I built stage-structured population models in a data fusion

framework that incorporates environmental variables such as the host population, relative humidity, and temperature, to predict the questing population of each life stage. I found that a four-stage model that includes the ecologically relevant dormant overwintering nymph state outperforms other models. The interplay between weather and host populations was also predictive.

In Chapter 2, I describe a data-assimilation scheme developed to update the tick population model iteratively and evaluate forecast uncertainty and sensitivities. Larval abundances were spatially heterogeneous, likely due to their limited dispersal capacity, and sampling efforts at this stage were less likely to reduce forecast uncertainty than efforts at later stages.

Chapter 3 evaluates the transferability and the structural components of this model for *I. scapularis* and *Amblyomma americanum* populations at NEON. *A. americanum* is arguably the second-most medically important tick species in the US. In general, forecasts were biased and tended to overpredict both species, this trend was on a latitudinal gradient, and forecasts for *I. scapularis* were more skillful than for *A. americanum*. Given the model framework, it appears that mouse abundance is less predictive of ticks at NEON than at Cary.

In Chapter 4, I estimated tick density at NEON sites and is used these estimates to constrain the parasitism state of mice through time, which has important implications for TBD management. Knowing when mice are parasitized could lead to management actions for mice removal and is another proxy for disease risk as this information tells us when ticks are active.

Overall, this dissertation focused on building mechanistic ecological forecasts from the ground up. I started with model calibration, then built a data assimilation scheme, and tested it at sites across the US. Therefore, this work represents the first of its kind pipeline from ecological model calibration to forecast implementation.

TABLE OF CONTENTS

LIST OF TABLES

LIST OF FIGURES

LIST OF ILLUSTRATIONS

LIST OF ABBREVIATIONS

AA ..... Amblyomma americanum

a-to-p ..... Absent to Present

BU ..... Boston University

C ..... Celsius

Cary ..... Cary Institute of Ecosystem Studies

CDC ..... Center for Disease Control and Prevention

CGDD ..... Cumulative Growing Degree Days

CRPS ..... Continuous Rank Probability Score

DA ..... Data assimilation

IX ..... Ixodes sacularis

JS ..... Jolly-Seber

LD ..... Lyme disease

L-N ..... Larvae to nymph transition

m ..... meters

MCMC ..... Markov Chain Monte Carlo

MEM ..... Multi-Event Model

mm ..... millimeters

MNA ..... Minimum Number Alive

N-A ..... Nymph to adult transition

NEON ..... National Ecological Observatory Network

NMME ..... North American Multi-Model Ensemble

p-to-a ..... Present to Absent

PSRF ..... Point Scale Reduction Factor

RH ..... Relative Humidity

RMSE ..... Root Mean Squared Error

TBD ..... Tick-borne disease

Introduction

Human incidence of tick-borne disease have more than doubled in the past decade (Eisen et al., 2016), which is mostly attributed to Lyme disease (LD). From its endemic regions in the Northeast and upper Midwest United States, LD has crawled its way into Canada, Michigan, Virginia, and Iowa (Hamer et al., 2010; Khatchikian et al., 2015; Oliver et al., 2017; Lantos et al., 2021). The rapid increase in tick-borne disease incidence warrants the need for iterative near-term forecasts of tick-borne disease risk, as they have the potential to relieve some of the public health burden while also providing valuable insights to researchers.

What follows is a brief overview of LD ecology, which is similar to other tick-borne diseases in the United States and will serve as a template for the chapters outlined ahead. By leveraging what we know about the tick-host-pathogen relationship, we can construct process-based, Bayesian state-space statistical models to provide inference on this system, which provide the foundation for iterative forecasts.

The Ecology of Lyme Disease

LD, caused by the bacterium *Borrelia burgdorferi* (Burgdorfer et al., 1982) is vectored by the black-legged tick (*Ixodes scapularis*), which has three post-egg life stages: larvae, nymph, and adult. For the tick to transition from one life stage to the next it must take a blood meal from a vertebrate host. Once the tick reaches adulthood, a female tick will take a third blood meal so that it can produce eggs, while male adults usually do not feed (Sonenshine, 2018).

The process of looking for a host is called “questing”, and the time of year, or phenology, that this occurs is different for each life stage (Lindsay et al., 1999; Levi et al., 2015). After hatching in the summer, *I. scapularis* larval ticks quest for and feed on hosts, after which they enter diapause to overwinter. Newly molted nymphs then quest the following spring/early summer and, if successful, molt into adults in the fall of the same year. Adults quest in fall/winter, laying their eggs in the spring, completing the cycle (Sonenshine, 2018).

Ticks would not vector disease if the landscape were without pathogens. *B. burgdorferi* is an obligate bacterial pathogen of small vertebrates, otherwise known as hosts (Tilly et al., 2008). Hosts serve two roles in this system, hosts for ticks and reservoirs for *B. burgdorferi*. Host species vary in how likely a tick successfully takes a blood meal from them (Brunner et al., 2011), and also how well they maintain and transmit *B. burgdorferi* to uninfected ticks. The white-footed mouse (*Peromyscus leucopus*) is an excellent reservoir host. They are ubiquitous on the landscape, can have high tick body burdens and feeding success, and can maintain *B. burgdorferi* infection (Donahue et al., 1987). Furthermore, none of these factors affect their mortality (Hersh et al., 2014).

While a blood meal is required for the tick to move from one life stage to the next, ticks spend roughly 90% of their lives off-host. This means that, as invertebrates, their metabolic activity and physiology, and by extension their day-to-day survival, are regulated by the environment by factors such as temperature (Bertrand & Wilson, 1996; Needham, 1991), precipitation (Hayes et al., 2015), and relative humidity (Berger et al.,

2014; Ginsberg et al., 2017).

The goal of this dissertation is to have automated, iterative forecasts of tick and small mammal populations running at multiple National Ecological Observatory Network (NEON) sites, and this dissertation describes the science to get us there.

Chapter one discusses building models from what's known about the ecology of tick-borne disease, but also filling gaps in knowledge of the LD system. Specifically, I use stage-structured matrix models and a data-fusion framework to build and test ecological hypotheses about *I. scapularis* including the role of instantaneous daily weather, host abundance, and how these to biotic and abiotic factors interact. We also quantify sources of uncertainty in predictions.

Chapter two validates these models through ecological forecasting at Cary and provides insight into 15 years of the LD system. This chapter also explores the effectiveness of a forward only Monte Carlo Markov Chain (MCMC) data assimilation technique. Here, we also explore the relative contribution of larvae data as it pertains to data assimilation and predictive capacity.

Chapter three is a true test of these models as I attempt to transfer them to NEON sites across the eastern US. Here, we focus on the ability of the stage-structured model formulation to describe population dynamics in space and across species. NEON collects multiple species of tick, and we focus on the most abundant of them, *Amblyomma americanum*.

Chapter four shifts the focus from modeling ticks to modeling their hosts. Specifically, we are interested in describing spatio-temporal patterns in parasitism, i.e.

when and where do mice have ticks attached to them. We use the NEON data again, as it provides large spatial coverage and spans multiple tick-borne disease systems. The outcomes here have direct implication for tick-borne disease management via host management.

CHAPTER ONE:

Instantaneous weather and mouse abundance increase predictability for the primary vector of Lyme disease (Ixodes scapularis)

Abstract

Lyme disease, the most prevalent tick-borne disease in North America, is caused by the bacterium *Borrelia burgdorferi* and is spread to humans by the black-legged tick (*Ixodes scapularis*) in the northeastern US. Of the three questing life stages, nymphs represent the largest public health concern, as they are most likely to transmit the bacteria to humans. Previous research has shown that the number of questing nymphs can be predicted using environmental drivers, but there is little work done on predicting the dynamics of the entire questing population at once. This is needed as adults are still competent vectors and while larvae are not, after their first blood meal they molt into nymphs. Therefore, a model that accurately predicts the dynamics of all life stages would be more accurate in describing the risk of encountering an infectious tick. To this end, we built stage-structured population models that incorporate environmental variables such as the host population, relative humidity, and temperature, to predict the questing population of each life stage. We found that a four-stage model that includes the dormant nymph state outperforms a three-stage model that only includes the questing states, and that by incorporating the host population and weather we reduced the amount of structural uncertainty that was present in the null model. We were able to accurately predict all three questing states at sites different than where they were calibrated, showing that this

model structure is generally transferable. Implications to ecological forecasting are discussed.

Introduction

In the United States, the total confirmed and probable cases of Lyme disease have more than doubled in the past decade (CDC, 2021). The disease is caused by the bacterium *Borrelia burgdorferi* (Stanek et al., 2012), and the increase in human incidence has been attributed, in part, to the range expansion of the principal vector of the bacteria, the black-legged tick (*Ixodes scapularis*) (R. J. Eisen & Eisen, 2018; Sonenshine, 2018).

I. scapularis has three post-egg life stages (larvae, nymphs, and adults), and of these stages, nymphs are the most epidemiologically important as their density is predictive of Lyme disease cases (Mather et al., 1996; Nicholson & Mather, 1996; Stafford et al., 1998; Pepin et al., 2012; Little et al., 2019). Furthermore, their peak questing activity, or phenology, each year coincides with peak human outdoor activity (Barbour & Fish, 1993). In the northeastern United States, this is roughly between May and June as nymphs emerge from dormancy (Lindsay et al., 1998)**.**

There have been numerous efforts to build predictive models of *I. scapularis* nymphs using varies modeling techniques and drivers (Ostfeld & Brunner, 2015). Mouse abundance, which itself is predicted from acorn abundance, is the most used biotic driver, shown to be predictive of *I. scapularis* nymphs almost two years in advance (Ostfeld, Jones, et al., 1996; Ostfeld et al., 2001). Abiotic variables, such as weather, have also been used to wide effect. Increasing winter precipitation is positively correlated with

nymph density in Connecticut (Jones & Kitron, 2000; Hayes et al., 2015; Kessler et al., 2019), and annual precipitation in Florida (Kessler et al., 2019). Furthermore, Jones & Kitron (2000) showed that cumulative rainfall predicts larval abundance.

Relative humidity has been shown to predict nymphs questing activity (Perret et al., 2004) and is a fundamental factor of their survival (Piesman et al., 1991; Ginsberg et al., 2017). Temperature has also been widely used, either untransformed or as cumulative growing degree days (CGDD). In Canada, tick survival decreased with decreasing temperature (Ogden et al., 2005), and spring temperature predicts nymph phenology (Levi et al., 2015). CGDD is positively correlated with tick observations by drag cloth (Jones & Kitron, 2000; Ogden et al., 2008) and peak occurrence (Levi et al., 2015). Vapor pressure deficit is also associated with immature tick survival and development (Lindsay et al., 1999).

These models are important because they connect life stage processes to climatic variables, which will be important to predict ticks into the future under an uncertain climate. However, estimating the abundance of future populations will need to take an even more mechanistic approach, either by modeling more than one life stage at a time or by including specific causal links to developmental, survival, and host processes (LaDeau et al., 2011; Ogden et al., 2014; Ostfeld & Brunner, 2015; Kilpatrick et al., 2017).

The use of hosts, such as mice, in the models above has been justified because of the important role mice play in the tick life cycle more generally, and in tick-borne disease ecology specifically. Larvae and nymphs require a blood meal to molt into the subsequent life stage, and adult female ticks require a blood meal to reproduce (Gray et

al., 2002; Stanek et al., 2012). In the northeastern United States, one of the primary hosts for larval and nymphal black-legged ticks is the white-footed mouse (*Peromyscus leucopus*) (Ostfeld, Jones, et al., 1996), which is also a competent reservoir species for *B. burgdorferi* (Schmidt & Ostfeld, 2001), and is the host most associated with high larval survival (Keesing et al., 2009).

Like nymphs, larvae and adults have their own phenology. Adults are primarily active between September and January (Levi et al., 2015), and are important because they are competent vectors of *B. burgdorferi* (Piesman et al., 1991) and their survival and host-finding success influence the number of larvae in the next year (Wilson et al., 1990). Larvae are active between July and October (Lindsay et al., 1998), and while not competent vectors of *B. burgdorferi,* as transovarial transmission does not occur (Richter et al., 2012; Rollend et al., 2013), they can become infected nymphs after their first blood meal if they feed on an infected host (Gray et al., 2002).

Identifying demographic rates (survival, transition, and fecundity) of an unmarked stage-structured population is a challenge (Gross et al., 2002). For example, a high larval survival rate and a low larvae-to-nymph transition rate can explain the number of larval and nymphal ticks from one-time point to the next equally as well as a low larval survival rate paired with a high larvae-to-nymph transition rate. Despite the challenges in estimating multiple unobservable transitions across life stages, data fusion and multi-model approaches have been used to identify demographic parameters in stage-structured populations of plants (Evans et al., 2010), salmon (Michielsens et al., 2008), and ticks (Dobson et al., 2011), which more than justifies a Bayesian approach.

Here we describe a Bayesian modeling approach that assimilates field data and mathematical processes contained within a daily stage-structured model. Our goal is to better identify critical life history transitions and evaluate the importance of external weather and host population drivers on the population dynamics of all three post-egg life stages.

This approach aims to quantify the demographic rates of each life stage to estimate abundances of each life stage and population growth through a data fusion approach, using a comprehensive and long-term dataset from the Hudson Valley Region in New York.

Specifically, we hypothesize that estimating life-stage specific survival rates with abiotic data will improve abundance estimates, as greater than 90% of a ticks life is spent off host and their micro-climatic conditions are intrinsically tied to their physiology (Needham, 1991) (i.e. estimating nymph survival as a function of weather improves nymph tick prediction skill and reduces adult prediction uncertainty) (H1). We also hypothesize that incorporating the mouse population will constrain larvae-to-nymph and nymph-to-adult transition rates and improve tick population estimates because of their outsized role in life stage development (Gray et al., 2002; Keesing et al., 2009) (H2).

Finally, we expect that including a completely latent state of dormant nymphs will improve nymphal predictions (H3), as this more accurately reflects the life history transition from larvae to nymph (Randolph, 2004; Dobson et al., 2011). Through our modeling approach, we also explore the spatial variability in tick demographic rates and analyze the uncertainty in population predictions at the three distinct field sites.

Illustration 1 Conceptual framework

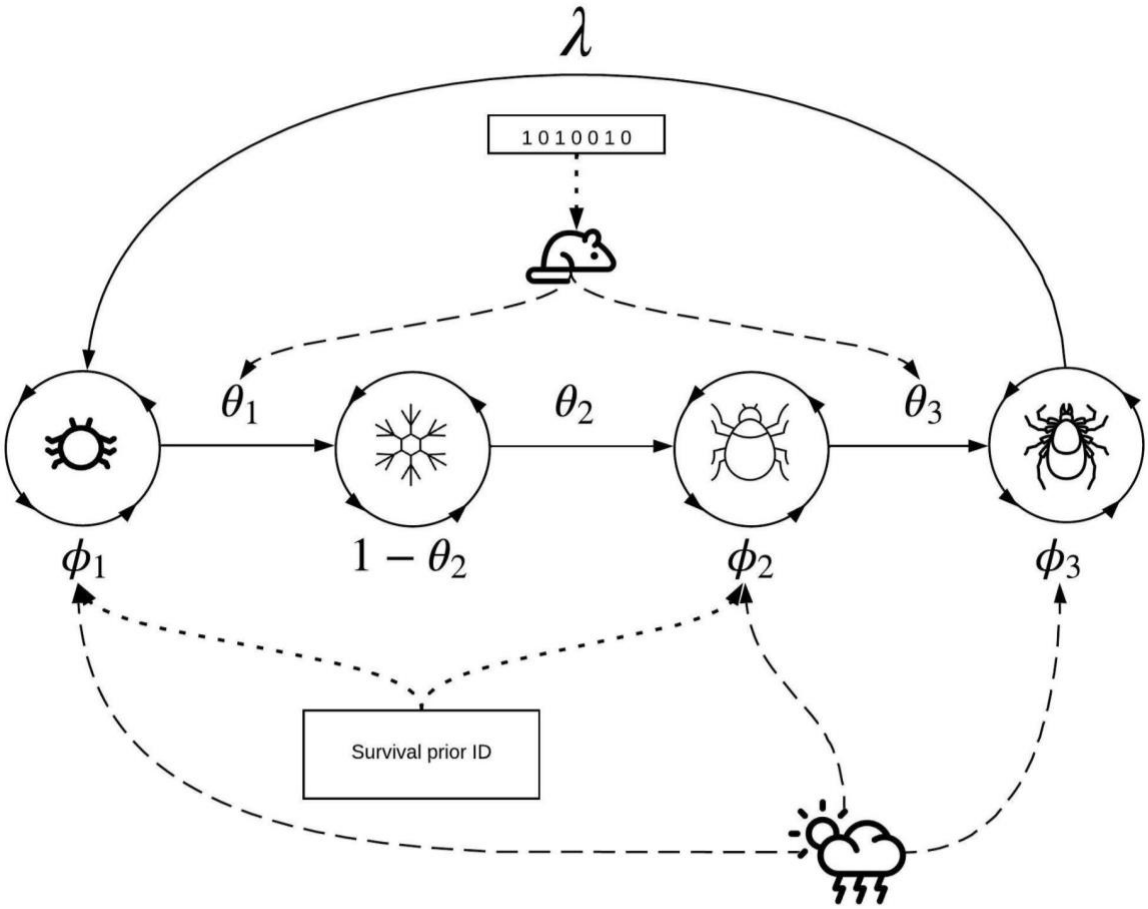

Illustration 1: Conceptual framework. Demographic parameters map to the transition matrix (Eq. 10). $\phi_{1\text{-}3}$ represent the daily survival rates of larvae, nymphs, and adults. $\Theta_{1\text{-}3}$ represent the transition rates from larvae to dormant nymph, dormant nymph to questing nymph, and questing nymph to adult nymph. λ is reproduction. Solid lines represent demographic processes, dashed lines represent where and what information was used as covariates (weather on survival (H1), mouse abundance on transition (H2)). Boxes and dotted lines represent the data-fusion framework and location of sub-models (building informed priors for larvae and nymph survival, estimating mouse abundance). The inclusion of the overwintering state represents H3.

Methods

Site Description and Data Collection

Three field sites were located at Cary Institute of Ecosystem (Cary) Studies in Millbrook, New York. Tick and mouse observations were collected at each site (Green, Henry, Tea), which are more than 100m apart and centered around 41.7851N, -73.7338W. All sites are 2.25 hectares and are post-agricultural oak-dominated stands (Ostfeld et al., 2001).

Tick and Mouse Observations

Tick (*I. scapularis*) abundances are derived from tick drags. A tick drag consists of pulling a 1 square meter cotton cloth along the ground on three randomly chosen transects, for a total of 450 square meters sampled per site. Ticks were counted and removed from the cloth every 30 meters. Drags were conducted every three to four weeks starting in the spring of 1995 through the fall of 2005. Tick drags did not occur in the winter.

Mouse (*P. leucopus*) population monitoring occurred via mark-recapture concurrent with the tick monitoring. The trapping grid was an 11 x 11 array of Sherman live traps, with each station spaced 15 meters apart, and two traps at each station. Traps were set for two consecutive nights every three to six weeks baited with oats, and mice were marked with a numbered ear tag upon the first capture. Mouse captures did not occur over the winter. The minimum number of mice alive (MNA) for each site was

estimated directly from these data. The three sites we chose to include in this study were the control sites of a long-term research program at Cary; mouse populations and vegetation were not manipulated at these sites. For more complete descriptions of the long-term tick and mouse monitoring at Cary see (Brunner & Ostfeld, 2008; Ostfeld et al., 2001; Schauber et al., 2005)**.**

Meteorology

Meteorology was collected through Cary's environmental monitoring program located on-site at a centralized location (the three Cary field sites used the same meteorological data). Precipitation was collected with a Belfort Instrument Universal Recording Rain Gauge Series 5-780, located 3m above the ground. Relative humidity was collected with a Phys Chem Corp. PCRC-11 or PCRC-55 (years 1995–1997) and a Campbell Scientific, Inc. HMP45C (years 1997-2005), and temperature was collected with a Campbell Scientific model 107 or 207 (years 1995-1998) and a Campbell Scientific, Inc. HMP45C (years 1998-2005). See Kelly (2020) for a complete description of Cary's environmental monitoring program.

Prior Distribution Identification

To identify the prior distribution of daily survival of black-legged ticks, we used data that were available from a related study (Brunner et al. *in prep*). Unfed larval and nymphal ticks were placed inside mesh bags and exposed to field conditions at three military installations distributed across the eastern US (specific coordinates

withheld due to funding requirements). The first bags were deployed on May 11, 2017, and the last used for this analysis were retrieved on August 23, 2017. Temperature and relative humidity were monitored with iButtons at each soil core.

Statistical Framework

This section describes our statistical framework to improve predictions of tick populations, which includes the main tick population model, and two sub-models (Illustration 1.1).

The tick population models we focus on are matrix stage-transition models, which use survival, transition, and fecundity rates to estimate the population density through time. The two sub-models were employed to help infer some of these demographic parameters in our focal model: a prior identification model for building informative priors on daily mean survival of larval and nymphal ticks, and a mouse population model where we use estimated mouse abundance as a constraint on transition parameters. Below we describe the two sub models that we used to parameterize our focal model.

Models were run until convergence was reached (point scale reduction factor less that 1.1). We determined convergence on marginal posterior distributions using the Gelman and Rubin's convergence diagnostic implemented via the coda package in R v.4.0.2 (Brooks & Gelman, 1998; Gelman & Rubin, 1992; Plummer et al., 2006; R Core Team, 2020). Workflow, data cleaning, and analysis were completed in R, and Bayesian models were built in NIMBLE (de Valpine et al., 2017, 2022)

Daily tick survival probability was estimated to construct informative priors for tick survival used in the tick matrix stage-transition model. We used a binomial process model to estimate daily tick survival.

$$y_t \sim binom(\phi, y_0) \quad [1]$$

Where y_t is the number of ticks alive at the end of the soil core experiment, y_0 is the total number of ticks that were placed in the soil and ϕ is the cumulative survival probability over the *n* days ticks were in the soil. We modeled the survival probability ϕ as

$$\log(\phi) = \sum_{n=1}^{d} \log(\lambda_n) \quad [2]$$

$$logit(\lambda_n) = \beta X_n \quad [3]$$

Where λ is the daily survival probability, beta is regression coefficients, and **X** is the matrix of daily covariates. To match the weather variables that are collected at Cary, we used above-ground daily temperature and relative humidity as covariates in this prior identification sub model. All weather variables were centered on their respective means. Uninformative priors with a mean of zero were used for regression coefficient β.

Mouse Population Models

To estimate the mouse population density over time, we used a Jolly-Seber (JS) model, which was developed specifically for mark-recapture data and estimates population-level demographic parameters. We modified the restricted dynamic occupancy model parameterization, which uses data augmentation to model the entry of not-previously-seen individuals into the population (Kéry & Schaub, 2012). Our modification estimates the daily survival of mice as a function of temperature and precipitation, then aggregates daily survival probabilities in-between capture events (eq. 4). We modeled survival on a daily basis because capture events were at irregular intervals.

$$logit(\lambda_d) = \beta_1 + \beta_2 * precipitation_d + \beta_3 * temperature_d \quad [4]$$

$$log\ (\phi_t) = \sum_{d=\Delta t}^{t}(log\ (\lambda_d)) \quad [5]$$

ϕ is the probability of surviving from one capture occasion to the next. Equation four describes daily survival rate, which is a logit transformed linear model of predictors. To get the survival rate between trapping occasions, we took the sum of the logged daily rates between trapping occasions (Δt), then exponentiated the sum (log link function), as shown in equation five. This was necessary to prevent numerical underflow. It is important to note that *d* represents each day in the time series, and *t* represents each

trapping occasion. See supplementary material section S1.1 for a complete description of this model.

Tick Population Models

We fit several models to test the effectiveness of model structure, biotic, and abiotic variables on their ability to improve predictions of tick abundance. Informative prior distributions for survival, as described above (from equation 2; prior identification sub model) were used in each of the models here, and each model was fit to each of the three Cary sites independently.

We first built a three-stage model corresponding to the questing larvae, nymph, and adult stages. We tried to fit a range of three-stage models using different environmental covariates, but are not presenting them because they performed poorly, and about the same as the static three-stage model, which does not include environmental covariates. Therefore, the only three-stage we report is the Static version.

We then built a four-stage model, where the added stage represents dormant nymphs. Because the four stage model performed significantly better than the three stage model (see Results), we then fit a series of five four-stage models, shown in Table 1, that include: a static (no covariates) model, one with daily weather variables to constrain questing tick survival, one that uses the raw mouse abundance data to constrain the transition rates from larvae to dormant nymph and from questing nymph to adult, one with the output of the estimated mouse abundance model instead of the raw mouse data, and a full model that uses both weather and estimated mouse abundance (Table 1.1).

Table 1.1 List of models and their structures.

Model Name	Model Description (stages)	Covariates	Parameters Constrained
Static (3)	Three-stage matrix model (questing larvae, questing nymphs, questing adults)		
Static (4)	(questing larvae, dormant nymphs, questing nymphs, questing adults)		
MNA (4)	Four-stage matrix model	Mouse abundance (Minimum number alive [MNA]) from data	Θ_1, Θ_3
Mice Estimated (4)	Four-stage matrix model	Mouse abundance from the level-two mouse population model	Θ_1, Θ_3
Weather (4)	Four-stage matrix model	Daily maximum temperature, daily minimum relative humidity, daily maximum relative humidity, daily precipitation	Φ_1, Φ_2, Φ_3
Weather + Mice (4)	Four-stage matrix model	Mouse abundance from the level-two mouse population model and daily maximum temperature, daily minimum relative humidity, daily maximum relative humidity, daily precipitation	Φ_1, Φ_2, Φ_3, Θ_1, Θ_3

Each transition matrix, $\mathbf{A_t}$, was estimated daily (Table 2). Parameterization of the non-zero elements can be found in S1.2. But briefly, survival and transition rates are logit transformed linear models. The models for survival used daily maximum temperature, daily minimum and daily maximum relative humidity, and daily precipitation in a regularized regression framework. To aggregate across observation days, we permuted the matrices as follows:

$$\boldsymbol{P_t} = A_t\boldsymbol{A_{t-1}}\boldsymbol{A_{t-2}}\ldots\boldsymbol{A_1} \quad [6]$$

$$\overrightarrow{x_{t+1}} \sim MVN(\boldsymbol{P}_t\overrightarrow{x_t}, \Sigma) \quad [7]$$

Where $\mathbf{P}_t$ is the permuted transition matrix (eq. 6) that is used to calculate the expected demographic transitions between sampling occasions. Then, the predicted latent state, x_{t+1}, was drawn from the multivariate normal distribution (eq. 7) based on the expected number of ticks, $\boldsymbol{P}_t\overrightarrow{x_t}$, and a process error covariance matrix $\boldsymbol{\Sigma}$. $\boldsymbol{\Sigma}$ was parameterized as a diagonal matrix of variances, assuming that process error across life stages is uncorrelated.

Observed tick counts were assumed to be Poisson distributed, where $y_{j,i}$ is the tick count of life stage *j* at time *t*, and *x* is the latent tick abundance:

$$y_{j,t} \sim Poisson(x_{j,t}) \quad [9]$$

$$\begin{pmatrix} \phi_1 * (1-\theta_1) & 0 & 0 & \lambda \\ \phi_1 * \theta_1 & 1-\theta_2 & 0 & 0 \\ 0 & \theta_2 & \phi_2 * (1-\theta_3) & 0 \\ 0 & 0 & \phi_2 * \theta_3 & \phi_3 \end{pmatrix} \quad [10]$$

Model Assessment

The mouse population models were assessed using posterior estimates of the total predicted mouse abundance (latent abundance multiplied by capture probability) compared to observed values using R^2 and bias. Tick population models were assessed by posterior predictive checks using one-step-ahead predictions within and across sites, where the one-step-ahead predictions iteratively cycle through the time series to predict the next observation from the current latent state.

As these matrix models were fit independently at each site, the within-site predictions test goodness-of-fit, while the across-site predictions represent a measure of transferability and out-of-sample validation. We evaluated the one-step-ahead predictions with the Continuous Ranked Probability Score (CRPS) (Gneiting & Raftery, 2007; Simonis et al., 2021), a metric that accounts for the probabilistic nature of our predictions, penalizing models not just for mean absolute errors, but also for predictive distributions that are under- or over-confident.

A perfect forecast is defined when CRPS is equal to zero. Therefore, forecast skill increases as CRPS approaches zero; lower scores are better. Moreover, as the magnitude of observations varies considerably across life stages, we evaluate model predictions for each life stage separately.

Variance Partitioning

Uncertainty in model predictions comes from four sources:; (i) initial condition (IC) uncertainty, (ii) parameter uncertainty, (iii) driver uncertainty, and (iv) process uncertainty. IC, parameter, and process uncertainties were propagated by sampling the joint posterior distribution of the matrix population models. Specifically, IC uncertainty came from x (eqn. 6), parameter uncertainty came from all the parameters in matrix **A** (Table 2), and process error came from $\boldsymbol{\sigma}^2$ (eqn. 7). In terms of driver uncertainty, we treated the weather as known (without uncertainty), but incorporated uncertainty in mouse population estimates, which was derived from the posteriors of the mouse population sub model (eqn. S8).

To determine the contribution of each source of uncertainty, we ran one-step-ahead predictions under several scenarios, sequentially adding each source of uncertainty. The first simulation only samples from the latent state (IC) while holding parameters and drivers (estimated mouse abundance) at their posterior means and setting process error to zero. We then added parameter uncertainty, then driver uncertainty (where appropriate), and finally process uncertainty. The final scenario includes all sources of uncertainty and is the simulation that was scored with CRPS, as this scenario represents the full

predictive posterior.

Population growth rate

Stochastic population growth rates were determined by sequences of the daily transition matrices **A**, under a mover-advancer model where the probability of advancing to the next environment is equal to one (Caswell, 2000). We estimated the growth rate for each sampling season, represented by the first tick drag to the last tick drag each year. Each stochastic population growth rate simulation used 2000 random draws from the joint posterior.

Results

Prior Identification

Posterior parameter estimates from the survival models are presented in Figure 1.1. To ease interpretation, intercepts were converted from the underlying (daily) survival rates to be expressed as the mean monthly (30-day) survival rate. In all models, nymphs have a higher monthly survival rate than larvae by approximately 5%. Weather variables were centered, meaning slope coefficients represent the effect that a given weather variable has on larvae or nymph survival as the weather variable departs from its mean. In all cases, parameters remained strongly overlapping with zero but tended to suggest higher climate sensitivity among nymphs, which responded positively to humidity and negatively to temperature, while larvae responded positively to temperature and were insensitive to humidity (Figure 1.1).

Figure 1.1 Prior identification: survival

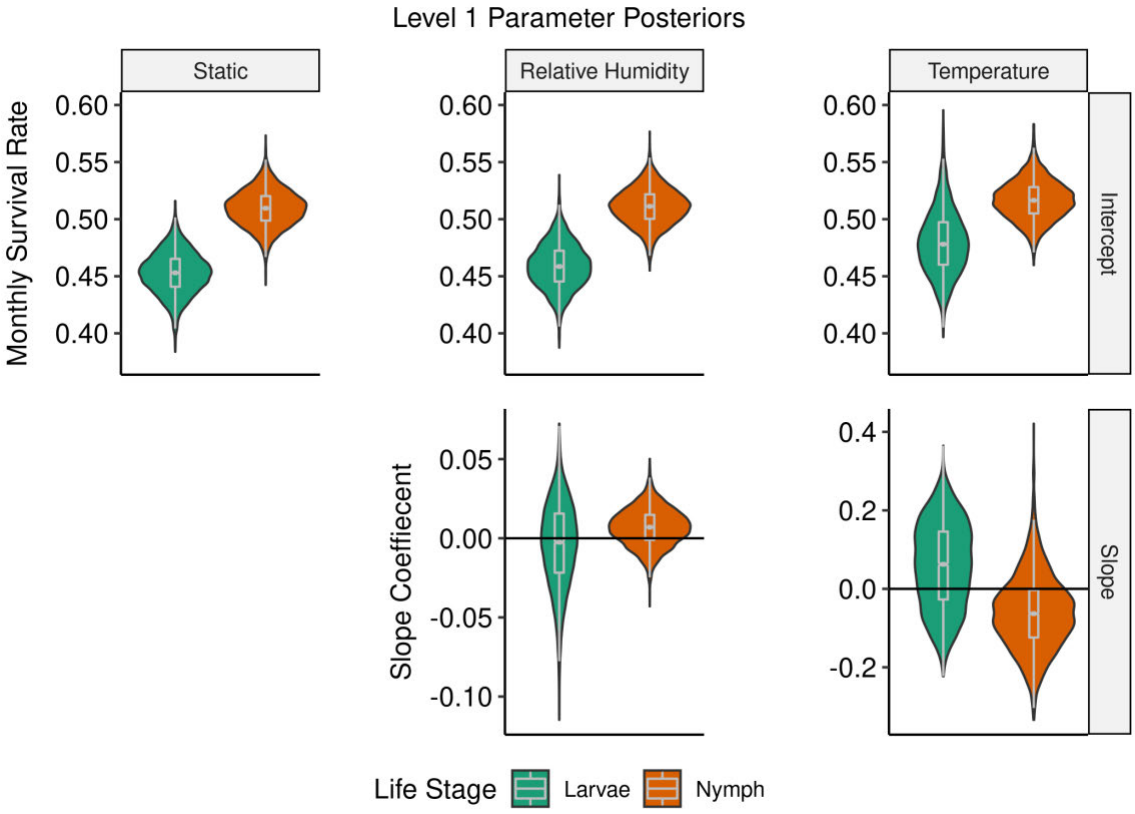

Figure 1.1: Posterior distributions from the stage 1 survival models. The Static model is the intercept-only model. The other covariates considered were daily relative humidity, daily temperature, and daily vapor pressure deficit. The top row is the intercepts, and the bottom row is the effect of each weather variable. Violin and box plots were drawn from 5000 random samples from the posterior.

Mouse Population Models

Demographic parameters describing the mouse populations were similar at the three Cary sites (Figure S1.1). Mean monthly survival rates were estimated as 0.815, 0.813, and 0.806 at Green, Henry, and Tea, respectively. While small, precipitation and temperature both have negative effects on mouse survival, with temperature having a stronger effect and more variable across sites. Capture probabilities were similar across sites, with Henry slightly higher at 60% compared to Green and Tea at 57 and 58%, respectively.

We evaluated the effectiveness of the mouse model by performing the one-step-ahead predictions described in section 2.4. R-squared values ranged from 0.74 to 0.77 across the three sites (Figure 1.2). On average, the model underpredicts by roughly 6, 3, and 5 mice per 2.25 hectares at Green, Henry, and Tea respectively. This is relative to a mean mouse abundance (MNA) of 51, 36, and 43 mice at Green, Henry, and Tea.

Tick Population Models

The 4-stage tick population models were able to recover observations in the one-step-ahead predictions more precisely than the 3-stage model. This was true both within and across sites for nymphs (Figure 1.3) and larvae (Figure S1.2), and less so for adults (Figure S1.3).

Figure 1.2 Mouse model accuracy

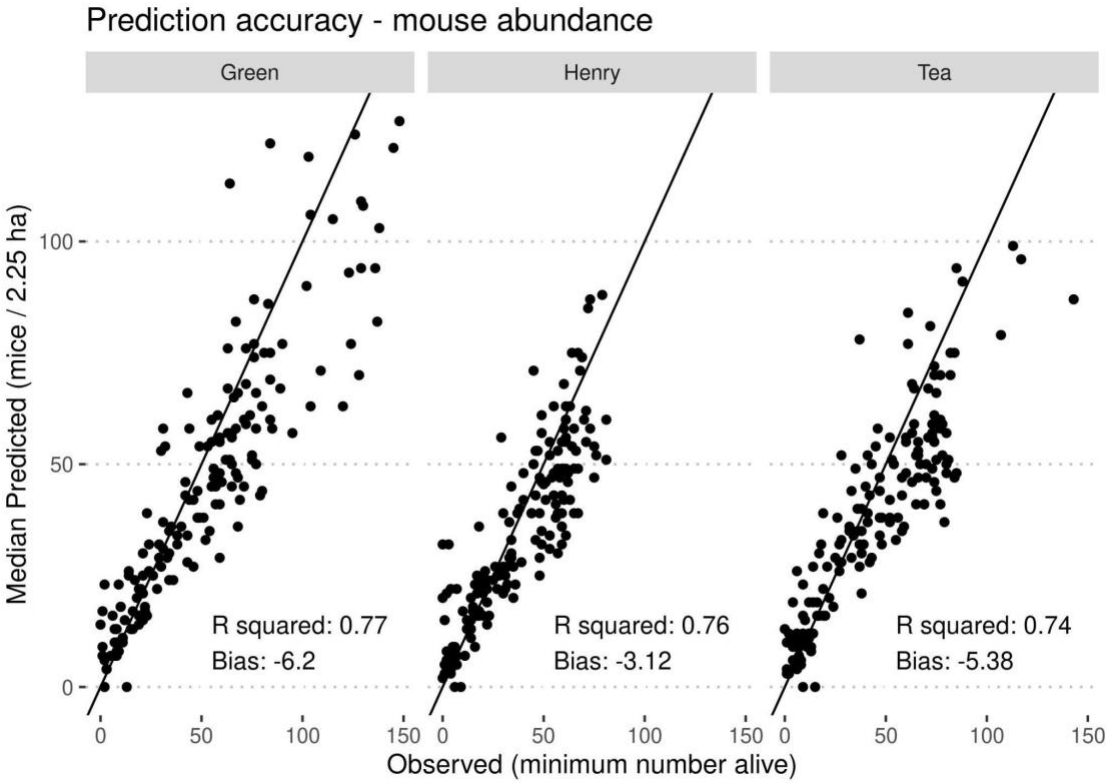

Figure 1.2: Model accuracy (the median prediction) with observation error compared to observed mice at each trapping occasion. The three sites are displayed independently. R-squared values are calculated relative to the one-to-one line. Bias represents the average number of mice underestimated per plot per trapping occasion.

Figure 1.3 Across-site nymph one-step-ahead predictions

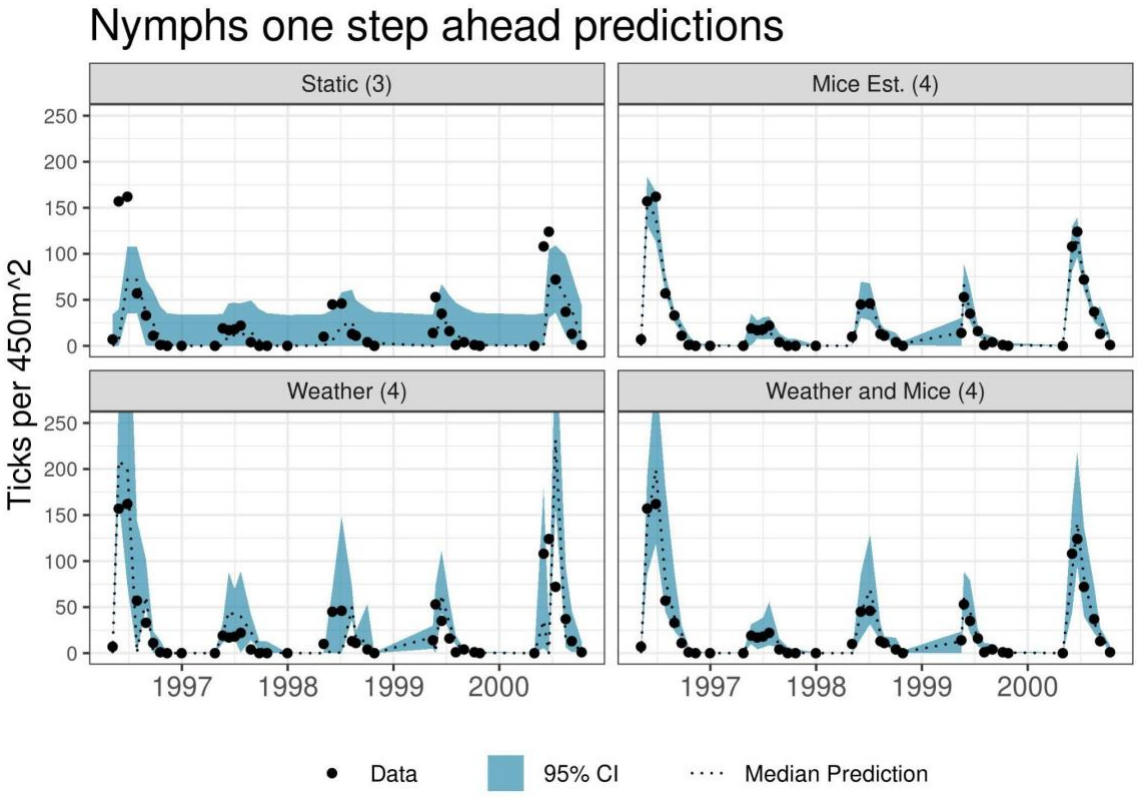

Figure 1.3: One-step ahead predictions from an across-site simulation for nymphs. The model was calibrated at Henry and simulated at Tea. Showing 1996 - 2000 because peak nymphal observations were in 1996 and 2000 at Tea. Displaying output from for models: Static (3) (top left), Mice Est. (4) (top right), Weather (4) (bottom left), and Weather and Mice (4) (bottom right). Models not displayed (Static (4) and Mice MNA (4)) were excluded because they have very similar predictions to the Mice Est. (4) model.

Demographic Parameters

Intercept terms for the survival equations represent mean daily survival rate because weather variables were standardized. We present them as monthly rates for easier comparison. The effect of covariates, either weather or mouse abundance,

represent the effect that a given variable has on mean survival or transition.

Survival intercepts

Median monthly larvae survival was mostly consistent across sites and models. At the low end, median monthly survival was estimated at 0.36 (90% CI 0.33 - 0.40) at Tea for the Static (3) model. The highest survival rate was at Green under the Weather (4) model with a median of 0.45 (90% CI 0.42 - 0.48). The models that included weather had nearly identical intercepts for larval survival. For nymphs, monthly survival was consistent across models where the minimum estimate was at Tea using the Mice MNA (4) model with a median of 0.48 (90% CI 0.45 - 0.50). The maximum estimate for nymphs was at Green under the Weather (4) model with a median of 0.52 (90% CI 0.49 - 0.54). Adult survival was less precise and more variable than nymphs and larvae. The minimum monthly survival rate for adults was 0.37 (90% CI 0.23 - 0.56) at Tea with the Static (4) model, and the maximum was 0.92 (90% CI 0.71 - 0.98) at Green with the Weather (4) model. All survival intercepts are in Table S1.1.

The effect of daily weather (H1)

The weather variable that had the largest impact on larval survival was precipitation, which increased survival at all sites (Figure 1.4).

Figure 1.4 The effect of weather on daily tick survival

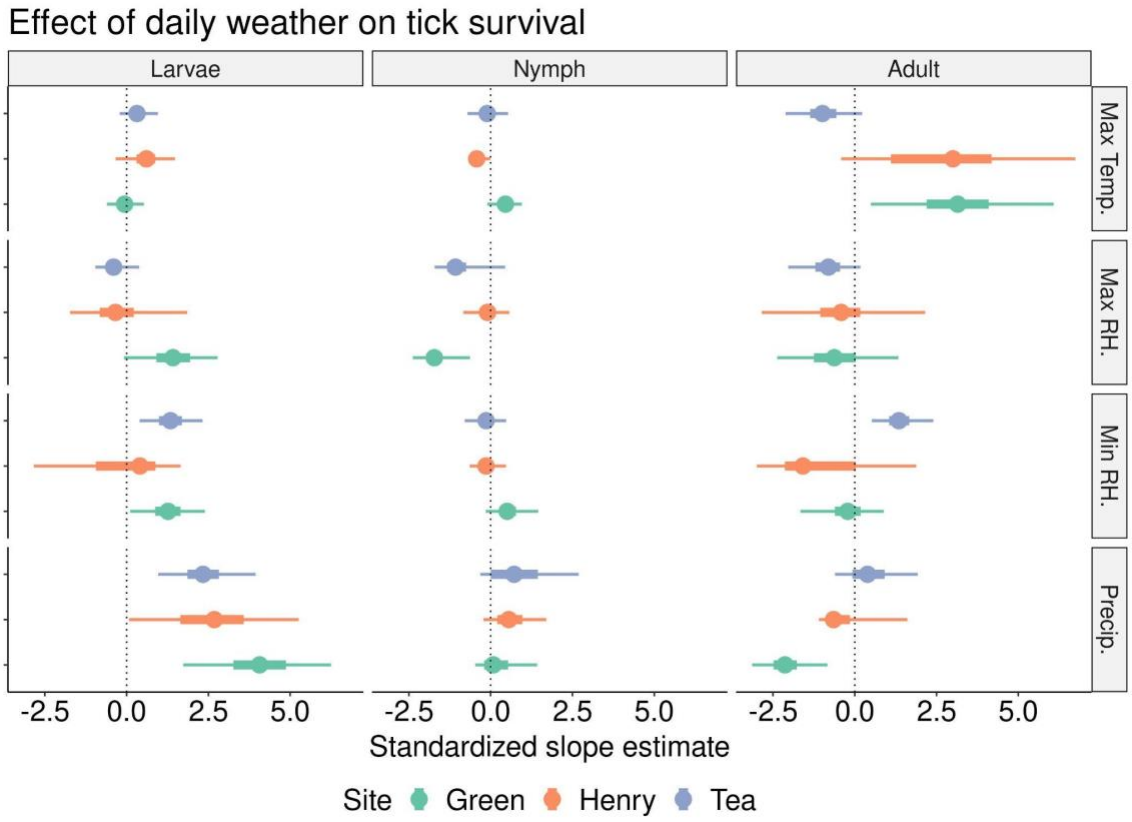

Figure 1.4: Standardized slope estimates for the effect of a given weather variable (rows) on the daily survival of a given life stage (columns) from the Weather and Mice (4) model. The width of the narrow whiskers represents the 90% CI, wide whiskers are the 50% CI, for each coefficient. Vertical dotted line to show which effects overlap with zero. Colors denote the site where the model was calibrated.

The effect of precipitation on larval survival was 4.06 (90% CI 2.01 - 5.97) at Green under the Weather and Mice (4) model. The effect of relative humidity (either minimum or maximum) was mixed, either increasing survival or having no effect (Figure 1.4). Daily maximum temperature did not have a significant effect on the survival of larval Ixodes ticks.

Like larvae, precipitation had the largest positive effect on nymph survival, the largest effect for the Weather and Mice (4) model being at Tea with a median of 0.73 (90% CI -0.22 – 2.02). The effect of relative humidity on nymphal survival was mixed.

Daily maximum relative humidity had a negative effect on nymph survival, where the largest effect was -1.73 (90% CI -2.16 – -1.11) at Green. Daily minimum relative humidity had no effect except at Green with a median of 0.5 (90% CI 0.03 – 1.07). The effect of temperature was also mixed, where there was no effect at Tea, a positive effect at Green (0.46; 90% CI 0.10 - 0.81) and a negative effect on survival at Henry (-0.43; 90% CI -0.62 – -0.18).

Daily maximum temperature had the largest positive effect on adult survival, where the largest effect was at Green with a median of 3.16 (90% CI 1.44 – 5.01). Daily maximum relative humidity reduced adult survival at all sites (Figure 1.4).

The effect of mouse abundance (H2)

The effect of mouse abundance on the daily transition rate from larvae to nymph or nymph to adult was mostly consistent across sites and model formulations. For the larvae-to-nymph (L-N) transition, mice either had a negative or null effect on the transition rate. The posterior distribution for effect of mice abundance on L-N transition included 0 for all Weather and Mice (4) model runs and in all model runs at Tea site. Numbers of mice had a negative association with this transition rate in models where mouse abundance (estimated or MNA) was an important effect (Figure S1.5).

The effect of mouse abundance on the nymph-to-adult transition was more pronounced. There was a positive effect of mice at Tea across all models, and at Henry estimated by the Mice Est. (4) and Mice MNA (4) models. There was no effect of mouse abundance at Green on the nymph to adult transition (Figure S1.5).

The effect of including a dormant stage (H3)

Larvae and nymph predictions benefited from the addition of the dormant state, and adults were agnostic. For larvae, process error (represented as standard deviations) is reduced from the Static (3) model only when daily weather covariates are in the model (Figure 1.5). Process error for larvae are estimated at range of 6 larvae/450^2m/day at Tea to 10 larvae/450^2m/day at Henry. The model with the most error was Mice Est. (4) at Green with an error of 22 larvae/450^2m/day. Model performance for larvae improved with the addition of the dormant state, where the three-stage model was the most skillful only 15% and 2% of the time for non-zero and zero counts, respectively.

Including the fourth stage to represent dormant nymphs reduced process error over the 3-stage model, and all 4-stage model process errors were similar. For example, the Static (3) model applied at the Green site estimated the error in nymph predictions to be 3.9 nymphs/450^2m/day, whereas all other models at that site had a nearly 10-fold decrease in error (0.4 nymphs/450^2m/day) (Figure 1.5).

Dormant nymph error was consistent within sites, where the models with daily weather have more error. For example, at Green, the error for the Weather and Mice (4) model is 8.5 dormant nymphs/450^2m/day, but for the Mice MNA (4) model the error was

6.3 dormant nymphs/450^{2}m. The other two sites follow the same pattern, with Tea having the most error in dormant nymphs. Adult process error was consistent within sites. All models at Henry showed adult process error to be between 1.73-1.87 adults/450^{2}m/day, Green was between 2.2-3.1 adults/450^{2}m/day, and Tea at 3.3-35 adults/450^{2}m/day.

Figure 1.5 Model process error

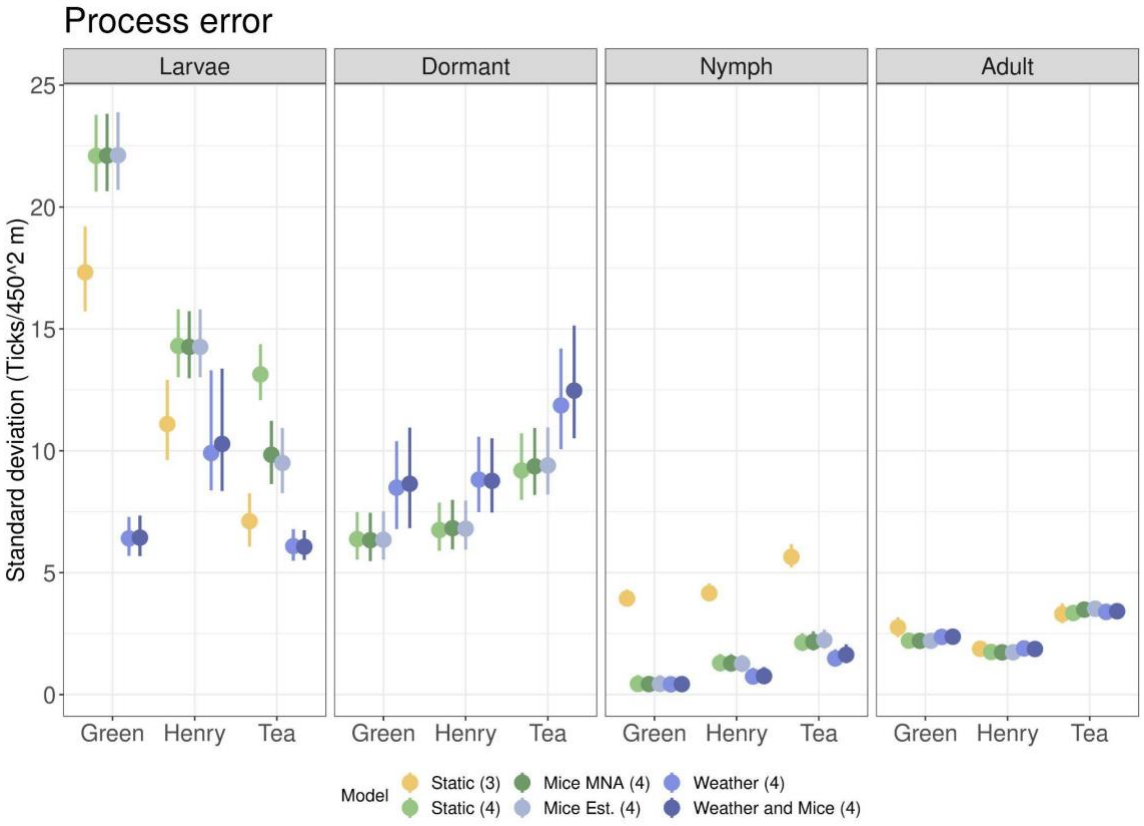

Figure 1.5: Process error distributions, represented as standard deviations. Facet columns are each life stage in the stage-structured matrix, the x-axis is the site a specific model (color) was calibrated. Whiskers are the 90% credible interval of the posterior, and points are the median value of process error. The dormant stage is not modeled in the Static (3) model.

Fecundity

We estimated variable fecundity rates among models and across sites (Figure S1.6). For example, the Mice MNA (4) model estimated a median fecundity rate (larvae/adult/day) of 0.88 (90% CI 0.06 - 5.04) at Green, 23.55 (90% CI 17.67 - 31.27) at Tea, and 32.15 (90% CI 24.45 - 41.49) at Henry. In general, the models that use weather to drive tick survival estimate a higher reproductive rate than other model formulations. For example, the Weather and Mice (4) model estimated a reproductive rate of 41.60 (90% CI 30.49 - 54.76) at Green, 44.48 (90% CI 33.79 - 57.35) at Tea, and 54.44 (90% CI 34.45 - 72.00) at Henry. For reference the prior on fecundity was set to a mean of 30 and a standard deviation of 10, which translates to a 90% CI between 13.83 and 46.82.

Population Growth Rate

Estimates of population growth rates were similar across all models and there was significant interannual variation (Figure 1.6). Over the 11 years of the study, population growth tends to increase across all three sites. Specifically, the tick population was growing (estimated by median population growth rate) in 1999 - 2000, and between 2000 - 2004. The three sites show similar annual trends in growth rate, except for years 1999 and 2005. In 1999, Green and Tea have growing tick populations while Henry is declining, and in 2005 Green and Tea have declining tick populations while Henry is growing.

Figure 1.6 Population growth rate

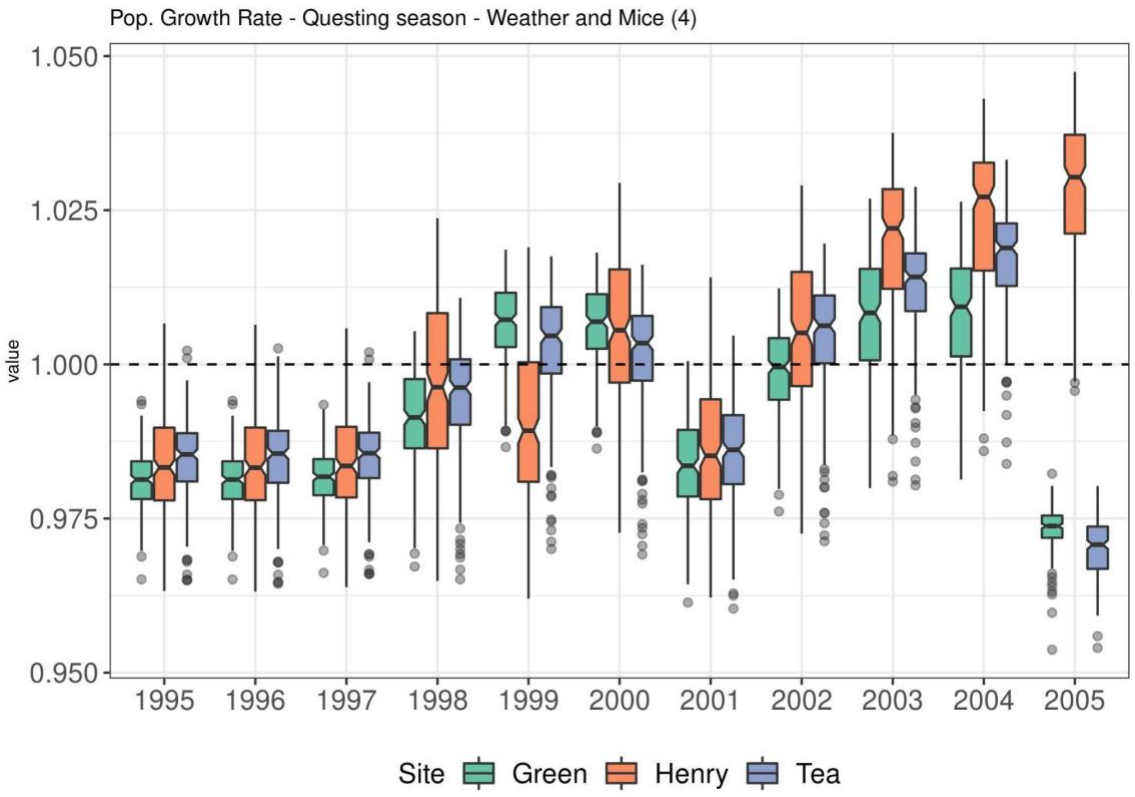

Figure 1.6: Population growth simulated during the questing season each year for the Weather and Mice (4) model at the three Cary field sites. The horizontal dashed line represents the threshold value of one (above the population is growing, below declining). Boxplots were drawn with 2000 simulations.

Model Assessment

Models were assessed by running one-step-ahead predictions. First, we need to distinguish between predictions made during the phenological period for each life stage and predictions made during other periods of the year.

Here, we make the simplifying assumption that predictions during the questing period are for non-zero counts, while predictions during the dormancy period are for zeros. Zero count observations can occur during questing periods, but over the 11-year period the distinguishment between zero and non-zero should give us an accurate estimate of how well each model predicts during questing and non-questing periods.

Two of the six models included weather, and they made the best one-step-ahead predictions (according to CRPS) for larval abundance 76% of the time for non-zero counts and 98% of the time when zero larvae were observed (Figure 1.7). The inclusion of daily weather variables made for better nymphal predictions more than half the time (51%) for non-zero counts, and for almost (98%) every zero count. Weather did not improve predictions of the adult ticks, where these models were the best performing for adults only 33% of the time for non-zero counts and 30% of the time for zero adult counts.

The 3-stage model was the most skillful at predicting nymphs only 2% and 0% of the time for non-zero and zero counts, respectively (Figure 1.7).

The effect that mouse abundance has on model performance is different between life stages. For larvae the models with mice only (estimated or MNA), made the best non-zero predictions 6% of the time compared to 26% for nymphs, and 19% for adults (Figure 1.7). However, if we include the model with that has both mice and weather, the three models with mice account for the best non-zero predictions 54%, 78%, and 34% of the time for larvae, nymphs, and adults respectively. If all models were equally skillful, we

would expect any combination of three (out of a total of six) models to be best roughly 50% of the time.

Figure 1.7 Model performance summary

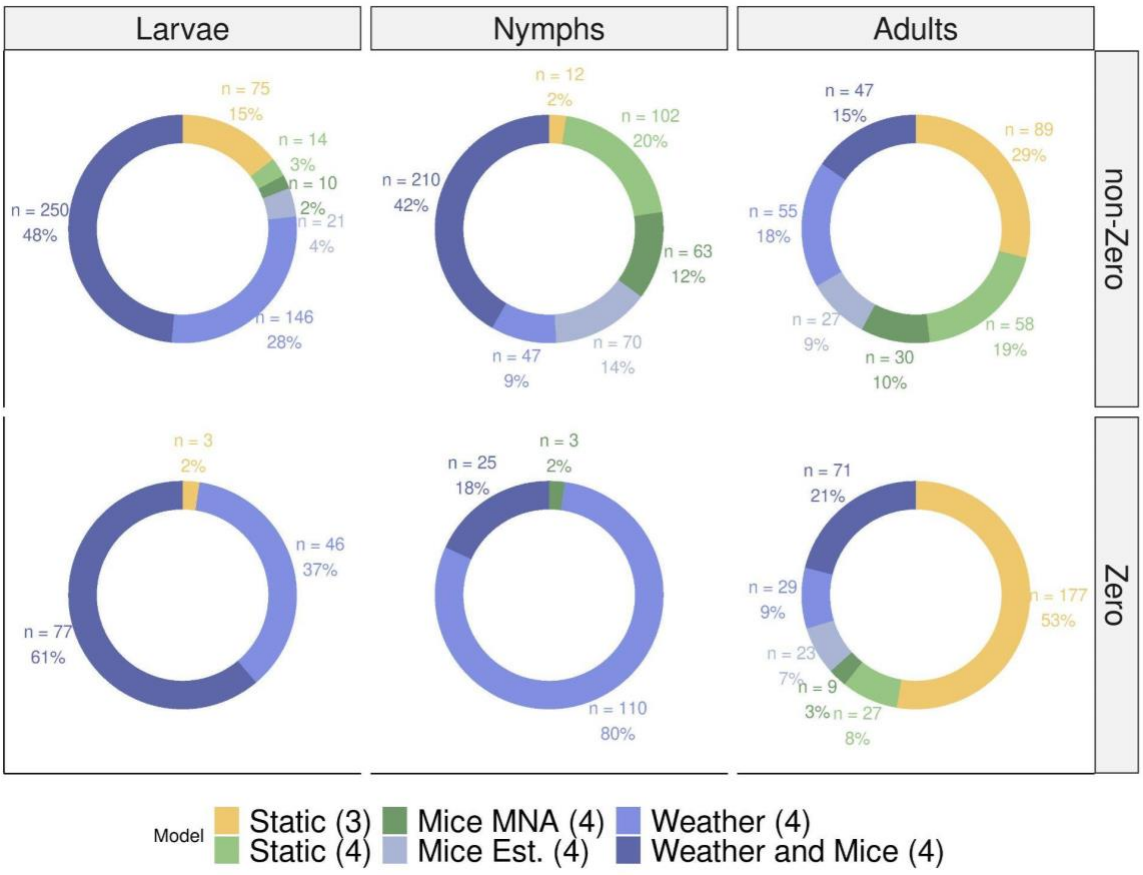

Figure 1.7: The relative performance of each model at predicting non-zero (top row) and zero (bottom row) observations for each life stage. Non-zero observations are during each life stage's questing period, and zero observations are during each life stage's dormancy period. n is the number of times a specific model had the best skill score, percent values are how often a specific model was most skillful relative to others.

CRPS scores, in general, scale with observations so that as the number of ticks observed increases prediction skill decreases. This pattern is most evident for larvae (Figure S1.8) and adults (Figure S1.9), the exception being larvae scores from the Weather (4) model, where within-site CRPS is higher than the across-site CRPS, on average.

The pattern for CRPS as nymph observations increase is different from that of larvae and adults. Most notably is that the Static (3) and Weather (4) model scores increase (i.e. get worse) faster than the other models (Figure 8). In contrast, the Static (4), Mice MNA (4), Mice Est. (4), and Weather and Mice (4) models all have relatively similar trends, in that CRPS gets slightly worse as observations increase. Of these last four models, the Weather and Mice (4) model has the biggest difference in score between across-site and within-site prediction skill, where within-site predictions are better on average (Figure 1.8).

Variance Partitioning

We partitioned the variance for each model and each life stage into the component parts that make up the total uncertainty (initial conditions, parameter, driver, and process error). Each life stage shows the same pattern in relative variance through time, where during the questing period the prediction variance is dominated by something other than process uncertainty, the total variance is larger during questing periods than during the dormant periods, and the relative proportion of uncertainty due to mouse estimates is small.

Figure 1.8 Nymph prediction skill

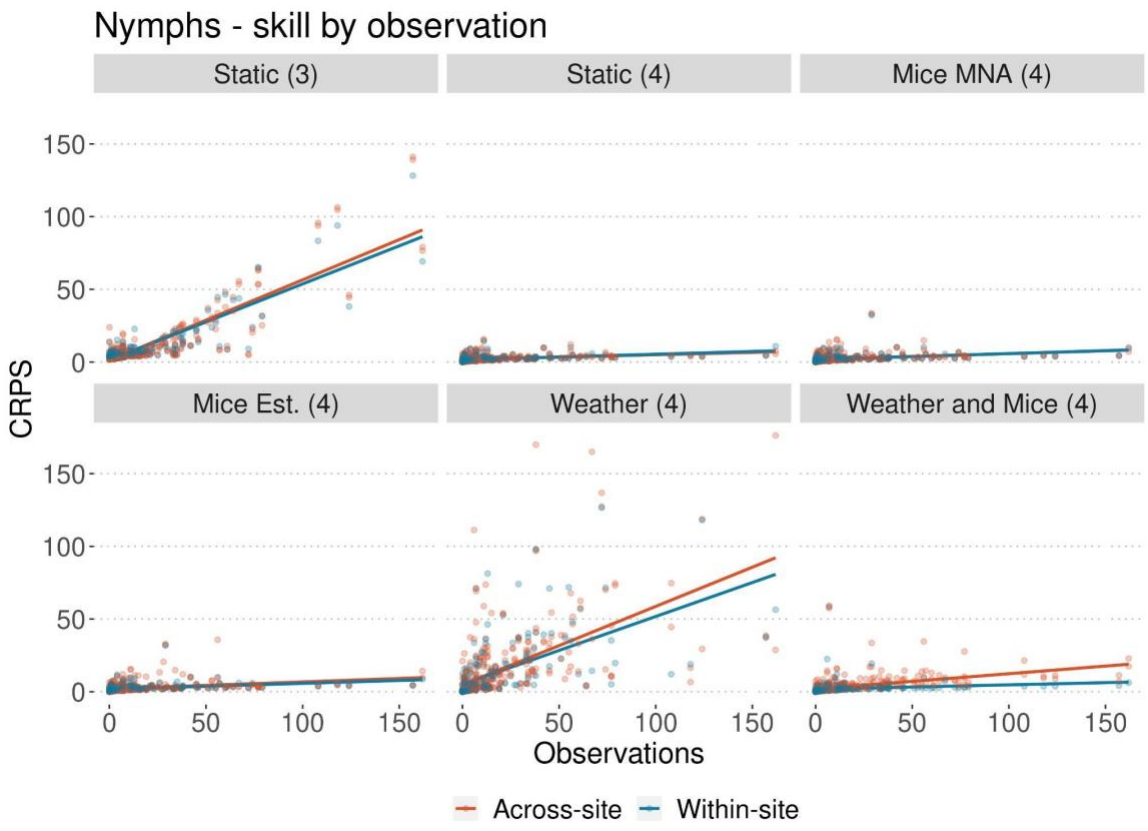

Figure 1.8: Trends in CRPS as observations increase. Each facet represents the performance of a single model. Blue corresponds to the scores for the within-site predictions, red to the across-site predictions. Lines are linear trends for each type of prediction.

For the larvae, initial condition uncertainty begins to make up about half of the total variance during their questing period for all models. In addition, the models that use weather have the most parameter uncertainty (Figures 1.9, S1.8, S.19).

Nymphal prediction variance is dominated by process error in the Static (3) model, and initial condition uncertainty in all other models (Figure 1.9). Additionally, the addition of the dormant stage between questing larvae and questing nymphs reduced the relative proportion of process uncertainty in nymph predictions drastically, from being dominant (>95%) to negligible (<5%). Excluding the Weather (4) model, total prediction variance decreased by a factor of 4 when including dormant nymphs in the model structure. Like the larvae, the Weather (4) model has the most parameter uncertainty. Additionally, late-season predictions are mostly made up of process uncertainty.

Adult prediction variance is low in the mid-season where it is dominated by process uncertainty. All models show that the beginning of the season is mostly comprised of parameter uncertainty, followed by initial condition uncertainty (Figure S1.9).

Discussion

This study quantitatively explored a series of stage-structured matrix models to predict all life stages of *Ixodes scapularis*, the primary vector of Lyme disease in North America. We found that including the dormant stage in the matrix between questing larvae and questing nymphs dramatically improved the predictability of nymphs (Figures 1.7 & 1.8), the life stage most responsible for Lyme disease cases in humans. We showed that over the 11 years of this study, the growth rate of the tick populations at Cary was variable from year-to-year and generally increasing, with periods of decline followed by a prolonged period of growth (Figure 1.6).

Figure 1.9 Nymphal prediction variance partitioning

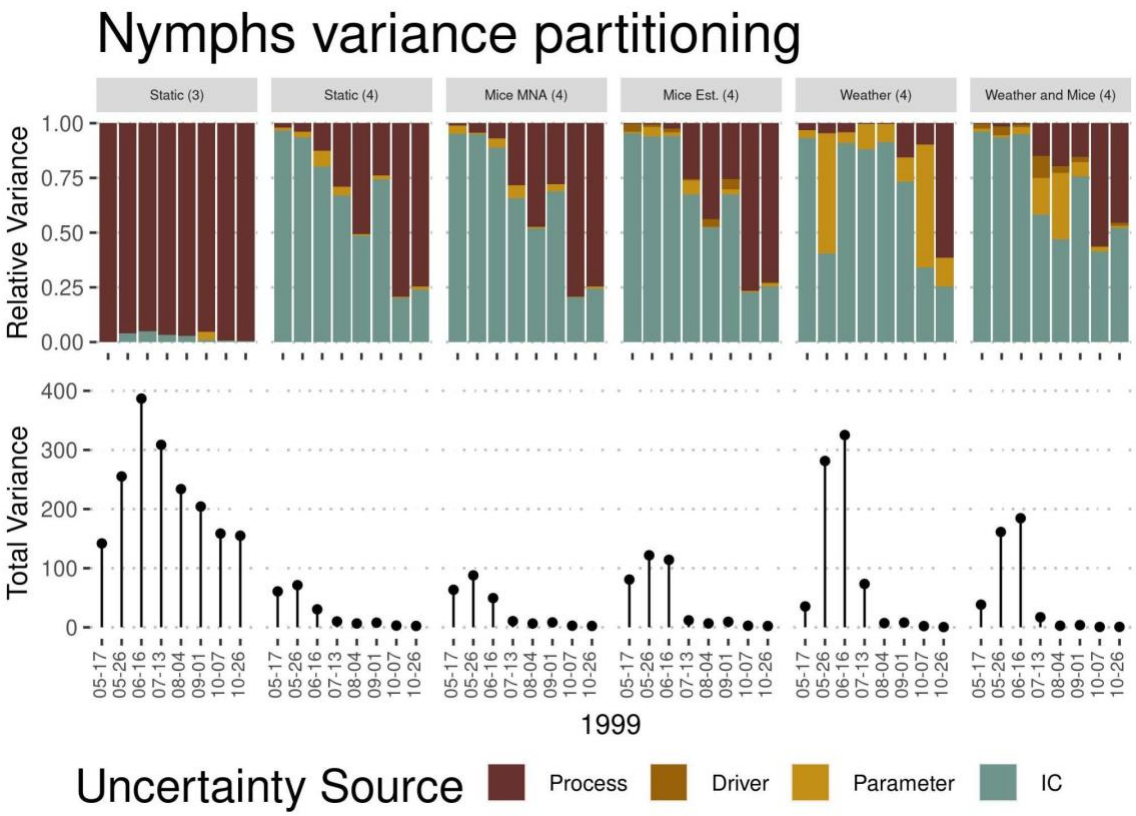

Figure 1.9: Variance partitioning for nymph predictions at Tea in 1999. The top row shows the relative proportion of the total variance that is made up of either process error (model structural uncertainty), driver error (from level 2 mouse population model, only present in Mice Est. (4) and Weather and Mice (4) models), parameter uncertainty (from parameter distributions), and initial condition uncertainty (errors in the latent state). The bottom row shows the total amount of variance in the prediction.

Both of these findings are relevant because quantitative predictions for nymphs and the trajectory of the population as a whole can aid in our understanding of Lyme disease risk (LaDeau et al., 2011; Kilpatrick et al., 2017). Additionally, an estimate of

population growth helps provide managers with a target for eradication efforts, an important goal of ecological forecasting (Galloway et al., 2021; Davis et al., 2022).

We also quantified the role of mice in constraining the transitions from larvae-to-nymph and nymph-to-adult, as well as the importance of key environmental drivers of tick survival. For nymphs, the model with both weather and with mice was the most skillful at predicting non-zero counts. This concurs with previous studies that show mice play a crucial role in the ecology of *I. scapularis* and can improve predictions of nymphs (Ostfeld et al., 2001, 2006). Furthermore, we do this in an ecologically relevant way, which has to do with the interplay between the dormant nymph stage and the negative effect of instantaneous mouse abundance. Nymphs are essentially held in the dormant stage until questing when they emerge as a single cohort, and then mice act as a removal mechanism from the questing state.

This explains the tendency of the Weather (4) model to overestimate nymphal predictions, as the most prominent effect of mice was on the nymph to adult transition (removing nymphs). Furthermore, incorporating the uncertainty in mouse estimates added little to the total variance of tick predictions.

For larvae and nymphs, weather had a significant effect on survival. Our results agree with (Dobson et al., 2011; Brunner et al., 2012) on daily density-independent mortality rates (explicit or implicit) of the questing states, with estimated monthly survival rates between 0.4-0.45 and 0.48-0.52 for larvae and nymphs. Our results also agree with (Ginsberg et al., 2014, 2017) that larvae survival drops as relative humidity (RH) decreases, and that average RH is not significant in predicting nymphs (Berger et

al., 2014). Out RH results contrast with Ginsberg (2014) which showed that high RH increases nymph survival. This could be due to the discrepancy between monitoring ticks from the field and monitoring ticks in the lab. Our model also uses precipitation as a daily driver of survival, and nymphs were estimated to have a positive association with precipitation (Figure 1.4). The precipitation effect could be overpowering the effect of RH, as days with precipitation will have higher RH.

Our model is similar to that of (Dobson et al., 2011) in that our model runs on a daily basis and incorporates biological processes into the model. However, our model is different in a few respects. For one, we model survival, transition, development, and reproduction within the daily transition matrix, which allowed us to estimate the population growth rate. Additionally, we were able to estimate the effect of host abundance, which allowed us to recover tick dynamics more effectively at other sites using their respective mouse populations. However, the model we present here combines host contact rate, feeding success, and development rate into one parameter (i.e. larvae-to-nymph transition), something that Dobson (2011) partitioned.

While we were able to recover tick observations of larvae and nymphs, we found it more difficult to accurately predict questing adults. All models considered were best some of the time (Figure 1.7). One factor contributing to this greater error in adult predictions is the lack of a dormant stage between questing nymphs and questing adults. While modeling this stage would be developmentally more appropriate (we tried to fit such a model but were unable to reach convergence), nymphs do feed, molt, and emerge as adults in the same year (Ostfeld, Hazler, et al., 1996). So our model formulation is not

unrealistic. Similarly, there is not a dormant stage between questing adults and questing larvae (i.e. an egg stage), but we were able to recover the larvae data. Also relevant to the adults is the smaller count numbers, and thus the potentially greater impact of sampling error and population stochasticity.

This work shows that a stage-structured model for *I. scapularis* is an appropriate formulation to describe the ecology of this important tick-borne disease vector. Especially when it comes to larvae and nymphs. Adult prediction accuracy varied, as such, we recommend future work focus on further constraining the adult stage. This could be done by using different drivers for survival or incorporating reproductive hosts in the fecundity term or adding a latent state in-between questing nymphs and questing adults. The penalized regression formulation on survival would make this straightforward.

Lastly, variance partitioning analysis shows interesting trends in both total and relative variance. For all life stages, total predictive variance tends to increase during the questing period. This was expected, as the model explicitly does not allow for stage transitions when not in a life stage's phenological (questing) window, meaning that the model is at stasis for most periods of the year. It was also expected, then, that during these non-questing periods most of the variance is comprised of process error because transition parameters are set to zero. Interestingly, the relative contribution of process error generally decreased during questing periods. This is either because process error is constant across all time while the other errors fluctuate, or during questing periods all error increases more rapidly than the other sources.

This means that the major obstacle to constraining predictions of peak tick abundance is mostly due to the uncertainty in the initial state. This has important implications for large-scale monitoring programs such as the National Ecological Observatory Network (NEON), which might have to make budgetary decisions about when and where to sample. We show that for predicting nymphs, the most important life stage of this species, sampling efforts should be directed towards monitoring nymphs.

CHAPTER TWO

A proof of concept for iterative ecological forecasts for the vector of Lyme disease (*Ixodes scapularis*)

Introduction

The expansion of black-legged tick (*Ixodes scapularis*) populations across North America (Sonenshine, 2018), coupled with the concurrent rise in Lyme disease incidence (Sharareh et al., 2019) necessitates more accurate and timely predictive models to inform stakeholders of the risk of Lyme disease (Ogden et al., 2020). There are numerous studies that show the relationship between peak density of the nymphal life stage of *I. scapularis* and Lyme disease incidence (Mather et al., 1996; Nicholson & Mather, 1996; Stafford et al., 1998; Pepin et al., 2012; Little et al., 2019). Therefore, land managers, public health officials, and outdoor recreational users could potentially plan their management actions or outdoor activities around the timing of peak tick abundance.

Unsurprisingly, there is a growing call for forecasts that can predict tick populations over space and time (Kilpatrick et al., 2017), with a focus on the nymphal stage. The emphasis on nymphal predictions stems from their competence as vectors of the etiological agent of Lyme disease (*Borrelia burgdorferi*) to humans (Stanek et al., 2012), their phenology is concurrent with peak human outdoor activity (Barbour & Fish, 1993; Pepin et al., 2012), and their small size makes them hard to identify and remove (L. Eisen & Eisen, 2016).

Therefore, the focus of this manuscript is to evaluate a proof of concept for iteratively forecasting the population dynamics of *I. scapularis* at the Cary Institute of Ecosystem Studies (Cary), located in Millbrook, NY. This evaluation is over a time period (2006-2021) where Lyme disease cases have increased dramatically in the US and are for a location in the northeastern US where Lyme disease is endemic (Diuk-Wasser et al., 2006). Furthermore, we place an emphasis on evaluating nymphal forecasts due to their inflated role in Lyme disease ecology.

For this proof of concept, we use the 4-stage process models that were previously calibrated in Chapter 1. The four stages are questing larvae, dormant nymphs, questing nymphs, and questing adults. The data provide information on the questing individuals only, meaning the dormant nymphs are in a completely latent state. Including dormant nymphs in the model drastically reduces model process error and increases the predictive capacity of questing nymphs (Chapter 1). We use two of the models from chapter one; one where weather drives the daily survival of each life stage with four daily weather variables; maximum temperature, maximum relative humidity, minimum relative humidity, and precipitation. The second builds from this model to also include the minimum number of mice alive (MNA) at each site to constrain the transitions from larvae to nymph and nymph to adult.

Furthermore, we defined phenology by setting transition parameters into the questing states to zero during the non-questing periods of the year (equation S1.7). For each life stage, the questing period was defined by cumulative growing degree days above zero degrees Celsius; i.e. questing only occurs if the cumulative growing degree

days were within the appropriate window for a given life stage. Therefore, our forecasting model explicitly defines phenology and uses current weather conditions to determine tick survival.

At its core, ecological forecasting is the *process* a forecaster uses to make predictions, and it is within the community standards and best practices of ecological forecasting we evaluate our proof of concept. Specifically, we focus on evaluating forecast accuracy and uncertainty, identifying end-users, iterative predictions, and using a null model (Dietze et al., 2018; Lewis et al., 2022).

Iterative predictions are central to the ecological forecasting process for several reasons. First, we can evaluate how accurate and precise our forecasts are by iteratively challenging the model with data, and making out-of-sample predictions (White et al., 2018; Taylor & White, 2020). This is particularly important for our use case, as we are using a process-based model. Our model represents certain hypotheses about how this tick-borne disease system works (Chapter 1), which means each iterative prediction represents a new quantitative evaluation of our current understanding of the system. Furthermore, under the correct data assimilation scheme, the model itself should be able to adapt through time, becoming more skillful with each iteration (Niu et al., 2014).

At each iteration, we evaluate the process model against the performance of a null model. Our null model is analogous to a climatology model, except here we use the historical mean tick abundance as a basis for the null prediction. This is an appropriate null model because of the consistent phenology from year to year in each life stage. For example, in the northeast US, nymphs begin questing in the late spring, peak in early

summer, and go dormant by late summer (Levi et al., 2015). While this pattern is consistent from year to year, the interannual variability in magnitude of questing nymphs varies substantially (Ostfeld, Hazler, et al., 1996). Therefore, comparing our models to this null model will allow us to determine if our models can predict known phenology and out-perform average annual abundance. A skillful forecast is one that has a lower continuous ranked probability score (CRPS) or lower root mean squared error (RMSE) than the null model.

As phenology is explicitly defined in our 4-stage process model (Chapter 1), we expect to have at least equal forecast accuracy at predicting zero counts (the non-questing periods for each life stage) as the null model, and we expect to out-perform the null model at forecasting peaks (the maximum count each year for each life stage). We also expect the forecast model to have larger forecast variance than the null model, because the forecast model propagates uncertainty while the null model does not. This added uncertainty may cause our forecasts to be less skillful than the null model, especially at dormant periods of the year. In this case, our models may be just as accurate as the null model, and the null model will be an overconfident forecast because it does not have propagated uncertainty.

Quantifying and partitioning forecast uncertainty is a pillar of ecological forecasting (Dietze, 2017). Additionally, uncertainty (usually paired with accuracy) is a key component in many proper scoring rules (Gneiting & Raftery, 2007), which are used as a measure of forecast skill. Uncertainty can arise from initial conditions, covariate data, parameter distributions, and the model structure itself (Dietze, 2017). Here, we

evaluate the role of the initial condition and covariate data uncertainty as it relates to forecasting skill.

The initial conditions for the forecasts are built by blending the observed tick density and the forecast for tick density, which occurs during the analysis step of the data assimilation (Dietze, 2017). This means the magnitude of initial condition uncertainty is in part due to the tick data itself. The tick observations at Cary are generated by conducting tick drags during the peak questing period of each life stage each year. Of the life stages, it is the larval data that has the most variability.

This variability is due, in part, to the behavior of adult female ticks, their hosts, and their offspring. After an adult female *I. scapularis* tick successfully feeds and mates, she drops off her host and lays eggs. Where this occurs is wherever the host happens to be at the time. Adult ticks tend to use larger hosts, such as deer, compared to juvenile ticks, who primarily attach to small vertebrates (Gray, J.S., 1998). Larger hosts tend to have larger home ranges that are both more heterogenous on the landscape and the individuals are more social than hosts for juvenile ticks (McNab, 1963). This means that the hosts, and subsequently tick egg sacks laid by female adult ticks, are clustered in space randomly (Ostfeld et al., 1996).

Therefore, successfully capturing larvae during their peak is almost random, as the observer has to encounter one or more of these clusters, and then the larvae have to attach to the drag cloth. One hypothesis is that removing these observations will have little effect on forecast accuracy and precision, as the heterogeneity in larval observations is large enough that the observations do not add information.

If this hypothesis is correct, future observation efforts could be shifted to more intensive sampling during the nymphal peak, which would be more informative as to actual disease risk as nymphs are the primary vector of *B. burgdorferi*. The counter hypothesis is that data collected during the larval questing season helps constrain forecasts for either abundance or phenology. As such, we set out to quantify the role of observations during the larval questing period by running parallel hindcasts with observations from the larval questing periods removed (Figure 2.1).

The other source of uncertainty we explore in this framework is that of covariate, or driver, data. Our process-based model uses current daily weather to constrain tick survival, which means we need a forecast of daily weather to forecast tick populations. In an effort to produce forecasts at both short to intermediate time scales, we quantify the impact of using the North American Multi-model Ensemble (NMME) (Kirtman et al., 2014). NMME is a seasonal weather forecast product with a 365-day horizon across ten ensemble members. Incorporating and estimating the uncertainty across ensembles enables us to propagate driver uncertainty into the forecast (Dietze, 2017), and to quantify the effect that this uncertainty has on the uncertainty in the tick forecast. We can quantify this effect by running parallel hindcasts.

The first of these hindcasts has zero driver uncertainty, using observed weather from the Cary meteorological station (Figure 2.1), and the second assimilates NMME. We hypothesize that incorporating this product will make the tick forecasts more uncertain (i.e. more total forecast variance) because we account for the variance across NMME ensembles. Consequently, we hypothesize that the tick forecast skill, as measured

Figure 2.1 Forecast timeline

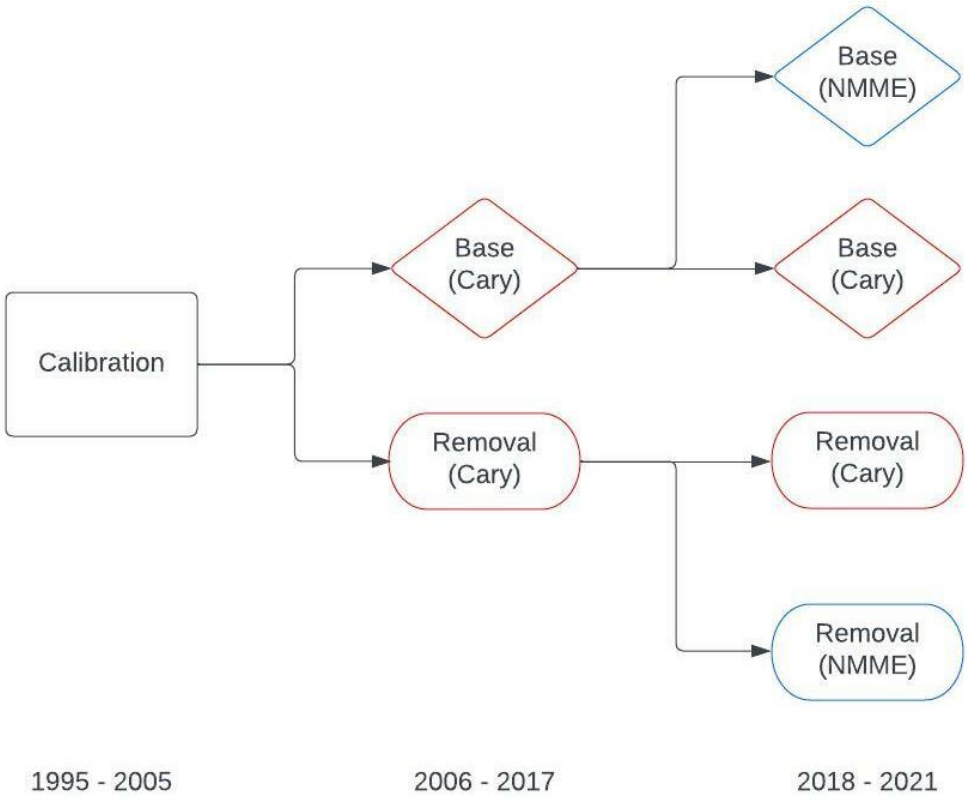

Figure 2.1 Timeline and conceptual flowchart for hindcasts. The model was calibrated from 1995 to 2005. Hindcasts started in 2006, where we ran the base hindcast (diamond) and the hindcast with peak larval data removed (ovals) until 2017, both with weather data from Cary (red). In 2018 the hindcasts from 2006 continue, where versions of each with NMME (blue) ran from 2018 to 2021.

by the Continuous Ranked Probability Score (CRPS) or root mean squared error (RMSE), will decay as the horizon increases. However, as the two forecasts differ only in their weather data source, patterns in forecast accuracy relative to the forecast horizon should be the same.

End-users of these forecasts, process-based or otherwise, will need them to be made for both short (days to weeks) and intermediate (seasonal to yearly) time horizons. The questing period for each life stage can be measured in terms of weeks (Levi et al., 2015), meaning forecasts could predict the onset, magnitude, and duration of tick activity (Ogden et al., 2005). Forecasts could then be used by land managers as part of their adaptive management plans to include activities that reduce tick density or tick survival such as invasive species removal (Allan et al., 2010), host-specific measures such as culling or fencing (Tsao et al., 2021), or prescribed burning (Gleim et al., 2014).

Within this framework, we set out to validate an iterative Bayesian forecast and data assimilation scheme and assess the sensitivity of these forecasts to common data limitation issues (e.g., weather forecast uncertainty, field sampling strategies). The two aspects of the data assimilation we explore are the effectiveness of the initial condition updates, and the second is on tick demographic parameter distributions and how they change over time.

In an appropriately specified model and data assimilation combination, we expect to see a weighted averaging of data and forecast distributions, where if the forecast is correct, then equal weight is placed on the forecast and data. If the forecast is wrong or too uncertain, we expect there to be more weight placed on the data. On the other hand, if a model is over-specified, we would expect the data assimilation to place more weight on the forecast, even if that forecast is wrong (Niu et al., 2014; Dietze, 2017).

Another validation of the data assimilation is on parameter distributions after data assimilation occurs. For each iteration, the parameter posterior distributions become the

priors for the next forecast, and we expect these to update over time and lead to an increase in forecast skill.

Methods

Data and Site description

Three field sites at the Cary Institute of Ecosystem Studies (Green, Henry, Tea) were used for tick, mouse, and weather observations. They are more than 100m apart centered around 41.7851N, -73.7338W. All sites are 2.25 hectares and are post-agricultural oak-dominated stands (Ostfeld et al., 2001).

Tick Data

Briefly, tick populations (*I. scapularis*) are derived from tick drags conducted at the Cary Institute of Ecosystem Studies in Millbrook, NY. A tick drag consists of pulling a 1 square meter cotton cloth along the ground on three randomly chosen transects, for a total of 450 square meters sampled per site. Ticks were counted every 30 meters. Drags were conducted every three to four weeks. Tick drags did not occur in the winter. For more complete descriptions of the long-term tick monitoring at Cary see (Brunner & Ostfeld, 2008; Ostfeld et al., 2001; Schauber et al., 2005)**.**

Cary Meteorology

Meteorology was collected from Cary's environmental monitoring program. Precipitation was collected with a Belfort Instrument Universal Recording Rain Gauge

Series 5-780 located three meters above the ground from 1995–July 2007, and using a Geonor Precipitation Gauge Model T-200B from July 2007–2021. Relative humidity was collected with a Phys Chem Corp. PCRC-11 or PCRC-55 (1995–1997) and a Campbell Scientific, Inc. HMP45C (1997–2021), and temperature was collected with a Campbell Scientific model 107 or 207 (1995–1998) and a Campbell Scientific, Inc. HMP45C (1998–2021). See (Kelly, 2020) for a complete description of Cary's environmental monitoring program.

For model calibration in Chapter 1, we centered and standardized the weather covariates (daily maximum temperature, daily maximum relative humidity, daily minimum relative humidity, daily total precipitation) by their respective means and standard deviations during the calibration period (1995–2005). Therefore, coefficients estimated in Chapter 1, and used as the initial parameter distributions during the hindcast period, represent the magnitude a weather variable has on tick survival as it departs from its historical mean. As such, we centered and standardized the observed weather variables during the hindcast period to the calibration period historical mean and standard deviations.

The tick data for this work is a direct continuation of the tick drag data used in Chapter 1, and has been described in detail elsewhere (Brunner et al., 2012; Brunner & Ostfeld, 2008; Ostfeld et al., 2006).

North American Multi-model Ensemble

As one of our goals with this manuscript is to investigate the feasibility of season-long forecasts, we chose to assimilate the North American Multi-model Ensemble (NMME) as our weather driver. Briefly, NMME is a year-long weather forecasting product produced monthly that has a one-degree resolution at a 6-hour time step with 10 ensemble members. See (Kirtman et al., 2014) for a complete description.

For each ensemble member on each day, we found the daily maximum temperature, maximum and minimum relative humidity, and total precipitation. Before data assimilation, each NMME variable was standardized to the historical mean and standard deviation as described above. We then applied a bias correction to the historical mean for all four weather variables. For temperature and minimum and maximum relative humidity, we calculated the mean (annual) for each ensemble of each variable, and calculated the difference between this and the calibration period observed means for each variable. This bias was added to each day of each variable of each ensemble for NMME. An example of the bias correction is in supplementary Figure S2.1.

The precipitation forecasts needed a different adjustment, as most days were predicted to have greater than zero precipitation, forecasting a constant drizzle throughout the year. To correct for this, we found the average annual cumulative precipitation at Cary over the calibration period (1134.16 mm). NMME has a horizon of a year, so we calculated the bias between the cumulative precipitation for each NMME ensemble and the Cary average annual cumulative precipitation, divided the bias by 365, and then

added this daily bias to each day in the NMME ensemble.

For each day of the tick forecast, we used an error in variables approach to estimate the true value for each weather variable and their associated uncertainties for each day. We used a multivariate censorship model to account for the theoretical bounds of relative humidity and precipitation, which are bound between 0 and 1 and bound at zero, respectively. Temperature was not censored.

$$\mu_t \sim MVN(\mu_0, \Sigma) \quad [1]$$

$$\Omega_t \sim wishart(\Lambda, k) \quad [2]$$

$$Yc_t \sim MVN(\mu_t, \Omega_t) \quad [3]$$

$$Yi_{t,j} \sim constraint(min_j \leq Yc_{t,j} \leq max_j) \quad [4]$$

Where on day *t*, μ is the vector of estimated means, **Ω** is the estimated precision matrix, *Yc* is the data from NMME, where any ensemble member that is censored (i.e. outside the theoretical bounds) was set to the boundary, and *Yi* is the indicator matrix indicating which ensemble members are censored. The priors for μ_t and $\mathbf{\Omega}_t$ were set as follows: μ_0 is a vector of zeros, **Σ** and ***Λ*** were set to a *j x j* diagonal matrix with 0.01, and *k* was set to *j+1,* where *j* is the number of weather variables). *min* and *max* are vectors of the theoretical minimum and maximum values for each weather variable. Where there

was no constraint (both temperature bounds and precipitation maxima), *min* and *max* were set to -1E4 and 1E4, respectively.

Cumulative growing degree days were calculated for each temperature ensemble member with a base of 10°C. We then used the mean (μ) and precision (τ) across ensemble members to estimate daily cumulative growing degree days with error:

$$cgdd_t \sim N(\mu_t, \tau_t) \quad [5]$$

The hindcasts that use NMME have a horizon that is slightly less than 365 days because NMME, which has a one-year horizon, is produced once a month. For example, a hindcast starting on April 15th will use the NMME forecast starting on April 1st of that year, meaning the end of the hindcast is March 31st of the following year, giving us a horizon of 350 days.

Statistical Framework

The hindcast ran from 2006 to 2021. Data processing and analysis were done in R v4.0.2 (R Core Team, 2020), and hindcast simulations were carried out in NIMBLE (de Valpine et al., 2017, 2022). When using the observed weather data from Cary, the hindcast horizon was 365 days. This process continued throughout the hindcasting period (2006 – 2021). Starting with the first state observations of 2018, we initialized a parallel hindcast that uses a seasonal forecasting product: the North American Multi-model Ensemble (Kirtman et al., 2014).

For both ticks and mice, the workflow for the hindcast is as follows: the first hindcast in 2006 was initialized using the historical mean abundance from the calibration period (1995 – 2005) for the month of May, and ran for 365 days. The next hindcast starts on the day of the next observation, assimilating the observation into the model, using the hindcasted estimate of ticks on the day of the observation as the initial condition. Parameter distributions were also estimated, using the previous hindcast's parameter distributions as priors (or in case of the first hindcast, the parameter distributions from the calibrated model). Therefore, the data assimilation scheme does the analysis and forecast step together (Dietze, 2017), and is essentially Bayesian updating.

The tick hindcasts were run in this way within-site, where model parameters were used to hindcast ticks at the site the parameters were calibrated, as well as across-site, where parameters were used to predict ticks at sites they were not calibrated.

Tick Forecast Model

We used the four-stage model from chapter one to simulate tick population dynamics. There were a few modifications made to the model calibrated in Chapter 1 to increase computational efficiency. First, the prediction step is done dynamically, where we predict tick populations every day from the day previous, instead of across days as done in Chapter 1 :

$$\overrightarrow{ex}_t = \boldsymbol{A}_{t-1}\overrightarrow{x_{t-1}} \quad [6]$$

Where on day *t-1*, **A** is the daily transition matrix, and *x* is the estimated latent state vector, which are used to predict the next days (*t*) expected tick population *ex*. For the hindcasts that use NMME, there is the added step of estimating the latent NMME variables as described in section 2.1.

To estimate shape (α) and rate (β) parameters for the informative inverse gamma priors on process error, we used the mean (μ) and variance (σ) from the posterior of the previous forecast using the method of moments (Llera & Beckmann, 2016):

$$\alpha = \frac{\mu^2}{\sigma} + 2 \quad [7]$$

$$\beta = \mu * (\frac{\mu^2}{\sigma} + 1) \quad [8]$$

All parameters in the model (survival, transition, weather and mouse effect coefficients, process error), except reproduction, were updated at each data assimilation step. Reproduction was held constant to help with convergence.

Data Removal Experiments

For the data removal experiment, we ran the hindcast without any larval data included, but predicted larval densities anyway. This means we set the value of all larval observations to NA so no information was provided during data assimilation. The other two questing states were still present and should help constrain the unknown larvae.

Null Model

Due to the consistent annual questing period of each life stage, we used a generalized additive model (GAM) smoothed over day of year for the null forecast. This will provide the average tick abundance for any day of year, including days when ticks are not sampled.

$$forecast_i = gam(y_i \sim s(day\ of\ year), family = "poisson") \quad [9]$$

Where the forecast on any given day of year for life stage *i* is a smoothed function over the day of year given the observed counts *y* for life stage *i*, using a Poisson observation model.

The null forecast itself was generated iteratively. For every new observation, a new null forecast was generated, so the number of observed counts used to smooth over increases throughout the hindcasting period.

Results

Removing larval data had little to no effect on forecast skill for nymphs and adults (Table 2.1). For larvae, models that assimilated weather from the Cary meteorological station had a better CRPS of four points when larval data was included for short term forecasts. For the NMME models, including larval data made the forecasts worse by a score of 10 when mice where included. For intermediate forecasts, average scores were

nearly identical when comparing across the larvae/no-larvae experiments for all life stages (Table 2.1).

Table 2.1 Average CRPS for each modeling scenario

Scale	Life Stage	Weather Source	Mice		No mice	
			Larvae	No Larvae	Larvae	No Larvae
Short	Larvae	CARY	71.72	75.02	69.87	72.47
		NMME	53.23	43.36	45.69	45.23
	Nymphs	CARY	7.87	7.50	7.50	7.48
		NMME	10.07	9.09	10.17	10.39
	Adults	CARY	3.04	2.95	3.06	3.11
		NMME	3.10	3.06	2.95	3.00
Intermediate	Larvae	CARY	116.57	116.29	117.83	117.20
		NMME	51.21	50.16	62.08	61.73
	Nymphs	CARY	8.08	7.95	8.02	7.99
		NMME	8.66	8.09	9.93	9.70
	Adults	CARY	4.06	3.96	3.95	4.02
		NMME	3.52	3.27	3.35	3.32

Table 2.1 The average CRPS for every modeling scenario, split between short (less than 31 days) and intermediate (90+ days) time scales. Larvae removal experiments are under the column No Larvae. Models that did not include mice are under the No Mice column.

The forecasts with NMME, on average, had less forecast variance than models that used weather from the Cary meteorological station. This was most apparent for nymphs and adults (Figure 2.2). This had interesting outcomes with respect to forecast skill.

For both short and intermediate-term larvae forecasts, the models with NMME outperformed the models with Cary data; the long-term forecasts where almost twice as skillful using NMME. For nymphs, the NMME models were less skillful for the short-

term forecasts, but for intermediate forecasts the two models were on parity. Adult forecast skill was the same across weather sources and time scale (Table 2.1).

Figure 2.2 Forecast variance

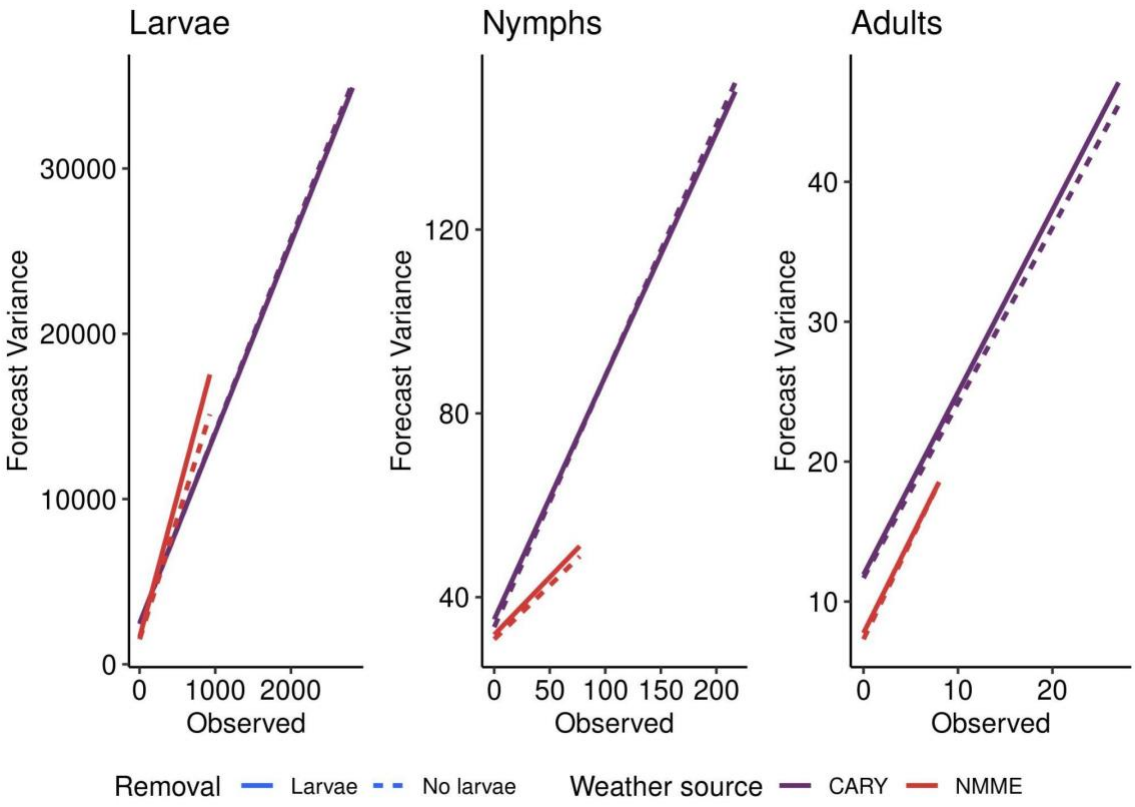

Figure 2.2 Forecast variance as it scales with the number of ticks observed on drag cloths. Purple lines are the models that used the Cary weather data, red are models that used NMME. Dashed lines were the larval removal experiments.

Larvae and nymph forecasts outperformed the null model during active periods of the year in all modeling scenarios (Figure 2.3). During the dormant periods of the year,

the null model tended outperform the process-based forecasts. Adult process-based forecasts were always worse than the null forecast (Figure 2.4, S2.3).

Larval (Figure S2.2) and nymphal (Figure 2.3) predictions from models that used mice and NMME were on average better than models without mice when forecasting peak values during the questing period. For intermediate length forecasts, larval and nymphal prediction skill benefited from having mice in the model. For example, during the nymph questing period and when using NMME, the models that used mouse data had a better RMSE compared to models without mice of eight ticks/450m^2 (Figure 2.3). Note that during the questing period larvae and nymph process-based forecasts were more skillful than the null during the questing period, regardless of weather data source, or if larval and/or mouse data was included.

In general, forecast skill increased with time (Figure 2.4). For larvae, average forecast skill for the processed-based models was high, about 800 larvae/450m^2. This contrasts with the null model error of 550 larvae/450m^2. However, as time progressed, larval forecast error was equal the null model in 2014, and by 2020 the process-based error had a better prediction error than the null by 250/450m^2; i.e., the rate of model performance increase was faster for the process-based models than the null model for larvae. Nymphal and adult prediction error also decreased, dropping from 25 nymphs/450m^2 to 10 nymphs/450m^2 for the process models and from 12 adults/450m^2 to 5 adults/450m^2 (Figure 2.4). Nymphs were an average always better than the null model, while adults were not.

Figure 2.3 How does the process model compare to the null model?

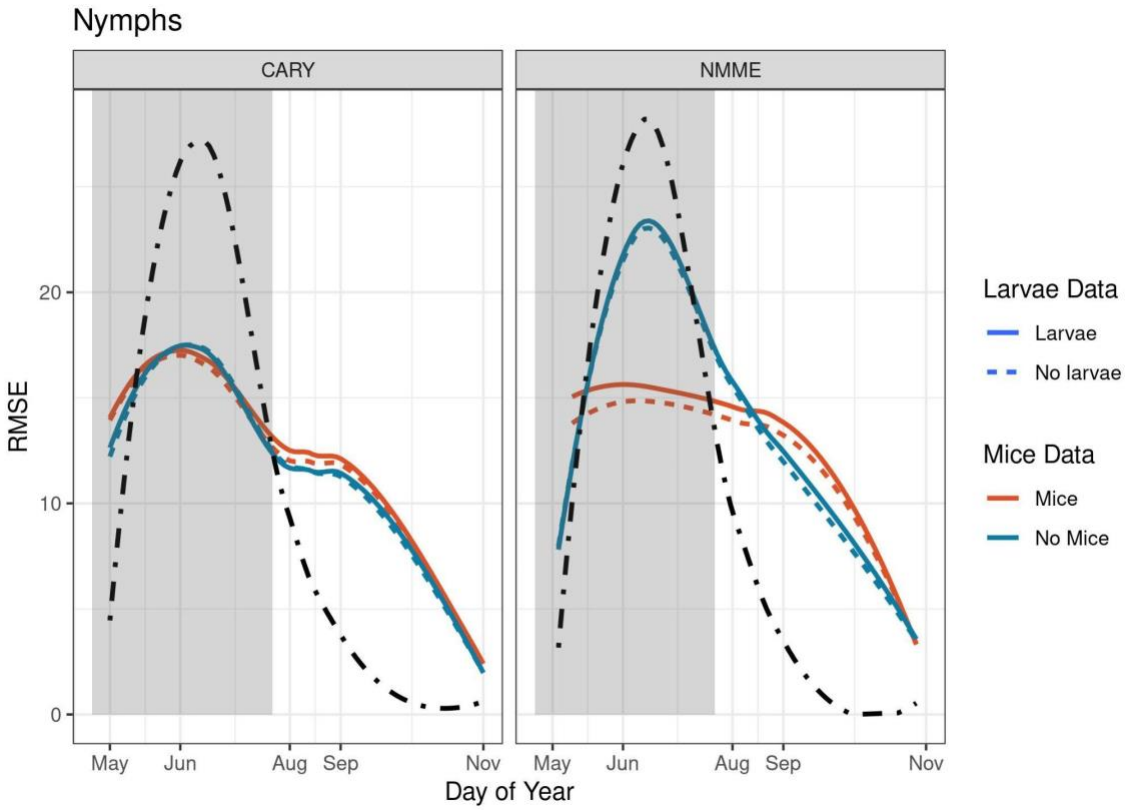

Figure 2.3 - Loess curves over the root mean square error (RMSE) for nymph forecasts. The left panel shows the models that used the Cary meteorological data as weather covariates, the right showing the models that used NMME. The black dot-dash line is the RMSE from the null model. Red shows RMSE for models that used mice to constrain transition rates, blue is those without mice. Solid lines show the RMSE of models that assimilates the larvae data, dashed lines those that did not assimilated larval data. The shaded region is the expected questing period for nymphs, and when peak counts are observed.

Figure 2.4 Process model vs Null - predicting peaks

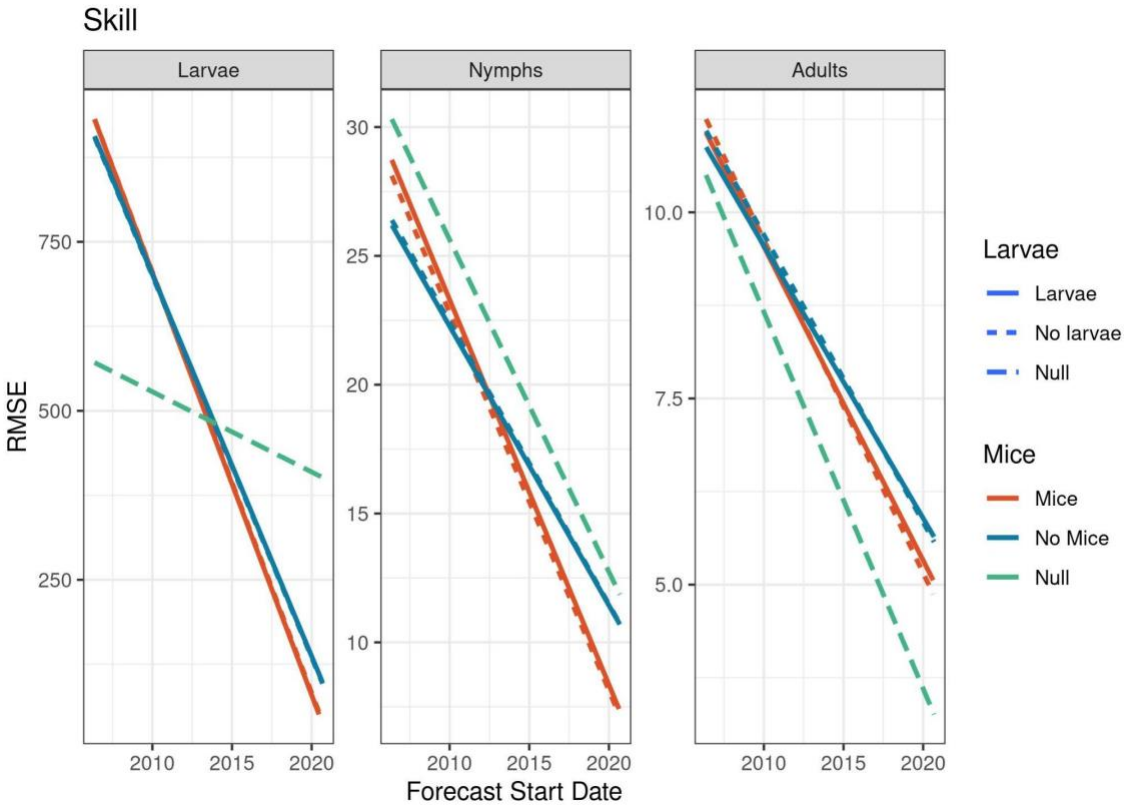

Figure 2.4 - The linear trend RMSE by forecast issue date for the peak observation each year for each life stage. The model RMSEs presented are from the models that use the Cary meteorological station as weather inputs. The green dashed line is the RMSE from the null model. Red shows RMSE for models that used mice to constrain transition rates, blue are those without mice. Solid lines show the RMSE of models that assimilated the larvae data, dashed lines those that did not assimilate larval data. Panels represent life stages, note the different y-axis for each panel.

The data assimilation scheme updated states and parameters as expected. When a good forecast was made it placed equal weight on forecast and data, and when bad forecast was made more weight was placed on the data (Figure 2.5).

Figure 2.5 Data assimilation

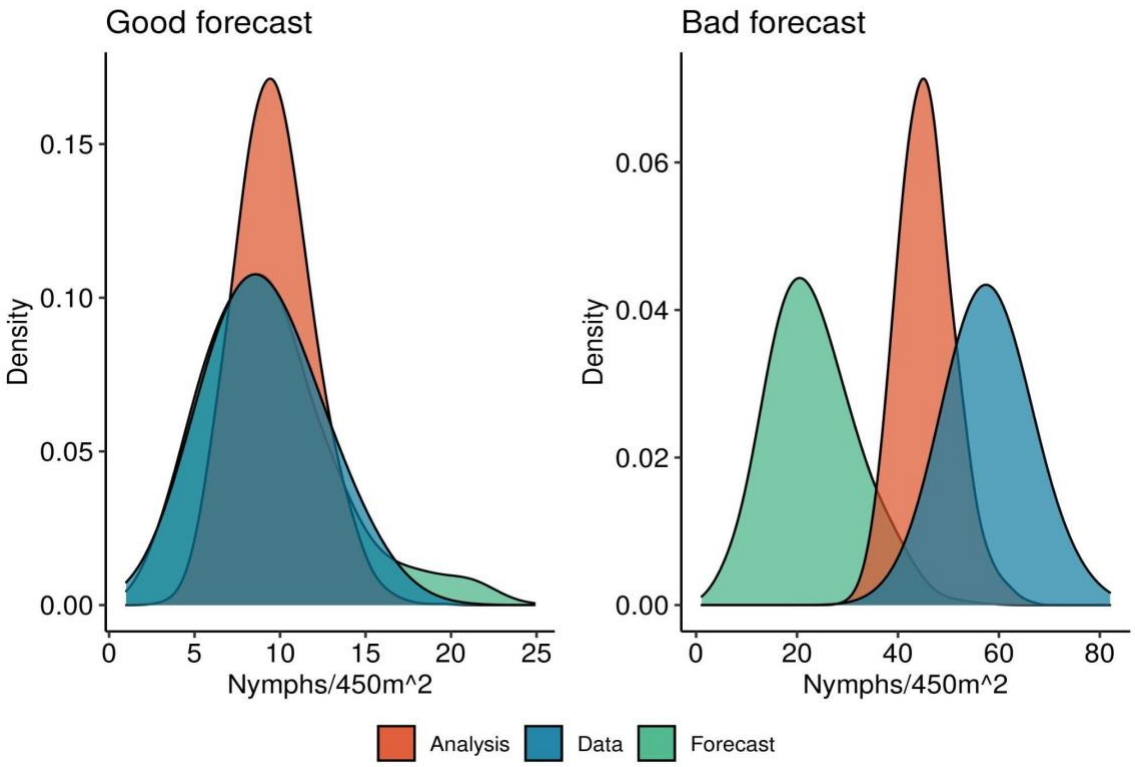

Figure 2.5 - State data assimilation. How the data assimilation works for two nymph forecasts. On the left, a good forecast on the left and a bad forecast on the right. The forecast distribution (green) is the distribution is what is given as the initial condition for the new forecast. The data distribution (blue) is a Poisson distribution with a mean equal to the observed number of nymphs. The analysis distribution (orange) is the estimate of the latent state on the observation day given both the forecast and data.

Figure 2.6 Parameter updates over time

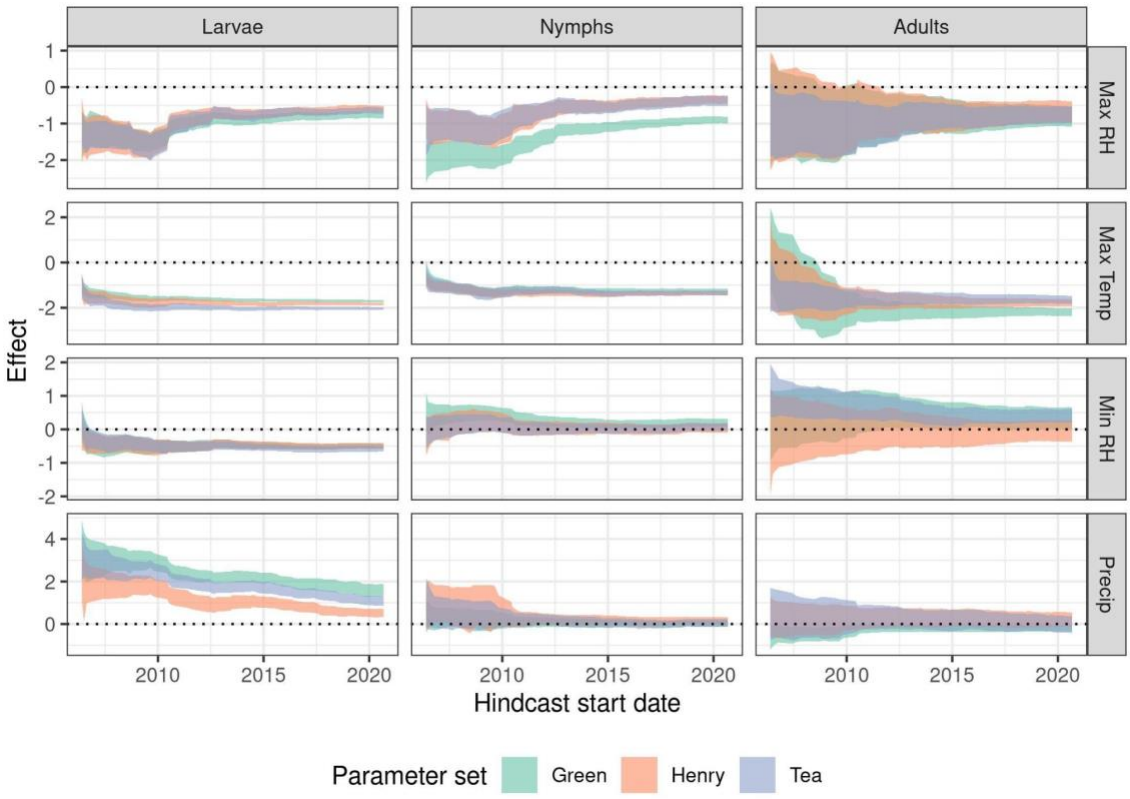

Figure 2.6 – Parameter distribution updates over time. Width of the 95% CI for weather effect parameters after data assimilation. Parameters came from three sites Green, Henry, and Tea, which are green, orange, and purple, respectively. Each life stage is a column, and each weather variable is a row.

Parameters also updated, becoming more precise over time. The largest change in parameter distributions was the effect of precipitation on larval survival, where posteriors moved towards a null effect (Figure 2.6). Another large shift was the effect of

temperature on adults, which started as a null effect but became more precise and negative with a mean effect of -2.2 (-2.02 – -2.4 95% CI) by the end of the forecast period.

Discussion

Our study was essentially a transferability-in-time experiment; we calibrated a model and tested it to data outside of the calibration period, and we were able to recover season dynamics for two of three life stages. We have shown the effectiveness of a proof of concept for iteratively forecasting the *I. scapularis* population at the Cary Institute of Ecosystem Studies and can predict peak nymph abundance once year in advance (Figure 2.8).

Larvae and nymph forecasts outperformed the null forecast, while adult forecasts did not. Our framework was not only able to recover observed weather dynamics (Figure 2.7), but also produced forecasts that had less variance on average than forecasts that used observed weather data (Figure 2.2). We therefore conclude that this stage-structured population model, given the current sampling strategy at Cary, is acceptable for short and intermediate forecasts for larval and nymphal ticks.

We tested two models in the overall framework, one that includes weather as covariates, and a more complex model that also includes mouse populations. On average, the more complex model with mice was more skillful for nymphs. This result is in contrast to (Johnson-Bice et al., 2021) which showed that more complex models

Figure 2.7 estimated latent weather

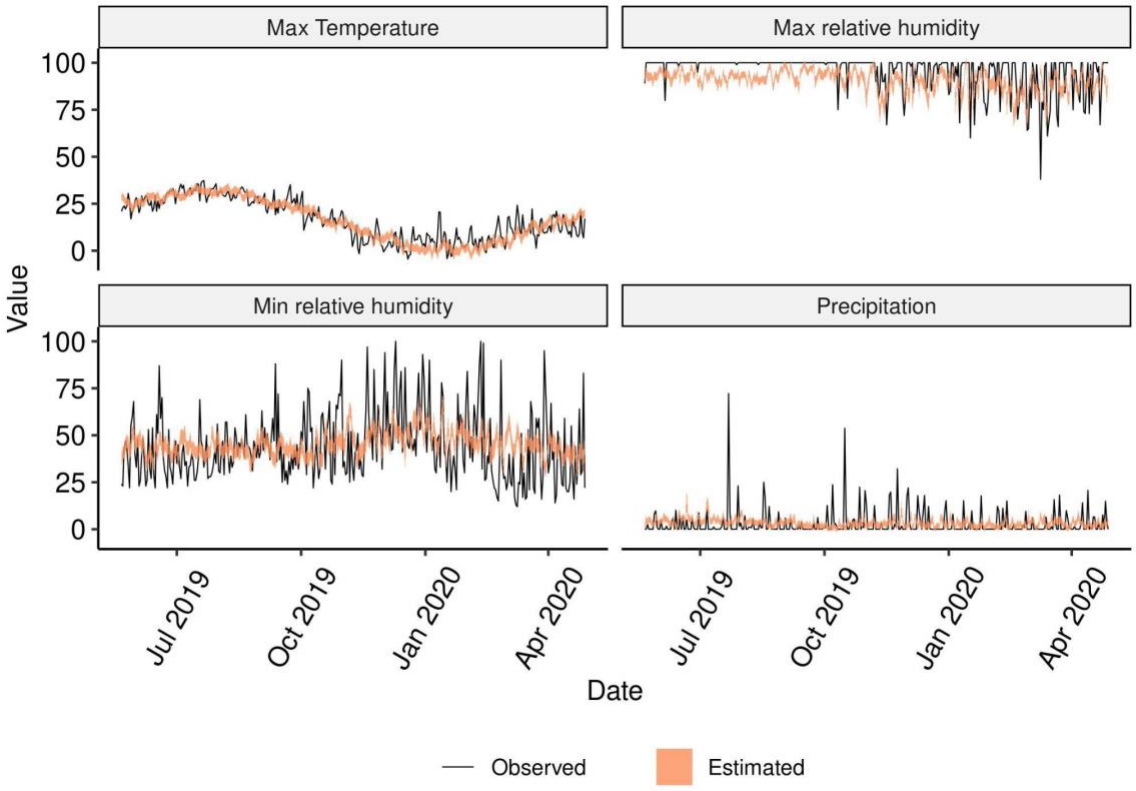

Figure 2.7 - The estimated values for the NMME variables under our errors in variables framework for a forecast issued on May 5, 2019. The orange envelope is what the model estimated, and therefore used as covariates in the forecast. The observed values from the Cary meteorological station are in black. Top left is daily maximum temperature (°C), top right is daily maximum relative humidity (percent), bottom left is daily minimum relative humidity (percent), and bottom right is total daily precipitation (mm).

performed worse out-of-sample. While we didn't explicitly test a static version of the stage-structure model (no covariates) we did test a complex model with biotic and abiotic drivers against the null GAM. As we were able to recover short and intermediate population dynamics for two of three life stages, we conclude that this model did not

Figure 2.8 Nymph forecast

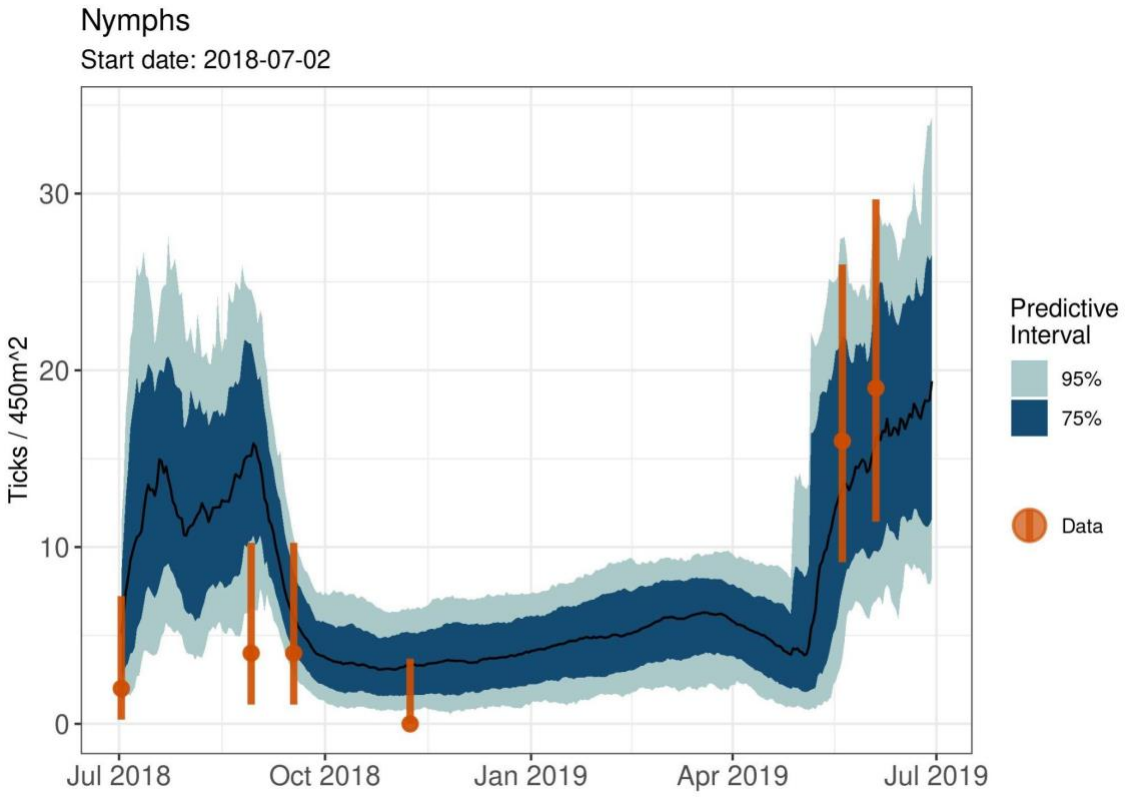

Figure 2.8 - Nymph forecast issued on July 2, 2018 from the model that used mice to constrain transition, NMME to constrain survival, and does not assimilate larval data. This forecast used parameters originally calibrated at the Henry site, while the forecast is at the Tea site. The forecast predictions are in blue (95% PI light, 75% PI dark), with the median forecast as the solid line. Orange points are observations with standard error. The phenology of nymphs is present in the forecast distribution, peaking in July/August 2018 and again in May 2019.

over-fit the training data. However, this is only true for the transfer-in-time at Cary. How this model may perform at other sites, or for other tick species, remains to be seen and should be considered for future research.

The partial recovery of seasonal dynamics is similar to that of (Kleiven et al., 2018) who performed a hindcast of their population model of Norwegian lemmings. While their issue was the difference between spring and autumn, we had issues between life stages. Our inability to predict adults may be do the low densities observed, which adds stochasticity to the data itself via sampling error.

For the larval data removal experiments, we removed larval data to test how this would affect forecast skill and found that removing them had remarkably no effect. We also tested a statistical framework for assimilating a year-long weather forecast, the North American Multi-Model Ensemble (NMME).

Our data assimilation scheme assimilated new tick observations as expected, and updated parameter distributions over time. The three parameter sets updated in similar ways, showing the same trends of the hindcasting period (Figure 2.6).

Weather effects becoming hyper-precise could be due to the estimated precision of NMME under our statistical framework. The four variables were able to match seasonal trends in observed values, but were much less variable day-to-day than observations (Figure 2.7). Also, the censorship of weather variables to their limits between zero and one for relative humidity and zero bound for precipitation, worked. Seasonal trends were best estimated for daily maximum temperature, and worse for precipitation. The error-in-variables model fails to predict large precipitation events and was the least variable day-to-day. It is not surprising, then, that the precipitation effect fell to zero for nymphs, and close to zero for larvae (figure 2.6). It is not that nymphs and larvae are now less sensitive to precipitation, but less sensitive to this particular

precipitation information because there is no variation.

The ability of the data assimilation to adapt parameters to make better forecasts matches expectations (Niu et al., 2014; Dietze et al., 2018). Our results are similar to Randon et al. (2022), which used MCMC methods for nowcasts of animal movements and found that their behavior persistence parameter adapted. We extend this further to show that a foreword only MCMC data assimilation scheme has the ability to update all model parameters when necessary. For example, the effect of temperature on nymph survival stays constant throughout the forecasting period while the effect of precipitation on larval survival updated constantly (Figure 2.6).

The biggest limitation to our framework is the inability to predict adult densities and our use of mouse data (in the form of minimum number alive) instead of a mouse abundance forecast. Our model was constructed with the instantons effect of mice on transition parameters. Therefore, in an actual forecasting scenario, mouse densities would also need to be forecasted. We currently do not have a forecast for mouse abundance, which is why we used the minimum number alive. A GAM smoothed over day of year, week, or month (such as the one used for the null model) is not practical as mouse abundance through time is highly variable. The Kleiven et al. (2018) study is a prime example of rodent seasonal dynamics being difficult to forecast. An immediate future need for this system is the ability to make accurate and precise year-long forecasts for mouse density.

This work as implications for the management of tick-borne disease risk. As we have shown that nymphal tick density can be forecasted at short and intermediate scales,

land managers could be more targeted in their mitigation efforts. Short-term forests could aid prescribed burning efforts as it is an effective tool for tick population management and requires little time or cost (Gleim et al., 2014), or invasive species removal (Allan et al., 2010). Other tools that could be used with little lead-time are pesticide applications, however the effectiveness of this strategy is mixed (Hinckley et al., 2016; Jordan & Schulze, 2019; L. Eisen & Stafford, 2020).

Intermediate forecasts could aid management strategies that take more planning and resources to accomplish. One such strategy is targeting host populations, by either removing hosts or using hosts to deliver acaracides to ticks (Tsao et al., 2021). However, it will be difficult to get management agencies to use products like these because this forecast is specific to Cary, and, less than half of vector-borne disease agencies engage in active surveillance (Mader et al., 2020).

The outsized role of initial condition uncertainty for nymphs during their questing period (Figure 1.9) and not needing larva here suggest we could sample nymphs more thoroughly. The shift in sampling could also be to sampling adults more intensively, as the model is currently not very good at forecasting them.

The next major step forward needs to be figuring out how to disseminate this information to land managers, but more importantly the public. People encounter ticks not just on public lands, but through activities around the home and neighborhood such as gardening or neighborhood parks. As tick control measures are often the responsibility of individuals (Piesman & Eisen, 2008) these forecasts need to be made publicly available. Not only will this help individuals, but hopefully it will shift responsibility from

individuals to tick-management programs. This is desperately needed to mitigate human incidence of tick-borne disease, especially given the effectiveness of mosquito-borne disease mitigation efforts by state and local agencies (L. Eisen, 2020).

CHAPTER THREE

Spatio-temporal mismatch in sampling design hinders model transferability

Predictive ecological models (and ecological forecasts) are increasingly used to inform adaptive management plans (Addison et al., 2013). However, managing ecosystems through the understanding of species dynamics and abundance is a challenge, and is dependent on several factors such as species diversity, trophic cascades, phenotypic variation, and species ecological function (Stuart-Smith et al., 2013; Atwood et al., 2015; Sequeira, Mellin, et al., 2018). Given the increasing pace of climate change, and the inherent spatio-temporal variability in ecological systems, ecological forecasts with the explicit goal of informing management decisions may have to be made at large scales. This means there must be a cohesion between local-scale management at the population level, with large-scale predictions at the ecosystem level (Atwood et al., 2015).

Data is collected at the population level, often by individual research projects or management agencies, making data availability at scale, and therefore large-scale forecasts difficult (Pennekamp et al., 2019). These data rich environments are where predictive models are calibrated and tested, because building models without sufficient data is impractical. However, important management decisions are needed for areas that don’t have active research or monitoring programs (Yates et al., 2018).

This highlights why model transferability is so important; the ability to make reasonably accurate predictions in data-poor environments (Yates et al., 2018). This is

particularly useful if the goal is to help inform adaptive management policies or to prioritize research objectives (Sequeira, Bouchet, et al., 2018). However, before we can transfer a model to a data-poor environment we need to assess the model's transferability skill in an otherwise non-data-limited environment. This is particularly important because data are a source of uncertainty (Dietze, 2017), and we don't want to make bad inference that leads to bad outcomes (Hernández-Camacho et al., 2015; Boettiger, 2022).

The goal of this paper is to explore the transferability of a stage-structured population model that was calibrated to a long-term data set at the Cary Institute of Ecosystem Studies (Cary), located in eastern New York state. The models were developed here because these data are the most comprehensive data available for *Ixodes scapularis*, the primary vector of Lyme disease (Ostfeld et al., 2006).

While Lyme disease is endemic to the northeastern and midwestern U.S., human incidence of the disease has been increasing for more than a decade (Diuk-Wasser et al., 2020), due in part to the geographic expansion of *Ixodes scapularis* (Sonenshine, 2018). The transferability of these models will be a challenge due to this expansion as we are dealing with new tick habitat.

To assess transferability, we use data from the National Ecological Observatory Network (NEON), which samples ticks in the same manner as the long-term study at Cary. Therefore, we quantify how well a stage-structured model calibrated to *I. scapularis* transfers to other *I. scapularis* populations.

Using NEON also provides an opportunity to transfer the model across species. *Amblyomma americanum* is another Ixodid tick and is the tick species that is most

abundant at NEON. Furthermore, it's of medical importance as it vectors Ehrlichiosis to humans. The secondary objective of this manuscript is then to quantify how well a stage-structured model calibrated to *I. scapularis* transfers to *A. americanum* populations. The transferability is spatio-temporal; the models were calibrated from 1995-2005 in NY and run at several sites across the US in 2018.

A proiri, the outlook on being able to transfer these models is mixed at best. In addition to the potentially suitable tick habitat from expanding populations, we have variable habitat within each NEON site.

Other attempts to transfer abundance models have also been made. A population model for the Norwegian lemming (*Lemmus lemmus*) was transferred in time and able to recover summer dynamics (Kleiven et al., 2018) but had trouble predicting winter populations. Furthermore, when surrogate data is used in the place of demographic data for sea lions, only one of two sites was able to be predicted (Hernández-Camacho et al., 2015).

Transferability of fish species abundance by taxonomic family from the Great Barrier Reef to Ningaloo Reef was poor (Sequeira, Mellin, et al., 2018) due to high variability in population levels across systems. Community models, which incorporate environmental variables and co-occurrence to predict community structure transferred better than species distribution models (Maguire et al., 2016). In general, mechanistic population models tend to overfit training data and therefore do not recover new observations, especially in a forecasting and transferability context (Johnson-Bice et al., 2021), even when biotic interactions are included (Soininen et al., 2018).

We include biotic interactions in our model through host abundance, as we know hosts increase the predictive capacity of *I. scapularis* nymphs in NY. We don't know how different *I. scapularis* populations are to each other, or how different *I. scapularis* might be to *A. americanum* when using the same statistical framework. We can, however, quantify the response to different biotic and abiotic interactions, which can further our understanding of how climate change may affect these two medically important tick species (Van der Putten et al., 2010)**.**

For abiotic interactions, we use weather to constrain survival and cumulative growing degree days (CGDD) to drive phenology, and we can test the extent to which the same CGDD thresholds can be used to estimate questing behavior. It is true that multiple studies have shown, including ours, that CGDD is a useful estimator of questing phenology. For example, at Cary, we have shown that we can predict the phenology of questing nymphs up to a year in advance using 400 cumulative degree days with a base of 0°C starting January 1st each year (Figure 2.8).We can therefore surmise that this aggregation correlates to nymphal development and/or diapause because once development is over the nymphs emerge and begin questing (Ogden et al., 2018). The question, then, is does this aggregation account for the development of all *I. scapularis* populations?

There is reason to think it could, as there is a latitudinal gradient in questing behavior of *I. scapularis* where they quest earlier in the south (I. M. Arsnoe et al., 2015; I. Arsnoe et al., 2019; Ginsberg et al., 2021). As the south gets warmer earlier in the year, southern tick populations will experience a quicker aggregation of degree days, reaching

the questing threshold of 400 earlier than northern populations.

As prediction error is expected to decrease as environmental novelty increases (Yates et al., 2018), and as abundance data often reflect site suitability, (Matthiopoulos et al., 2015; Paton & Matthiopoulos, 2016), we hypothesize that the NEON sites most similar to Cary (HARV, TREE, i.e. the northernmost sites) will have better-performing forecasts.

Abundance data has more information about a particular species' dynamics than occupancy data, so in theory, models calibrated with abundance data should transfer better than those built on presence/absence data (Howard et al., 2014). Indeed, (Estrada & Arroyo, 2012) found that models on abundance data were more favorable for species that are heterogenous on the landscape. As *I. scapularis* are heterogeneous in space, both across and within populations (Ripoche et al., 2018), we can expect a degree of transferability. Therefore, we also expect forecasts for *I. scapularis* to be more precise and have less error than forecasts for *A. americanum* because models have greater transferability within populations than across populations (Peñalver-Alcázar et al., 2016).

Transferring this model using iterative ecological forecasting and uncertainty partitioning is an ideal process for this experiment. First, our data assimilation scheme can adapt model parameters, including model uncertainty, over time (Figure 2.6), which leads to more skillful forecasts (Figure 2.4). If this stage-structured model can predict the *A. americanum* population dynamics, which was parameterized with *I. scapularis* data, then we can infer that these two species are more alike than different.

Methods

Tick Data

The tick data product used was DP1.10093.001 *Ticks sampled using drag cloths* (National Ecological Observatory Network (NEON), 2022b). Within each NEON site, there are six plots where tick sampling occurred. The plots are square at 40 meters to a side and spaced at least 500 meters. Tick sampling occurs by dragging a $1m^2$ cloth along the perimeter of the plot for a total of $160m^2$ of searched area. Tick drags occur during the growing season at each site; within two weeks after green-up and two weeks before senescence. Frequency of tick collection is either once every three weeks or once every six weeks, depending on whether or not more than five ticks are collected at a site within a 365 day window (Paull et al., 2022).

The two most abundant tick species found across NEON sites are *Amblyomma americanum* and *Ixodes scapularis*, so we filtered the data to include only these species, and we used data from the high intensity (sampled every three weeks) plots only.

From the taxonomic data, we combined the total number of female and adult counts from each drag to get the total number of adults collected as adult ticks are the only ticks that were identified to sex (Paull et al., 2022). For taxonomic classifications, NEON identifies each tick to the lowest taxonomic rank possible for nymphs and adults, as such we only used records that were identified to species. The larvae are most often identified to either the class or family level, to keep enough larval records in the data we filtered out all larvae identifications that were not to the family (Ixodidae) level or below.

We next visually inspected time series to identify sites with sufficient ticks of all life stages to permit model calibration, which left us with data from 10 NEON sites (Table 3.1). We removed plots that did not have at least three tick drags each year otherwise models did not converge.

Mice data

The small mammal data product used was DP1.10072.001 Small mammal box trapping (National Ecological Observatory Network (NEON), 2022a). Like the ticks, the small mammals are identified to taxonomic rank, and we kept all individuals identified to the genus Peromyscus, which included *P. leucopus* and *P. maniculatus*. We constructed a standard capture history matrix at each site where watch individual mouse was a row, and trapping day was a column.

We used the minimum number alive of mice as a covariate for the Weather & Mice model. The number of alive is the sum of all alive mice captured on any trapping day, and any mice that we can infer are alive an any trapping day. For example, if a mouse was captured on trapping occasions one and three, we can infer the mouse was alive on trapping occasion two. To keep this data stream relevant to a forecasting context, we did not interpolate between trapping occasions. Rather, we kept the minimum number alive constant from one occasion to the next to reflect our unknown number of mice alive into the "future." For example, if there are 12 mice alive on day one and 22 mice alive on day eight, then days two through seven were assigned a minimum number alive of 12.

Daymet

We used the coordinates on table 3.1 to download the gridded product daymet (Thornton et al., 2020) for weather meteorology at the site level. We downloaded temperature, relative humidity, and precipitation on a daily time step.

We did not use the weather observed from the NEON metrological towers because as of this writing, the NEON product has too many missing values. We did however use the NEON data to downscale daymet to match site characteristics. For relative humidity and temperature, we calculated the average value for each day of year from both the NEON and daymet data, then calculated the difference (bias) between the NEON average and daymet average for every day of year. We then added in the bias back to each date in the daymet data with respect to the day of year. Cumulative growing degree days were calculated from the downscaled daily maximum temperature with a threshold value of zero degrees Celsius.

The null model was designed much like that of Chapter 2, where we used a generalized additive model smoothed over day of year. There was a null model generated for each site, and a new null forecast was generated after data assimilation.

All data intake and cleaning, and statistical and graphical analysis were done in R v4.0.2 (R Core Team, 2020). NEON data was downloaded from NEON's API using the neonstore package (Boettiger et al., 2021), Daymet meteorological data was downloaded with the daymetr package (Hufkens et al., 2018), and Bayesian modeling was implemented in NIMBLE (de Valpine et al., 2017, 2022).

Table 3.1 NEON site descriptions

Site Code	Site Name	Tick Species	# Plots (tick / mice)	Latitude	Longitude	State	NEON Domain
BLAN	Blandy Experimental Farm	AA & IX	6 / 5	39.03	-78.04	VA	Mid-Atlantic
HARV	Harvard Forest & Quabbin Watershed	IX	7 / 8	42.54	-72.17	MA	Northeast
KONZ	Konza Prairie Biological Station	AA	6 / 8	39.10	-96.56	KS	Prairie Peninsula
LENO	Lenoir Landing	AA & IX	6 / 7	31.85	-88.16	AL	Ozarks Complex
OSBS	Ordway-Swisher Biological Station	AA	9 / 6	29.69	-81.99	FL	Southeast
SCBI	Smithsonian Conservation Biology Institute	AA & IX	7 / 7	38.89	-78.14	VA	Mid-Atlantic
SERC	Smithsonian Environmental Research Center	AA & IX	6 / 8	38.89	-76.56	MD	Mid-Atlantic
TALL	Talladega National Forest	AA	6 / 8	32.95	-87.39	AL	Ozarks Complex
TREE	Treehaven	IX	6 / 6	45.49	-89.59	WI	Great Lakes
UKFS	Kansas University Field Station	AA	6 / 6	39.04	-95.19	KS	Prairie Peninsula

Table 3.1: Overview of the NEON sites included in the analysis. Tick species shows which tick species are modelled at each site (AA: *Amblyomma americanum*; IX: *Ixodes scapularis*). # plots is the number of plots at each site for each organism.

Forecast workflow

For the first forecast, we used the calibrated posterior of the model validated at the Cary Institute of Ecosystem Studies. We had three parameter sets from the calibration period, one for each of the three field sites. Here, we used the average parameter values across the three sites for initial parameter distributions. We ran the forecast from the first observation in 2018 through the last observation in 2019 at the site level. At each site, we ran four models; static (no covariates), Weather (daily weather drive survival of each life

stage), Mice (mouse abundance driver transition parameters), and Weather and Mice (includes weather driving survival and mouse abundance on transition). At each time step, each model was run four times to add uncertainty components.

We performed the uncertainty partitioning as one-at-a-time, meaning the first simulation only included initial condition uncertainty, then we added parameter uncertainty, then driver uncertainty, and then finally process uncertainty. For example, if parameter (i.e., node β) uncertainty was included it was given a prior equal to that of the last forecast $\beta \sim N(\mu, \tau)$, where μ was the mean and τ the precision of β from the previous forecast. If parmeter uncertainty was not included, β was treated as deterministic, $\beta = \mu$, and therefore no uncertianty was propagated.

When driver error was included in the simulation, we used a simple error-in-variables framework to account for the uncertainty in daymet.

$$temp_{daymet,t} \sim N(\widehat{temp}_t, \tau_{temp}) \quad [1]$$

$$\widehat{temp}_t \sim N(0,1) \quad [2]$$

$$\tau_{temp} \sim exponential(1) \quad [3]$$

Using temperature as an example, the latent temperature $\widehat{temp}$ at time *t* was given a standard normal prior (inputs were standardized), and then constrained using the observed temperature from daymet $temp_{daymet}$ and an estiamted precison τ_{temp}, which

represents the error in temperature. τ_{temp} was given an unformative zero-bound prior. When driver uncertainty was not included in the simulation the observed temperature from daymet was used without error; $\widehat{temp}_t = temp_{daymet,t}$.

Process error was simulated using the multivariate normal distribution.

$$\overrightarrow{x_{i,t+1}} \sim MVN(\overrightarrow{x_{i,t}}, \Sigma) \quad [4]$$

Where Σ is a diagonal matrix of variances. When process error was included the diagonal terms were estimated by giving them informative inverse gamma priors built by moment matching (Llera & Beckmann, 2016) from the last forecast. We set these process variance terms to 1e-10 when process uncertainty was not included in the simulation. This added a negligible amount of uncertainty, as evidenced by the amount of total variance added when simulations included process uncertainty (Figure 3.1).

The NEON domain is hierarchical, meaning several plots are within a site. To take advantage of this, we made forecasts at the site level, and used plots as replicates.

$$y_{i,t,p} \sim Poissson(\frac{x_{i,t}{}^{*}area_{t,p}}{450}) \quad [5]$$

$$\vec{x}_t = \boldsymbol{A}_{t-1}\overrightarrow{x_{t-1}} \quad [6]$$

Where, within a site, the observed number of ticks *y* for life stage *i* at time *t* for plot *p* is Poisson distributed with a mean equal to that of the latent state *x* of life stage *i* at

time *t* multiplied by the sampled area (m^2) at time *t* in plot *p*, scaled by a factor of 450. Here, the numerator represents the number of ticks per square meter, but the spatial scale of sampling at the Cary Institute is at $450m^2$. The parameters in the model were thus calibrated at this sampling design, so we had to scale the latent states here to match the scale of the latent states from model calibration at Cary.

The actual forecast was made where on day *t-1,* **A** is the daily transition matrix, and *x* is the estimated latent state vector, which are used to predict the next days (*t*) expected tick population.

Results

To determine the relative skill for each model at a NEON site, we subtracted the null model CRPS from the process model CRPS for each forecast at each site (thus a positive difference indicated the process model was more skillful), then calculated summary statistics from these distributions.

For the larval Ixodes forecasts with all uncertainty included, the median difference between the process models and the null model over the forecasting period was negative (worse than the null model) for most models and sites, except at LENO for the Weather model (median 7.25, 95% CI -136.37 – 37.45), and the Weather and Mice model (5.52, -150.76 – 36.58), both under the constant parameter scenario (Figure S2.1).

Ixodes larval forecasts that included weather variables performed better at HARV than TREE (Figure S2.1). The Weather model's median difference in CRPS to the null model's CRPS was -5.66 (95% CI -97.03 – 50.56) at HARV and -14.05 (95% CI -202.2 –

122.73) at TREE. Similar differences were evident in the Weather and Mice model for larval Ixodes forecasts.

The same was true for the larvae Amblyomma forecasts, were LENO had the best relative scores to the null model with the Weather model (6.64, -146.57 – 37.6), and the Weather and Mice model (5.98, -174.16 – 36.41), again both under the constant parameter scenario (Figure S3.2).

The nymphal Ixodes forecasts with all uncertainty were, at the median, always worse than the null model (Figure 3.1). In contrast, the Amblyomma nymph forecasts on average outperformed the null model with updated parameters at SERC, TALL, and UKFS, and with constant parameters at UKFS (Figure S3.3).

The adult forecasts for both *Ixodes scapularis* (Figure S3.4) and *Amblyomma americanum* (Figure S3.5) were on average worse than the null forecasts at all sites.

For the two NEON sites that closely match the environment and tick species composition of Cary (HARV and TREE), nymph process model forecasts were more skillful at TREE than HARV. For example, the Weather and Mice model forecasts that updated parameters, the CRPS difference to the null at TREE was -0.8 (95% CI -43.76 – 33.86), while the difference at HARV was -1.49 (95% CI -12.54 – 10.77). The higher median difference (and higher 95% CI) at TREE compared to HARV for nymphs was evident across forecast scenarios (Figure 3.1).

Figure 3.1 Average difference in CRPS for *Ixodes scapularis* forecasts relative to the null model

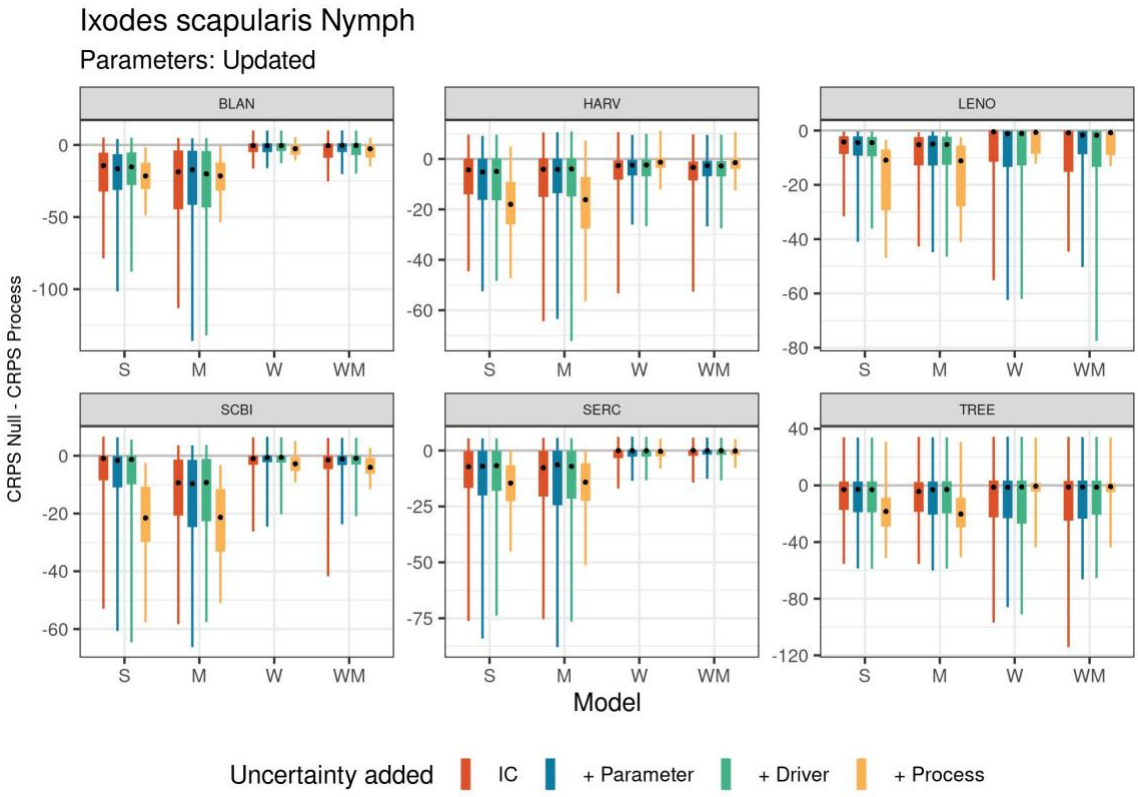

Figure 3.1 - The distribution of the difference in CRPS over the entire forecasting period for *I. scapularis* nymphs. For each forecast, the difference between the null model score and the process model score was calculated, values are the average of these differences with 95% CI. Colors represent forecasts as uncertainty is added, starting with initial condition uncertainty (IC, red), then parameter uncertainty was added (blue), followed by adding driver uncertainty (green), and the forecast with all uncertainty included (Process, yellow). Models are shown on the x-axis as the Static model (S), Mouse model (M), Weather model (W), and the model with both weather and mice (WM). Negative values indicate the process model was worse than the null, positive values when the process model was better. The null model is a GAM smoothed over day of year for each life stage at each site.

Figure 3.2 Median prediction vs. observed for nymph forecasts

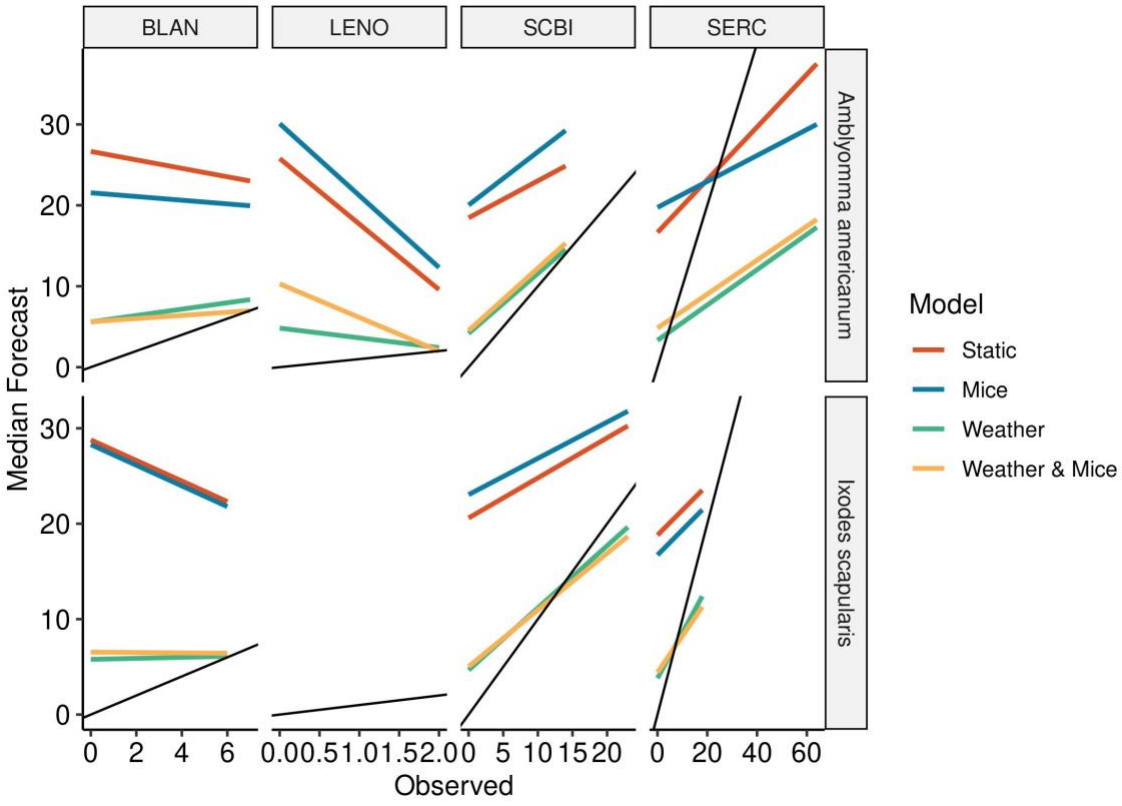

Figure 3.2 - The median forecast (ticks on drag cloths) from the simulations that include all uncertainty at the four sites (columns) where both species (rows) were modeled. Color represents the line of best fit for each model, individual forecasts are not plotted to reduce noise. The black line is the 1:1 line.

At the NEON sites where both *I. scapularis* and *A. americanum* are present, relative model performance was mixed (Figure 3.2). In general, *I. scapularis* forecasts were more skillful or on parity with *A. americanum*, especially for larvae. For nymphs, the model that included weather but not mice were more skillful at forecasting *A.*

americanum than *I. scapularis* at three of the four sites where these two species overlap. All models and life stages were dominated by process error, even during the questing period (Figure S3.1).

In general, forecasts for nymphs improved over time, except for the parameter and driver uncertainty forecast scenarios at BLAN (Figure 3.3). Furthermore, the data assimilation updated model parameters throughout the forecasting period. The most dramatic of these changes was to the process variance terms (Figure 3.4), which in some cases dropped by an order of magnitude from their initial distribution. For example, the starting distribution for process variance (units are $(ticks/450m^2)^2$) for Ixodes adults at the Henry Cary site had a 95% CI range of 2.05 – 3.56. This dropped to 0.127 – 0.155 at the end of the transferability experiment (Figure 3.4). However, larval process variance increased from a starting 95% CI range of 30.8 – 55.7 (at Cary) and ending with a 95% CI range of 161.63 – 355.79 (at HARV).

The other change in parameters worth noting is the effect of mice on state transitions (Figure 3.5). Compared to the starting parameter distributions, the effect of the mouse population on the larvae-to-nymph transition increased for both species. For example, the 95% credible intervals of the posterior distribution from model calibration overlapped zero at all three Cary sites for the larvae-to-nymph transition, while this effect was positive at five sites and negative at one site for *Ixodes scapularis* (intervals are 95% CI range): 0.624 – 0.922 at BLAN, 0.953 – 1.13 at HARV, 1.79 – 2.12 at SCBI, 0.817 – 1.07 at SERC, and 0.378 – 0.583 at TREE, -0.258 – -0.067 at LENO.

Figure 3.3 Change in nymphal CRPS over time

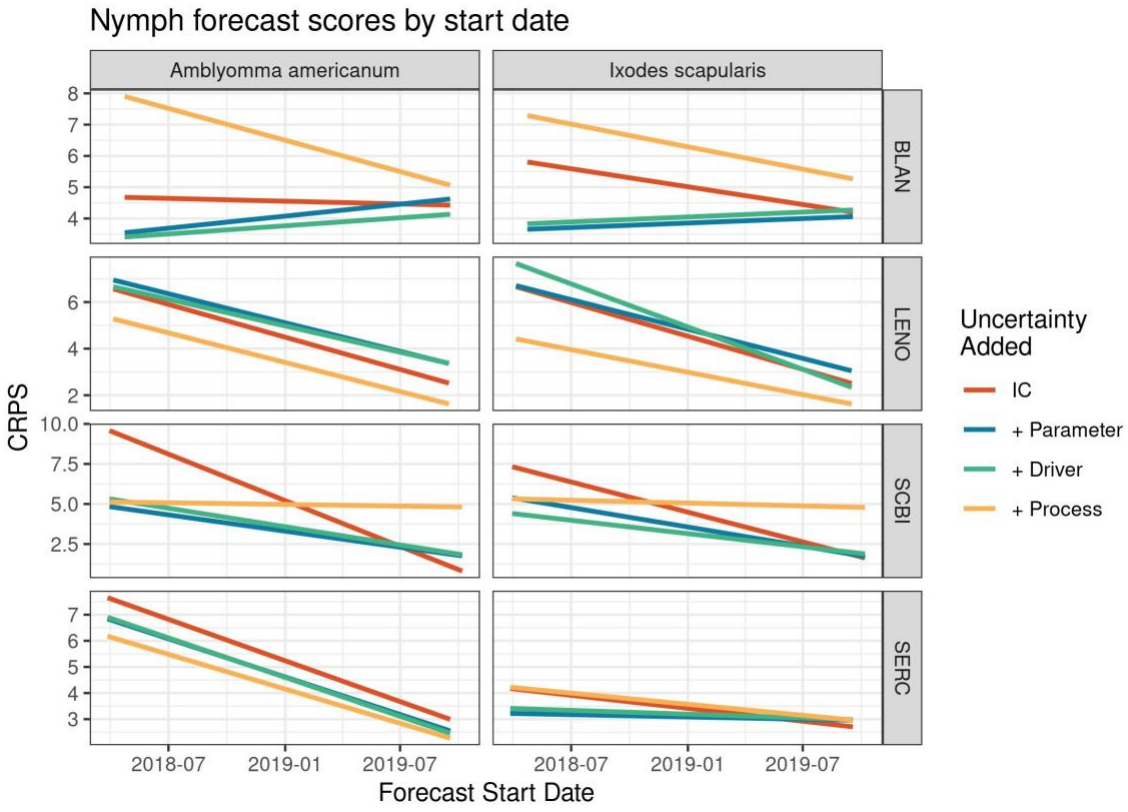

Figure 3.3 - Linear trend in CRPS with respect to forecast start date for nymphs at the four sites where both species were modeled. Color represents one-at-a-time uncertainty scenarios where the first forecast only included initial condition (IC, red) uncertainty, then parameter (+ Parameter, blue) uncertainty was added, followed by driver (+ Driver, green) uncertainty, and the forecast with all uncertainty (+ Process, yellow).

Figure 3.4 Change in process variance terms

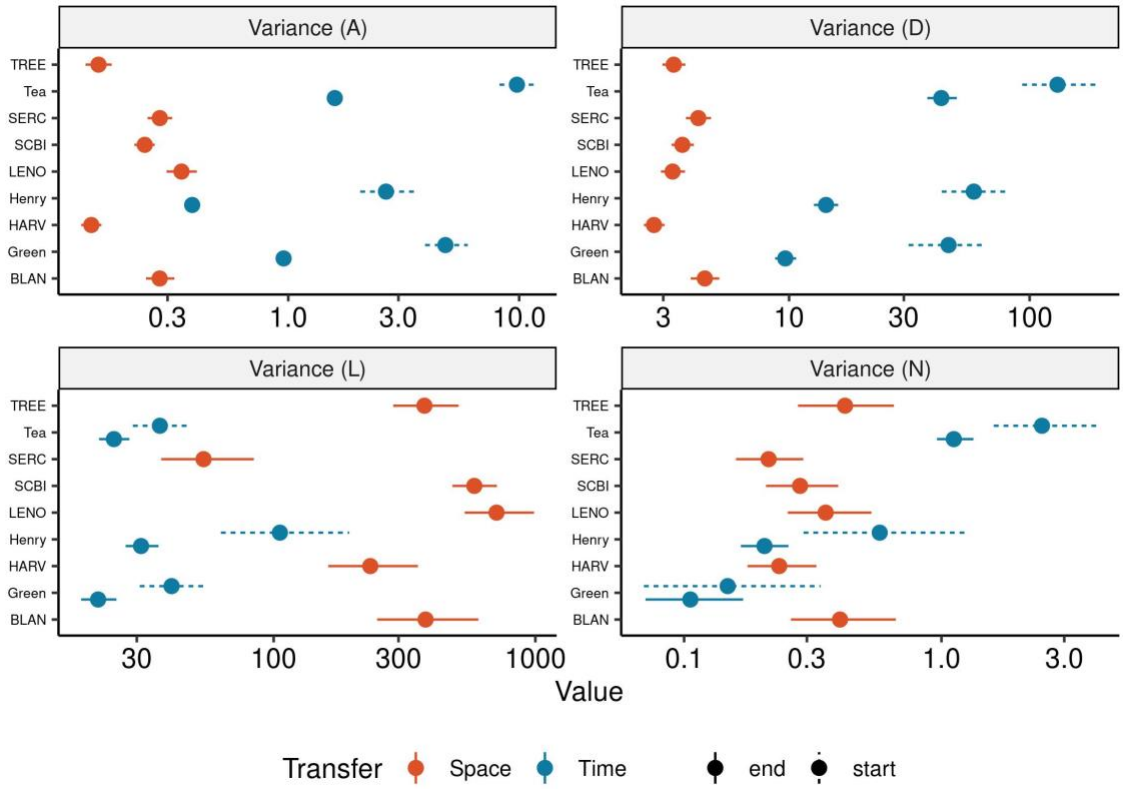

Figure 3.4 - The change in process variance terms for *I. scapularis*. X-axis units are $(ticks/m^2)^2$. The forecasts started with informative priors on process variance for each state, represented by the blue dashed 95% interval. The red intervals are posterior widths for each state after the last forecast of 2019 at NEON sites (transfer-in-space). For comparison, the solid blue interval is the posterior after the last forecast from chapter 2 (transfer-in-time) experiments. The four states are adult (A) , dormant nymphs (D), larvae (L), and nymph (N).

Discussion

Here, we tested the effectiveness of a stage-structured population model by transferring the model in space and across species. Model transferability was better than expected, especially to the NEON sites that were most like Cary (HARV and TREE) due their environmental characteristics such as climate and habitat type (Figure 3.6). Furthermore, scaling the latent state to match the spatial effort of the NEON data (m^2) to the effort used at Cary (450 m^2) increased transferability, which was expected (Sequeira et al., 2016).

However, forecasts at NEON were biased, either over- or under-predicting depending on the site (Figure 3.2). This suggests the correction we applied to the latent state, while helpful, was not enough to account for the difference in magnitude of observed abundance between NEON and Cary. This difference has been shown to lead to biased estimates (Sequeira, Bouchet, et al., 2018). Forecast bias could also be attributed to the difference in habitat structure between Cary and NEON. The Cary sites sit in an oak dominated forest, which NEON would classify as deciduous forest. We transferred the models into other habitat types such as evergreen forest, pasture, wetlands, crops, and grasslands. While forecasts were biased in all land cover types, the deciduous forest forecasts had the most even distribution in bias, whereas the other land cover types were heavily weighted as consistently under- or over-predicting (Figures S3.7, S3.8, and S3.9 for larvae, nymphs and adults, respectively). As transferability is expected to be low when moving into more novel environments (Yates et al., 2018), it is not surprising that our forecasts were more biased in non-deciduous forests.

Figure 3.5 Change in Mouse effect

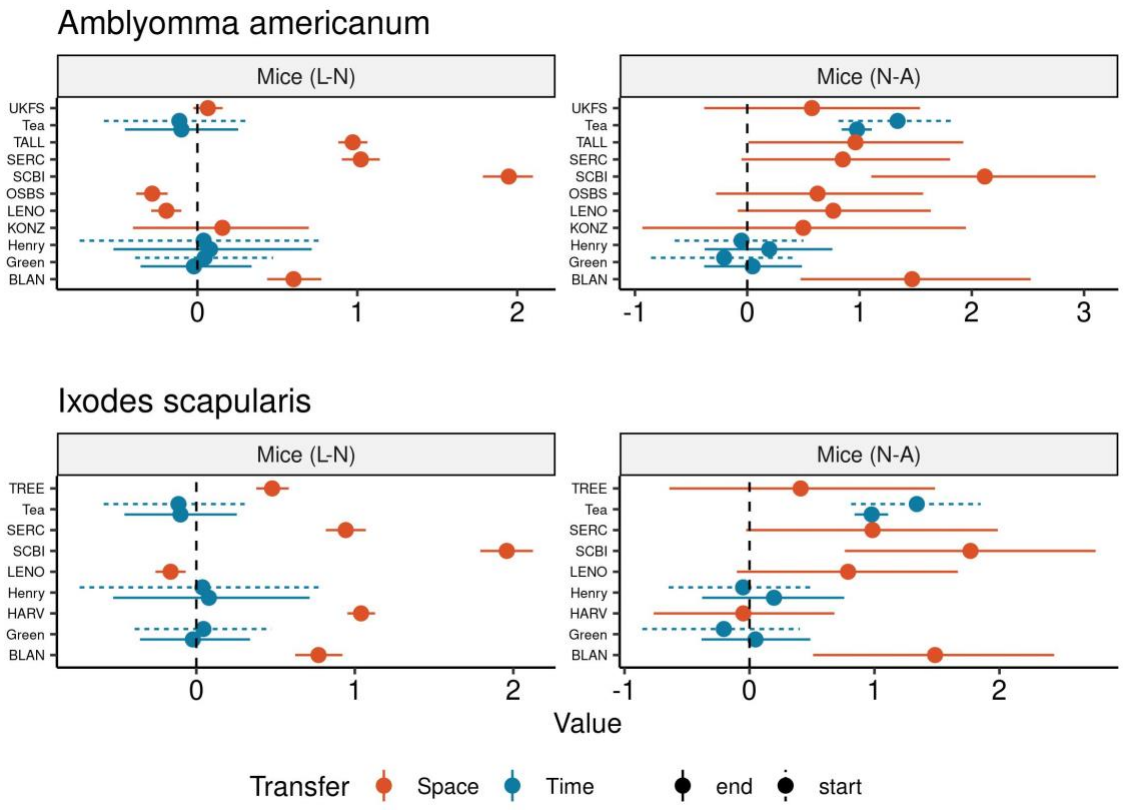

Figure 3.5 - The change in effect of mice on state transitions for *A. americanum* and *I. scapularis*. The forecasts started with informative priors for each effect, represented by the blue dashed 95% interval. The red intervals are posterior widths for each effect after the last forecast of 2019 at NEON sites (transfer-in-space). For comparison, the solid blue interval is the posterior after the last forecast from chapter 2 (transfer-in-time) experiments. The effects are the transition from larvae to nymph (L-N) and nymph to adult (N-A).

Further evidence that the NEON sites contain more novel environments, we can look at the difference between that last parameter distributions from this experiment (transferring the models in space) to the last distributions from the hindcast experiments (transferring the models in time) from chapter 2. Parameter distributions were allowed to

update after each data assimilation step, which means the last posterior from each experiment represents the most realistic demographic parameters for each site. We can justify this reasoning because in both chapters, forecast skill increased through time with parameter updating (Figure 3.3).

When comparing the forecasts, we see that process variance terms updated relative to the chapter 2 parameters. The process variance term represents the unexplained demographic stochasticity at each site. For adults and dormant nymphs both species, process variance fell substantially at the NEON sites compared to the Cary sites (Figure 3.4). This could be explained by one of two reasons. The first is that demographic parameters at NEON more accurately describe population trends at NEON compared to Cary, and therefore less stochastic error is needed. The second is that the data itself is less variable. We argue for the latter, as forecast bias was substantial and adult forecasts were almost never better than the null forecast, regardless of uncertainty scenario (Figures S3.4 and S3.5).

On average the best performing process model for *A. americanum* larvae and nymphs included weather but not mice. For adult ticks, it was the model that had both weather and mice included. This result matches other studies in that mouse abundance does not explain *A. americanum* populations because they are host generalists (Kollars et al., 2000; Hroobi et al., 2021).

Figure 3.6 *Ixodes scapularis* forecast at HARV

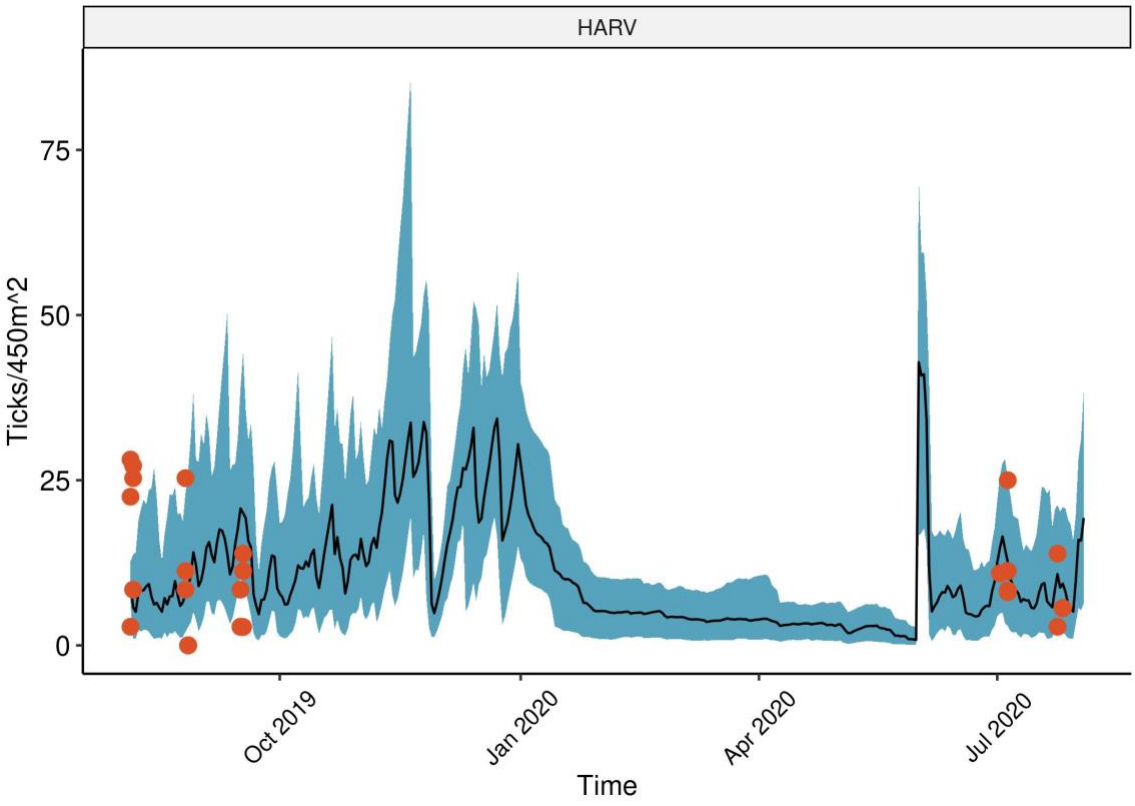

Figure 3.6 - Forecast issued at HARV for *I. scapularis* nymphs from the Weather & Mice model. The blue ribbon is the 95% predictive interval with the median (black line). Orange dots are tick observations at each plot within the HARV site.

This reflects the data assimilations' ability to update parameters as needed, which is particularly relevant for the process error terms as noted above. Interestingly, other demographic parameters did not change with as much magnitude as the process error terms. See supplementary Figures S3.10 & S3.11 for survival and S3.12 & S3.13 for transition terms.

Interestingly, coefficients responsible for the effect of mouse abundance on the transition from nymph-to-adult also updated substantially. For the Ixodes, this seems to match with other studies showing that nymph abundance can be constrained by mouse abundance (Dobson et al., 2011; Ginsberg et al., 2020; Ostfeld, Levi, et al., 2018). The same shift for *A. americanum* is interesting, and is at odds with others that have shown that mouse density is not predictive of *A. americanum* populations (Hertz et al., 2017). This could be due the tradeoff between the rise in this effect and the drop in *A. americanum* adult survival (Figure S3.11). However, the model with weather, but did not include mice, was on average the best process model for *A. americanum*, which would support the current literature.

We attempted to transfer in space a stage-structured model that has been proven to work in a forecasting context, and failed to do so, confirming that transferring models in space is difficult (Yates et al., 2018; Kleiven et al., 2018; Johnson-Bice et al., 2021) . However, we have shown that our data assimilation scheme updates model parameters in a way that makes the forecasts more skillful over time.

The prevalence of process error and overprediction would suggest that the model is not structurally sound for these populations. However, this won't truly be known without calibration such a model to these specific data. To that end future research should focus on calibrating this type of model, along with others, to the NEON data.

CHAPTER FOUR

A data-fusion framework to describe the change in parasitism status of mice at several sites in the National Ecological Observatory Network

Introduction

Tick-borne diseases are complex systems where ticks, hosts, and pathogens interact. The prior chapters have focused primarily on the ecology of *Ixodes scapularis*, the vector for Lyme disease (LD) in the northeastern United States. However, the ecology of their hosts is equally as important to understanding how tick-borne disease (TBD) risk may change in space and time (Goodwin et al., 2001; Ostfeld et al., 2001; Linske et al., 2018).

The primary hosts for *I. scapularis* larvae and nymphs are small vertebrates, such as mice, chipmunks, squirrels, birds, and in the southeast lizards and skinks (Ginsberg et al., 2021). Hosts are a critical component within the life cycle of ticks, which require a blood meal to survive and reproduce, it also where pathogens reside (Gray et al., 2002; Stanek et al., 2012). With respect to TBDs, some hosts are more important than others (Barbour et al., 2015; Levi et al., 2016). Mice (*Peromyscus leucopus*) are an important blood-meal host for early life stage ticks (Ostfeld et al., 2018), and are unaffected by tick burden by tick burden (Brunner & Ostfeld, 2008; Hersh et al., 2014; Dhawan et al., 2018), and they are competent reservoirs for the etiological agent of Lyme disease, *Borrelia burgdorferi* (LoGiudice et al., 2003).

I have shown that mouse abundance is useful to predict the density of questing *I. scapularis* ticks, especially nymphs, which has been demonstrated via model selection in Chapter 1and for short and intermediate forecasts in Chapter 2. The models developed in prior chapters included information flow from mice as a driver to tick juvenile transition. The mechanism underlying this impact on transition rate is that mice remove individuals from the questing nymph pool, thereby constraining nymph forecasts. In the current model we leverage paired sampling of off- and on-host ticks at NEON sites to estimate both tick demographic rates and presence on mouse hosts. Further, we specifically examine frequency of state changes in mouse hosts, which itself has important implications for tick-borne diseases.

The current model estimates parasitism state as the presence/absence of ticks on mice. Quantifying how this state changes intra- and inter-seasonally has important implications for TBDs (Brunner & Ostfeld, 2008). It is a measure of successful tick questing, which will further our understanding of tick phenology and the risk of humans encountering ticks (and potentially contracting a TBD).

To describe the parasitism states of mice, we employ the use of multi-event models (MEM) (Pradel, 2005), which are an extension of multistate models. A multistate model keeps track of the state of an individual (disease status, site found). The multi-event approach adds the step (event) of parametrizing the identification the individual to a certain state. This approach allows us to use censored, or “unknown” state observations, rather than discarding them, which leads to less biased and more precise parameter estimates (Conn & Cooch, 2009; Desprez et al., 2013). Additionally, MEM allows for the

ability to distinguish detection probabilities by ecological state (i.e., presence/absence); i.e. partitioning observation probability from state assignment probability. This has shown to an important modeling technique to identify and constrain breeding status (Couet et al., 2019) and disease prevalence (Jennelle et al., 2007). For example, using this approach (Murray et al., 2009) found that chytrid fungus (*Batrachochytrium dendrobatidis*) infection did not affect detection rates of the rainforest treefrog (*Litoria pearsoniana*).

MEMs have been used in ecology for over a decade to estimate demographic parameters such as survival and reproduction (Couet et al., 2019; Lebreton et al., 2009). These models have also been used in disease ecology to estimate disease status (Buzdugan et al., 2017), cause-specific mortality (Ruette et al., 2015), and sex uncertainty (Genovart et al., 2012). And while these models are useful for classifying individuals to a certain state, a key feature is their ability to estimate the rate of transition between states. For example, the transition to a disease-positive state (seronegative to seropositive) was more likely than the reverse in rabbits with respect to myxoma virus and Rabbit Hemorrhagic Disease Virus (Santoro et al., 2014). Likewise, (Choquet et al., 2013) showed found the same likelihood in a seabird (Black-legged Kittiwake, *Rissa tridactyla*) with respect to *Borrelia burgdorferi*/. (Conn & Cooch, 2009) used MEM approach show that being able to include individuals marked as unknown reduced parameter error in a MEM of conjunctivitis in house finches (*Carpodacus mexicanus* Müller).

MEM models can also be used in a data-fusion framework, combining multiple sources of information to estimate the state of interest. For example, (Ruette et al., 2015)

used radio-tracking and recoveries of dead martens (*Martes foina*) to estimate sex- and age-specific survival rates. Furthermore, (Buzdugan et al., 2017) were able to identify a temporal trend in infection status for wild badger (*Meles meles*) populations by blending ecological and epidemiological data.

The objective of this chapter is to quantify temporal trends in host use by ticks using the MEM approach. Specifically, we make use of data from the National Ecological Observatory Network (NEON). NEON data should be representative of data quality and types more generally available, include missing data, capture & detection challenges, and also represent more unique pairing of drags with tick on mice observations.

We use a data fusion approach, that begins by estimating tick density through time, and then uses this to constrain the presence/absence of ticks on mice. Ticks collected by NEON include multiple species which are recovered in multiple land cover types. Here, we focus on the two most abundant tick species collected by NEON; *Ixodes scapularis* (Ixodidae) and *Amblyomma americanum (*Ixodidae). *I. scapularis* has a broad geographic range in the eastern and midwestern United States (Sonenshine, 2018), which overlaps with the geographic extent of *A. americanum* and is also found throughout the eastern U.S. (Monzón et al., 2016; Springer et al., 2015). This means there is a substantial overlap in geographic extent between these two medically important tick species. Both species have three post-egg life stages (larvae, nymph, and adult), and they are both generalist host feeders.

In both species, the ability to find a suitable host affects molting success and

fecundity (Brunner et al., 2011; Labruna et al., 2000; Wilson et al., 1990).Where they differ is in their host-seeking behavior and phenology (Kollars et al., 1999, 2000; Schulze et al., 2005; Hroobi et al., 2021). In general, *I. scapularis* has a "wait-and-see" questing strategy, where they quest vertically along the vegetation column, but in general do not actively seek hosts (Mathisson et al., 2021). Meanwhile, *A. americanum* has a more aggressive host-finding strategy, actively searching for hosts and moving more horizontally through the vegetation (Mays et al., 2016; Schulze et al., 2005).This behavioral difference has implications for off-host survival, and potentially reproduction. For example, *I. scapularis* seems to be more susceptible to desiccation than *A. americanum*, presumably because they spend less time exposed, and/or quest at different times of day (Bacon et al., 2021; Schulze et al., 2001, 2002). This may be because, in terms of habitat, both species can be found in a variety of vegetation types but *A. americanum* tends to be more habitat generalists, and *I. scapularis* tend to be found in more covered (i.e. forested) landscapes (Mathisson et al., 2021).

To explain tick population dynamics across NEON sites for two species of ticks, we use the same four-stage matrix modeling approach described in Chapter 1, which employs a generalized mixed-effects model framework to parameterize demographic rates for each species. Specifically, we use fixed effects of species (*A. americanum* and *I. scapularis*) and forest type (forest and non-forest) to describe demographic parameters and ultimately estimate tick density. We also hypothesize that *A. americanum* will have higher survival rates in non-forested plots compared to *I. scapularis* because of the habitat preferences of *I. scapularis*.

We hypothesize that estimated tick density will have a positive effect on mice acquiring ticks; the more ticks are on the landscape, the chances of a mouse having just a single tick on it will go up, as tick burden is positively associated with tick density (Brunner et al., 2011). We hypothesis, then, that as tick density increases the probability of a mouse switching from ticks present to ticks absent will go down.

Furthermore, due to differences in questing strategy we expect this relationship to be stronger at NEON sites that are predominantly *I. scapularis* dominated because of the stronger predictive relationship they have with their hosts (Brunner & Ostfeld, 2008).

Methods

All data intake and cleaning, and statistical and graphical analysis were done in R v4.0.2 (R Core Team, 2020). NEON data was downloaded from NEON's API using the neonstore package (Boettiger et al., 2021), Daymet meteorological data was downloaded with the daymetr package (Hufkens et al., 2018), and Bayesian modeling was implemented in NIMBLE (de Valpine et al., 2017, 2022).

Tick Data

The tick data used here is the same for Chapter 3, which has a complete explanation of the data, data cleaning, and NEON sampling design. Briefly, we used data from the product DP1.10093.001 *Ticks sampled using drag cloths* (National Ecological Observatory Network (NEON), 2022b; Paull et al., 2022). We used *Amblyomma americanum* and *Ixodes scapularis* identified to species, and larvae records identified to family (Ixodidae).

Table 4.1 NEON site descriptions

Site Code	Site Name	Tick Species	# Plots (tick / mice)	Latitude	Longitude	State	NEON Domain
BLAN	Blandy Experimental Farm	AA & IX	6 / 5	39.03	-78.04	VA	Mid-Atlantic
HARV	Harvard Forest & Quabbin Watershed	IX	7 / 8	42.54	-72.17	MA	Northeast
KONZ	Konza Prairie Biological Station	AA	6 / 8	39.10	-96.56	KS	Prairie Peninsula
LENO	Lenoir Landing	AA & IX	6 / 7	31.85	-88.16	AL	Ozarks Complex
OSBS	Ordway-Swisher Biological Station	AA	9 / 6	29.69	-81.99	FL	Southeast
SCBI	Smithsonian Conservation Biology Institute	AA & IX	7 / 7	38.89	-78.14	VA	Mid-Atlantic
SERC	Smithsonian Environmental Research Center	AA & IX	6 / 8	38.89	-76.56	MD	Mid-Atlantic
TALL	Talladega National Forest	AA	6 / 8	32.95	-87.39	AL	Ozarks Complex
TREE	Treehaven	IX	6 / 6	45.49	-89.59	WI	Great Lakes
UKFS	Kansas University Field Station	AA	6 / 6	39.04	-95.19	KS	Prairie Peninsula

Table 4.1: Overview of the NEON sites included in the analysis. Tick species shows which tick species are modelled at each site (AA: *Amblyomma americanum*; IX: *Ixodes scapularis*). # plots is the number of plots at each site for each organism.

One characteristic recorded for each NEON plot is land cover classification, which includes cultivated crops, deciduous forest, emergent herbaceous wetlands, evergreen forest, grassland herbaceous, mixed forest, and pasture-hay, and woody wetlands. Ticks collected by drag cloths are not equally distributed among the land cover classifications and most ticks are found in the forested (deciduous, evergreen, mixed forest) plots. To increase the number of non-forest plots to use, we grouped plots into forest and non-forest groups.

Small Mammal Data

The small mammal data product used was DP1.10072.001 *Small mammal box trapping* (National Ecological Observatory Network (NEON), 2022a). Like the ticks, the small mammals are identified to taxonomic rank, and we kept all individuals identified to the genus Peromyscus, which included *P. leucopus* and *P. maniculatus*. A trapping bout could include anywhere from one to three nights of trapping, however as our model works daily, we created the capture history matrix so that every capture day is represented as a column, and individuals as rows.

The small mammal data keeps track of the status of each mouse (captured alive or found dead), and whether or not the individual mouse has ticks attached, does not have ticks attached, or the presence/absence of ticks is unknown. Therefore, our capture history matrix includes the following four observed states: mouse alive with ticks attached, mouse alive without ticks attached, mouse alive with unknown tick status, and recovered dead.

The mouse analysis was conducted at the same 10 NEON sites as the ticks. Furthermore, trapping grids, and therefore individual trap nights, were observed at the same NEON plot level. However, because some animals were caught across plots capture matrices were constructed at the site level.

Cumulative growing degree days

Daily weather variables were extracted from the Daymet data product (Thornton et al., 2020) using the latitude and longitude for each site Table 4.1. Specifically, we used

daily maximum temperature at each NEON site to calculate daily cumulative growing degree days (CGDD) within each year with a threshold temperature of 0°C. We then used the CGDD to determine the phenological periods that each life stage of each species should be questing at each site. The determination of start and end of the questing period was determined by sorting the counts (of each species-life stage-site group) by CGDD and removing observations that were less than one percent of the maximum observed count. This not only removes zeros but also removes small counts before the onset and behind the tail of the questing period. This done at the site level because some plots' time series were not variable enough to calculate thresholds. We confirmed these thresholds by graphical analysis and adjusted as necessary. Thresholds were adjusted for adults at LENO and TREE because the start and end of the questing period were calculated to be the same because the adult data was not variable enough at these sites.

Statistical frameworks

Species were kept separate but were in the same model, which was a stage-structure matrix model with four stages: questing larvae, dormant nymphs, questing nymphs, and questing adults. This is a similar structure to the "static" models used in previous chapters (no time-varying covariates on survival or transition), except now we extend across species and forest and non-forest groups.

Daily demographic parameters were modeled as

$$logit(\theta_{j,k}) = \beta_0 + \beta_1 S_j + \beta_2 F_k \quad [1]$$

$$log(\lambda_{j,k}) = \beta_0 + \beta_1 S_j + \beta_2 F_k \quad [2]$$

where Θ is our daily (non-reproductive) demographic parameter of interest (larvae survival, nymph survival, adult survival, larvae-to-nymph transition, nymph-to-adult transition), and λ is fecundity, for species *j* in land cover type *k*, β_0 is the mean demographic rate for *I. scapularis at forested sites*, *S* as the indicator variable for *A. americanum*, and *F* as the indicator variable for non-forest.

To aggregate across observation days, we permuted the matrices as follows:

$$\boldsymbol{P_{i,j,t}} = A_{\boldsymbol{i,j,t}}\boldsymbol{A_{i,j,t-1}A_{i,j,t-2}\ldots A_{i,j,1}} \quad [3]$$

$$\overrightarrow{x_{\boldsymbol{\iota,J,t+1}}} \sim MVN(\boldsymbol{P_{i,j,t}}\overrightarrow{x_{\boldsymbol{\iota,J,t}}}, \Sigma_j) \quad [4]$$

Where **A** is the transition matrix (Table S4.1) at plot *i* for species *j*, on day *t*. **P** is the permuted transition matrix that is used to calculate the expected demographic transitions between sampling occasions. Then, the predicted latent density of ticks (ticks/m^2), $x_{i,j,t+1}$, was drawn from the multivariate normal distribution based on the expected number of ticks, $\boldsymbol{P}_{i,j,t}\overrightarrow{x_{\iota,J,t}}$, and a process error covariance matrix $\boldsymbol{\Sigma}_j$, which was parameterized as a diagonal matrix of variances, where there is a different covariance matrix for each species *j*. $\boldsymbol{\Sigma}_j$ does not permute.

The data model for nymph and adult ticks is:

$$y_{l,j,i,t} \sim Poisson(x_{l,j,i,t} * a_{i,t}) \quad [5]$$

Where *x* is the estimated latent density of life stage *l* of species *j*, at plot *i*, at time *t*, *a* is the area sampled (effort), and sampling error is modeled with a Poisson distribution using the observed counts *y*.

At sites where only one species is present, larvae were modeled using the same data model as nymphs and adult ticks. For sites where we cannot assume what species that larvae belong to, we modeled the proportion of the larval pool that belongs to each species as follows:

$$\psi_{i,t} = \frac{d * a_{i,t}}{1 + d * a_{i,t} + x_{2,i,t} * a_{i,t}} \quad [6]$$

$$L_{i,t} \sim binomial(\psi_{i,t}, y_{i,t}) \quad [7]$$

Where $\Psi_{k,t}$ is the probability that larvae in plot *i* at time *t* are *A. americanum*, which is given by the estimated larval count of *A. americanum* at plot *i*, at time t over the sum of both species. We add one to the denominator so that we don't divide by zero when the estimated count is zero for both species. The count of *A. americanum* larvae observed in each plot at time t, L is then estimated using $\Psi_{k,t}$ constrained by the total number of larvae observed, *y* in plot *i* at time *t*.

Mouse parasitism

We fit the multistate model below using a marginalized distribution implemented in NIMBLE, which drastically reduces computation time, especially over a large capture history matrix (in this case 4950 mice by 364 trapping occasions). The marginalization was conditional on the first capture.

Mouse status was modeled under a multievent Jolly-Seber framework. In the transition matrix (Table xx) rows represent the true state of a mouse at time *t*, and the columns represent the true state of a mouse at time *t+1*, where *t* marks capture events, and the probability of moving from one state to another from *t* to *t+1* is within the matrix. The four latent states are: the mouse is alive with ticks present (AP), mouse alive with ticks absent (AA), a mouse recently died (RD), and the absorbing dead state (D).

Transition matrix of mouse states from *t* (rows) to *t+1* (columns)

$$\begin{array}{c} \\ AP_t \\ AA_t \\ RD_t \\ D_t \end{array} \begin{array}{c} \begin{array}{cccc} AP_{t+1} & AA_{t+1} & RD_{t+1} & D_{t+1} \end{array} \\ \begin{bmatrix} \phi_{p,s}(1-\psi_{pa,s}) & \phi_{p,s}\psi_{pa,s} & r(1-\phi_{p,s}) & (1-r)(1-\phi_{p,s}) \\ \phi_{a\,s}\psi_{ap,s} & \phi_{a,s}(1-\psi_{ap,s}) & r(1-\phi_{a,s}) & (1-r)(1-\phi_{a,s}) \\ 0 & 0 & 0 & 1 \\ 0 & 0 & 0 & 1 \end{bmatrix} \end{array} \quad [8]$$

Within the transition matrix $\phi_{p,s}$ is the survival probability of mice with ticks present at site *s*, and $\phi_{a,s}$ the survival of mice without ticks attached. $\Psi_{pa,s}$ is the

probability a mouse switches from having ticks attached to not having ticks attached (p-to-a), and $\Psi_{ap,\,s}$ is the probability a mouse switches from not having ticks attached to having ticks attached (a-to-p). *r*, the probability of recovering a mouse that has recently died (does not vary by site), is in the state transition matrix (instead of the observation matrix) to allow for better MCMC mixing (Kéry & Schaub, 2011). The parameters inside the transition matrix varied by site.

Survival was modeled hierarchically by mouse state:

$$\alpha_p \sim N(\mu, \sigma) \quad [9]$$

$$logit(\phi_{p,s}) \sim N(\alpha_p, \sigma_p) \quad [10]$$

Where α_p is the base daily survival rate of mice with ticks present. This was given a semi-informative prior where $\mu = 5$ and $\sigma = 1/\sqrt{0.1}$. This is semi-informative because the mean reflects our prior knowledge from Chapter one that the daily mouse survival rate is high, but the prior standard deviation is still relatively wide. The base survival rate, α_p, was then used as the mean for site-specific survival rates of mice with ticks present. The same formulation was used for estimating the daily survival rate of mice with ticks absent, $\phi_{a,s}$.

Our data fusion framework uses tick densities from the models above to constrain the daily transition parameters $\Psi_{pa,\,s}$ and $\Psi_{ap,\,s}$ following a simple linear model:

$$logit(\psi_{k,s,t}) = \beta_{1,s} + \beta_{2,s} * tickDensity_{s,t} \quad [11]$$

Where $\Psi_{k,\,s,\,t}$ is the transition parameter *k* at site *s* at time *t*, which is a function of site-specific slopes and intercepts and estimated site-specific tick density accounting for

error following a Gaussian errors-in-variables model. As ticks were estimated at the plot level, and mice at the site level, we summed the mean site densities across plots to get the total tick density at each site. Site-level variance was estimated as:

$$Var(y) = \sum_{i=1}^{n} var(x_i) + 2\sum_{i<j} cov(x_i, x_j) \quad [12]$$

where *y* is the total site-level variance across *x* plots from *1…j*. Tick densities were centered and scaled by site-specific tick density standard deviations.

To estimate survival and transition probabilities across trapping occasions, which are heterogeneous in time, we used the following:

$$log\ (\theta_t) = \sum_{d=\Delta t}^{t}(log\ (\theta_d)) \quad [13]$$

Where Θ is our parameter of interest in the transition matrix (ϕ or Ψ), *d* indexes the daily estimate of that parameter over the number of days between trapping occasions (Δt). *t* is then the aggregated rate from trapping occasion *t-1* to *t*.

The observation matrix ties the true state of the mouse at trapping occasion *t* to the observed state of the mouse at trapping occasion *t*. There are five types of observations; mouse alive with ticks present (AP), mouse alive with ticks absent (AA), mouse alive with unknown tick status (AU), a mouse recovered dead (RD), and a mouse not captured, or unobserved (U). Note that the row title RD stands for a mouse that recently died (the mouse state), and the column heading RD is for a mouse recovered

dead (the observation made).

Observation matrix: the probability of observing mice (columns) in state *t* (rows) at time *t*

$$\begin{array}{c} \\ AP_t \\ AA_t \\ RD_t \\ D_t \end{array} \begin{array}{c} \begin{array}{ccccc} AP_t & AA_t & AU_t & RD_t & U_t \end{array} \\ \begin{bmatrix} \theta_{p,s}\Gamma_{p,s} & 0 & \theta_{p,s}(1-\Gamma_{p,s}) & 0 & (1-\theta_{p,s}) \\ 0 & \theta_{a,s}\Gamma_{a,s} & \theta_{a,s}(1-\Gamma_{a,s}) & 0 & (1-\theta_{a,s}) \\ 0 & 0 & 0 & 1 & 0 \\ 0 & 0 & 0 & 0 & 1 \end{bmatrix} \end{array} \quad [14]$$

Within the observation matrix define $\Theta_{p,s}$ and $\Theta_{a,s}$ as the probabilities of capturing a mouse with ticks present (p) or absent (a), respectively, at site *s*. θs represent the observation event, and is why the unobserved (column U) probabilities are $1-\theta$. The identification events are defined as $\Gamma_{p,s}$ and $\Gamma_{a,s}$. $\Gamma_{p,s}$ is the probability of identifying a mouse as having ticks attached *given* that its latent state is that it is alive with ticks present *and* it was captured. $\Gamma_{a,s}$ is the probability of identifying a mouse as not having attached *given* that its latent state is that it is alive without ticks attached *and* it was captured.

Results

Mouse observation model

The probability of capturing a mouse was variable across sites and tick status (Figure 4.1, Table S4.2). At the southern sites, the probability of capturing a mouse with ticks attached was low. For example, at OSBS the median capture rate of mice with ticks attached was 0.02 (95% CI 0.0 – 0.06). The site with the highest capture probability for mice with ticks attached was SERC, with a median rate of 0.52 (95% CI 0.46 – 0.59). The probability of capturing mice without ticks attached was less variable across sites. The lowest estimate was at SCBI with a median capture rate of 0.19 (95% CI 0.17 – 0.23), and the highest capture rate of mice without ticks attached was at BLAN with a median capture rate of 0.62 (95% CI 0.57 – 0.68).

The estimated rate of correctly identifying whether mice had ticks attached (Γ) or not was high (Table S4.2). The median rate of correctly identifying that a mouse has ticks attached when ticks were truly attached was 0.76 (95% CI 0.74 – 0.78). Correctly identifying a mouse without ticks when ticks were truly absent was 0.97 (95% CI 0.96 – 0.98). The probability of recovering a mouse dead was very low, with a median of 0.005 (95% CI 0.008 – 0.011).

Figure 4.1 - Capture probability by site

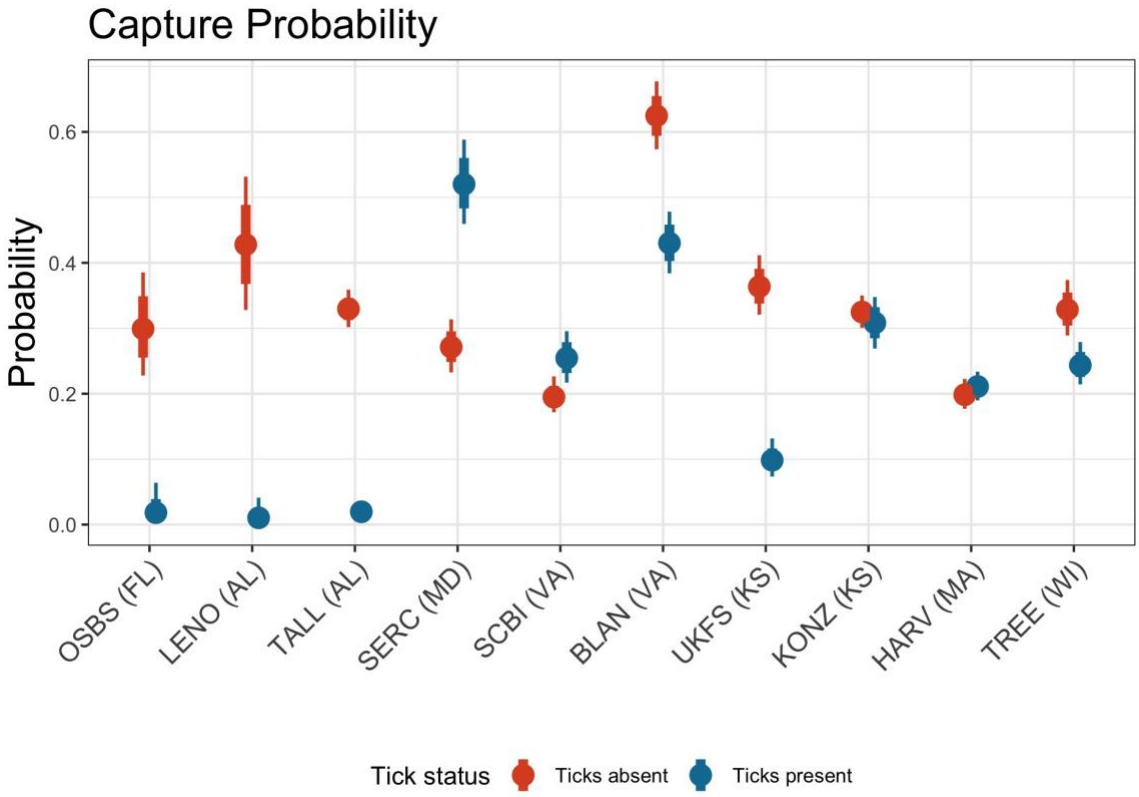

Figure 4.1 - Site-specific capture probabilities ($\boldsymbol{\theta}$) estimated from models fit to data at each of the 10 NEON sites (state), which are ordered on x axis by latitude. The capture rates for mice with ticks present are in blue, and mice without ticks in red. Points are the median estimate, thin whiskers are the 95% CI, and wide whiskers are the 75% CI. These rates are very precise, which is why some whiskers are not shown (covered by the point).

Process (state-transition) model

Mean mouse survival (α) was higher for mice with ticks absent than for mice with ticks present (Figure 4.2). Mice with ticks absent had a mean monthly survival rate of 0.68 (95% CI 0.57 – 0.77), while mice with ticks present survived at a monthly rate of 0.61 (95% CI 0.47 – 0.72).

Figure 4.2 – Base monthly mouse survival rate

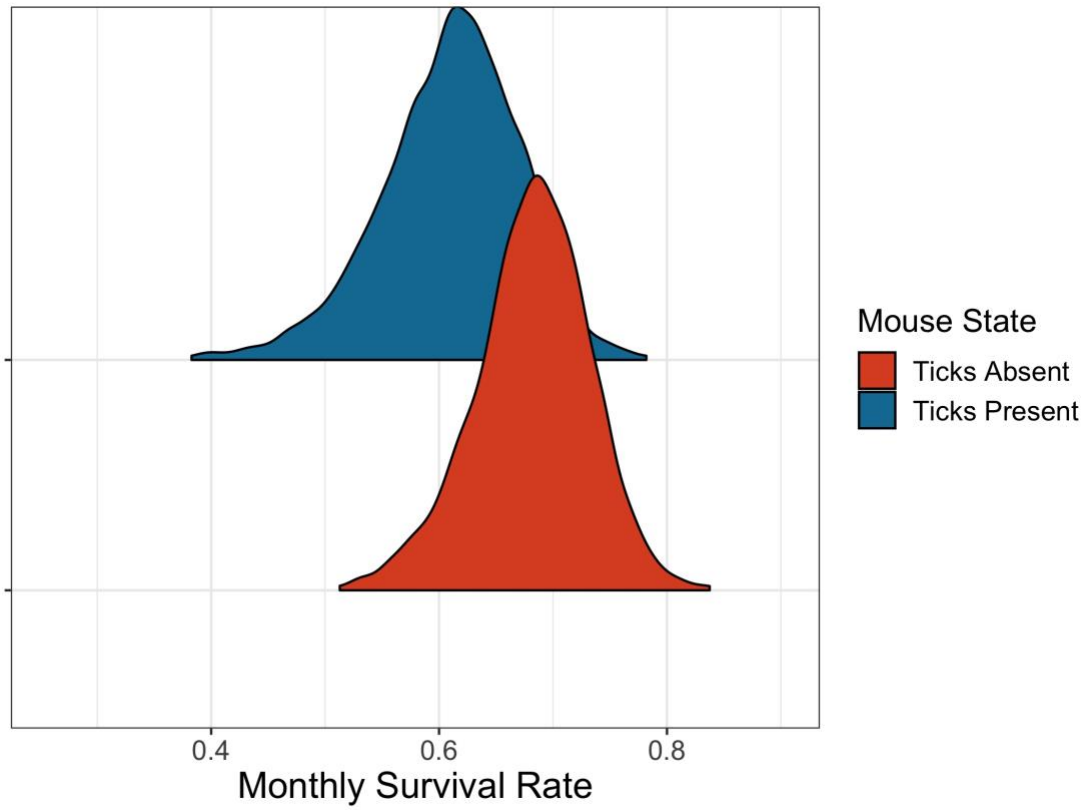

Figure 4.2 – Mean monthly survival rate or mice ($\boldsymbol{\alpha}$, eqn. 9) for each mouse state. Survival of mice with ticks absent is in blue, those with ticks present in red.

Monthly survival rates varied across mouse status and site (Figure S4.1). On the low end, mice with ticks absent survived at a monthly rate of 0.46 (95% CI 0.4 – 0.49) at SCBI. Mice with ticks absent had the highest monthly rate of survival at TALL of 0.76 (95% CI 0.72 – 0.78). Mice with ticks present generally survived at a lower rate at each site compared to mice without ticks present, except at SERC, SCBI, and BLAN. The highest monthly survival rate for mice with ticks present was at SCBI of 0.73 (95% CI 0.66 – 0.8), and lowest was at TREE with a median of 0.47 (95% CI 0.38 – 0.56).

The daily rate of changing states (intercept, eq. 11) for the present to absent (p-to-a) or absent to present (a-to-p) transition was variable across sites, and generally increased from south to north (Figure S4.2). At the most southern site, OSBS, the p-to-a transition was estimated at a daily rate of 0.74 (95% CI 0.36 – 0.94). At the most northern site, the daily p-to-a transition was estimated at 0.86 (95% CI 0.82 – 0.91). The a-to-p transition at OSBS was estimated at 0.38 (95% CI 0.15 – 0.63), and at TREE it was a daily rate of 0.94 (95% CI 0.92 – 0.95).

The effects of tick density on mouse state transitions (either direction) were inconsistent across sites, or effects were generally small (Figure 4.3). For the sites that are dominated by *Ixodes scapularis* (HARV and TREE), there was little effect of tick density on the a-to-p transition, and a small but negative effect of tick density on the p-to-a transition; at HARV the effect of tick density on the p-to-a transition was -0.12 (95% CI -0.3 – 0.08), at TREE the effect was -0.23 (95% CI -0.57 – 0.13). The median effect of tick density at sites dominated by *Amblyomma americanum* (UKFS, TALL, OSBS, KONZ) varied across sites, but in general the effect was not different than zero except at TALL. At TALL the effect of tick density was negative for both transitions; -0.67 (95% -1.93 – -0.09) for the a-to-p transition and -0.28 (95% -0.72 – 0.04) for the p-to-a transition.

The sites were both tick species are found (SERC, SCBI, LENO, BLAN) had similar estimates of the effect of tick density within each site, and the effects decreased from south to north. For example, the effect of ticks on the p-to-a transition at LENO (located in Alabama) was 2.17 (95% CI 1.11 – 3.38) and at BLAN (located in Virginia)

Figure 4.3 - Slope estimates for the effect of tick density on mouse state transitions

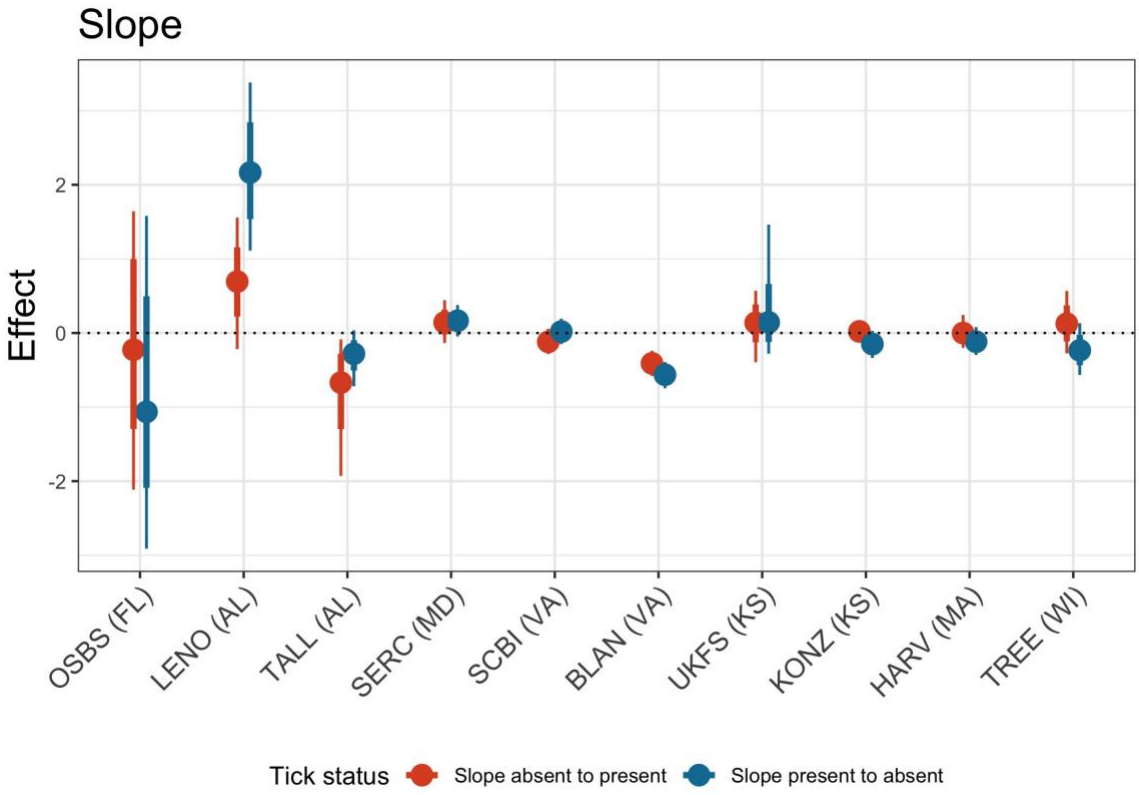

Figure 4.3 - Site-specific slope estimates, mouse transitions arranged on the x-axis by latitude (south to north) - The effect of modeled tick density on the state transition of mice. Effect of tick density on the mice transition rate from ticks present to absent are in blue, the other direction (absent to present) in red. Points are the median estimate, thin whiskers are the 95% CI, wide whiskers are the 75% CI. The dotted horizontal line at zero is plotted to show the limit of no effect.

the effect was -0.56 (95% CI -0.75 – -0.39). For completeness, the effect of tick density on the a-to-p transition at LENO was 0.69 (95% CI -0.22 – 1.56) and at BLAN the effect was -0.41 (95% CI -0.58 – -0.24).

Tick-stage structured model

Here we present the posterior estimates for demographic parameters, which includes the influence of the fixed effects, that are in Figure 4.4. Larvae *A. americanum* had a median monthly survival rate of 0.71 compared to < 0.01 of *I. scapularis*. Nymph survival was similar for both species, where *A. americanum* survived at a rate of 0.37/month and *I. scapularis* at a rate of 0.29/month. Like the larvae, the non-forest effect was centered on zero with a wide interval estimate. Median monthly adult survival varied considerably across species, where *I. scapularis* survived at a rate of < 0.01, *A. americanum* had a median monthly survival rate of 0.22.

The daily transition rate from larvae to nymph was the same within species. *A. americanum* had daily larvae to nymph transition rate of 8.80E-06 (3.02E-06 – 2.07E-05 95%CI) and 8.62E-06 (8.13E-07 – 9.68E-05) in forest and non-forest plots, respectively. *I. scapularis* had a slightly higher daily larva to nymph transition rate of 2.20E-03 (6.03E-04 – 0.01) and 2.12E-03 (1.86E-04 – 0.03) in forest and non-forest plots, respectively.

Median nymph to adult transition rates was slightly higher than from larvae to nymph, and similar for both species. *A. americanum* had a median nymph to adult transition rate of 3.41E-03 and 3.10E-03 in forest vs non-forest plots, whereas *I. scapularis* had a rate of 4.41E-03 and 4.08E-03 in forest vs non-forest plots. Precision was higher in forested groups (Table 4.2).

Table 4.2 Summary of tick demographic parameters

Parameter	Life Stage	Species	Cover Type	Median	Lower 95%	Upper 95%
Survival	Larvae	AA	Forest	0.71	0.56	0.83
			Non-forest	0.71	0.04	0.97
		IS	Forest	1.49E-03	1.95E-08	0.13
			Non-forest	1.49E-03	1.53E-18	0.56
	Nymphs	AA	Forest	0.37	0.30	0.43
			Non-forest	0.37	3.38E-04	0.89
		IS	Forest	0.29	0.22	0.35
			Non-forest	0.29	4.97E-05	0.87
	Adults	AA	Forest	0.22	0.10	0.37
			Non-forest	0.23	6.07E-06	0.85
		IS	Forest	4.61E-05	3.20E-10	0.02
			Non-forest	5.78E-05	2.00E-23	0.37
Transition	Larvae to nymph	AA	Forest	8.80E-06	3.02E-06	2.07E-05
			Non-forest	8.62E-06	8.13E-07	9.68E-05
		IS	Forest	2.20E-03	6.03E-04	0.01
			Non-forest	2.12E-03	1.86E-04	0.03
	Nymph to Adult	AA	Forest	3.41E-03	1.27E-03	0.01
			Non-forest	3.10E-03	2.77E-04	0.03
		IS	Forest	4.41E-03	1.61E-03	0.01
			Non-forest	4.08E-03	3.66E-04	0.04
Reproduction	Adult to Larvae	AA	Forest	3.17	0.74	8.56
			Non-forest	2.98	0.22	34.03
		IS	Forest	39.12	8.67	119.75
			Non-forest	36.96	2.93	426.40

Table 4.2 – Posterior estimates of tick demographic parameters for *A. americanum* (AA) and *I. scapularis* (IS) in forest and non-forest plots.

Reproduction differed between species but not between forest and non-forest sites. *A. americanum* had a median reproduction rate (number of larvae produced from a single adult per day) of 3.17 (0.74 - 8.56 95%CI) and 2.98 (0.22 - 34.03) in forest and non-forest habitats. *I. scapularis* had a median reproduction rate of 39.12 (8.67 - 119.75) and 36.96 (2.93 - 426.4) in forest and non-forest habitats. Despite the difference in data source type, the current model's estimate for *I. scapularis* reproductive rate was

consistent with the median reproductive estimate from the Cary data (Chapter 1). For all demographic parameters, and their comparison to the Cary fits from Chapter 1, see supplementary Figures S4.3 (survival) and S4.4 (transition).

Discussion

In this study, we used a multievent capture-recapture model to explore the role that tick densities have on the parasitism status, and the rate of change in parasitism status, of mice across several NEON sites. We also quantified how demographic parameters differ across habitat (forest vs. non-forest), and species (*I. scapularis* vs *A. americanum*). Generally, the temporal change in tick density drives the temporal variation of parasitism status in mice as an inverse relationship (Figure 4.5), most notably on the transition from ticks present to ticks absent. On the first pass, it would seem like this relationship is different than that of (Brunner & Ostfeld, 2008). They found a positive relationship between the densities of larval and nymphal ticks and actual tick burden (the number of ticks attached), while our study focuses on the presence/absence transition rates of ticks on mice.

Figure 4.4 - Tick model fixed effects

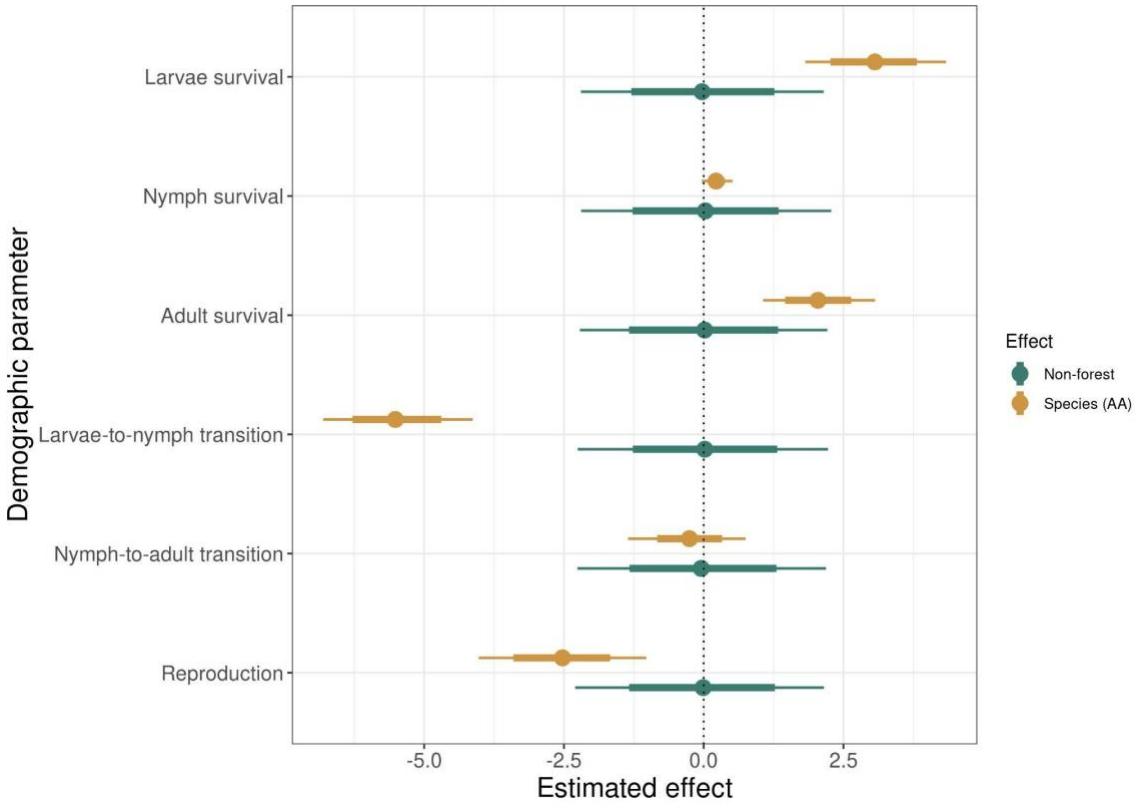

Figure 4.4 - Fixed effects on demographic parameters for ticks - The effects for a tick being *A. americanum* are in yellow and being in a non-forest habitat are in green. Fixed effects were placed on each demographic parameter, which is on the y-axis. Points are the median estimate, thin whiskers are the 95% CI, and wide whiskers are the 75% CI. Note the log scale on the y-axis.

Our results estimated a small effect of tick parasitism on mouse survival and are in line with other studies (Brunner & Ostfeld, 2008; Hersh et al., 2014; Dhawan et al., 2018), suggesting that mouse mortality is largely due to other factors, such as predation (Collins & Kays, 2014). We also showed that monthly mouse survival differed across

NEON sites and parasitism status (Figure S4.2). Moreover, monthly survival rates were often above 0.5, confirming that mice are capable of surviving in a wide range of habitats (Geier & Best, 1980; Nupp & Swihart, 1996, 2000; Linske et al., 2018).

The inverse relationship between tick density and the presence/absence transition rates of ticks on mice also means that as tick density increases, the probability of remaining in the same state increases. The NEON sites used in this analysis were chosen, in part, because consistent tick observations were available. Therefore, we know that ticks are consistently present at these sites. Ticks require a blood meal to survive (Childs & Paddock, 2003; Anderson & Magnarelli, 2008), which means we know that ticks are feeding on hosts at these sites. This would suggest that our results are in agreement with (Brunner & Ostfeld, 2008) that most ticks aggregate on a subset of mice, and that a small percentage of ticks find hosts (Ginsberg et al., 2020).

Furthermore, we extend this relationship to show that the degree of aggregation appears to be of the same magnitude at both southern and northern sites, where *I. scapularis* and *A. americanum* are found, respectively (Figure 4.2). Interestingly, this result also supports the literature that ticks aggregate on mice less in southern sites, particularly during peak tick density (Ginsberg et al., 2021) (Figure 4.6). This is most likely due to the differences in questing behavior between northern and southern *I. scapularis* ticks, and between *I. scapularis* and *A. americanum*.

Figure 4.5 The relationship between tick density and mouse state transition

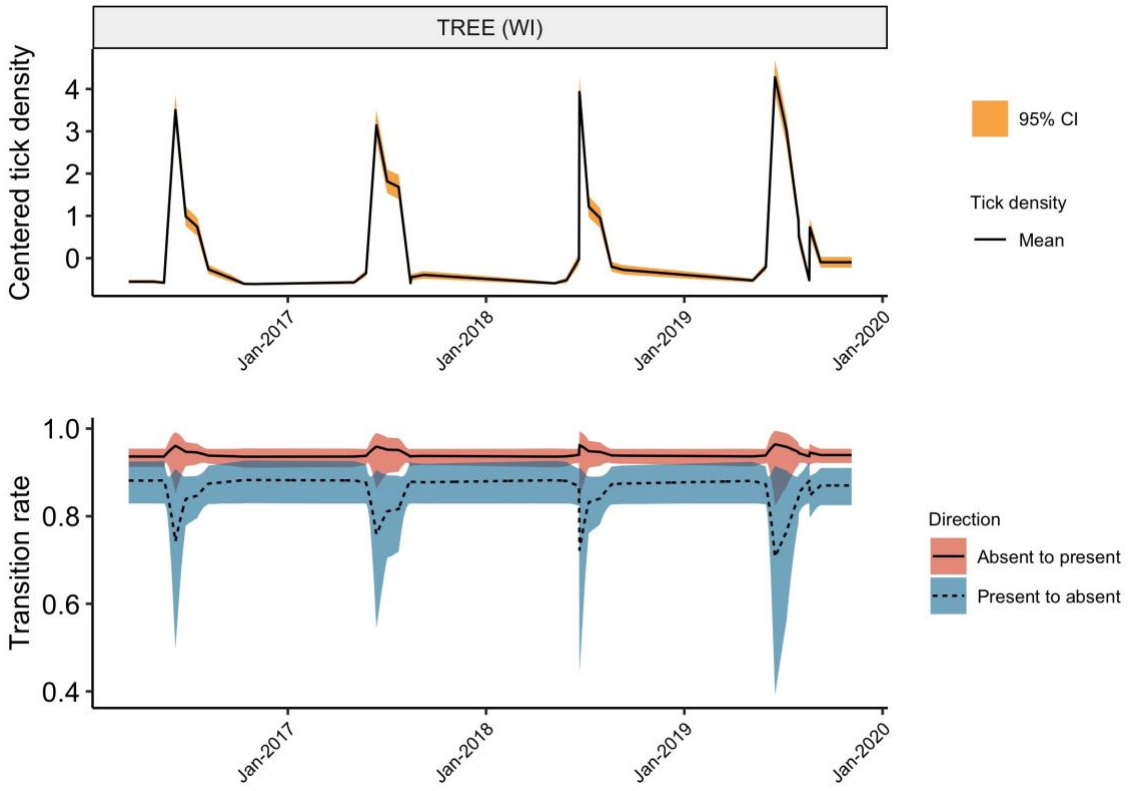

Figure 4.5 - Time series showing the relationship between estimated tick density (top row) and mouse state transitions (bottom row), for the northern TREE (located in Wisconsin, *I. scapularis* dominated) site. The yellow envelope around the tick densities is the 95% CI for estimated tick density. The red and blue envelopes are the 95% CI around estimated mouse state transition rates, red being the transition from ticks absent to ticks present, and blue the other direction.

For *A. americanum*, their primary host is white-tailed deer, meaning their aggregation on mice is reduced overall (Kollars et al., 2000; Paddock & Yabsley, 2007; Hertz et al., 2017), as their ability to find hosts, such as white-tailed deer, is far higher than small mammals (Mount et al., 1993).

With respect to *I. scapularis*, host aggregation on mice in southern environments is less because there is a more diverse community of hosts used by ticks (I. Arsnoe et al., 2019; I. M. Arsnoe et al., 2015) (Hertz et al., 2017; Ginsberg et al., 2021). However, even in northern environments (NEON sites HARV, TREE) where *I. scapularis* is the primary tick species, there was a total of 1344 individual mice captured, of which 35.7% (n = 480) never had ticks attached. Additionally, during periods of above average tick density at these two northern sites, roughly the same proportion, 34.6%, of mice never have ticks attached (299 mice never captured with ticks over 865 individual mice captured during peak tick density).

For ticks, demographic parameters that describe their populations vary by species and not by forest cover (Figure 4.4). Our result that forests vs non-forest habitats have no effect on demographic parameters should be viewed with some caution. To reach convergence in the stage-structured tick model, we had to remove NEON plots with less-than-ideal time-series data, and these removed plots were mostly classified as non-forest. Therefore, the absence of a clear habitat type effect is most likely due to sample size.

When we compare tick demographic parameters, there is an apparent trade-off between survival and reproduction exhibited by *A. americanum* ticks. Relative to *I. scapularis*, the daily reproduction estimated for *A. americanum* was reduced, and the daily survival rate of all life stages was higher. The survival reproduction trade-off could be viewed through the lens of individual heterogeneity, where individuals are competing for resources, i.e. hosts, which translates to fat and energy allocation (Alasmari & Wall,

2021). Essentially, energy expended on reproduction compromises survival (Cox et al., 2010).

Figure 4.6 Relative mouse parasitism status with respect to average tick density

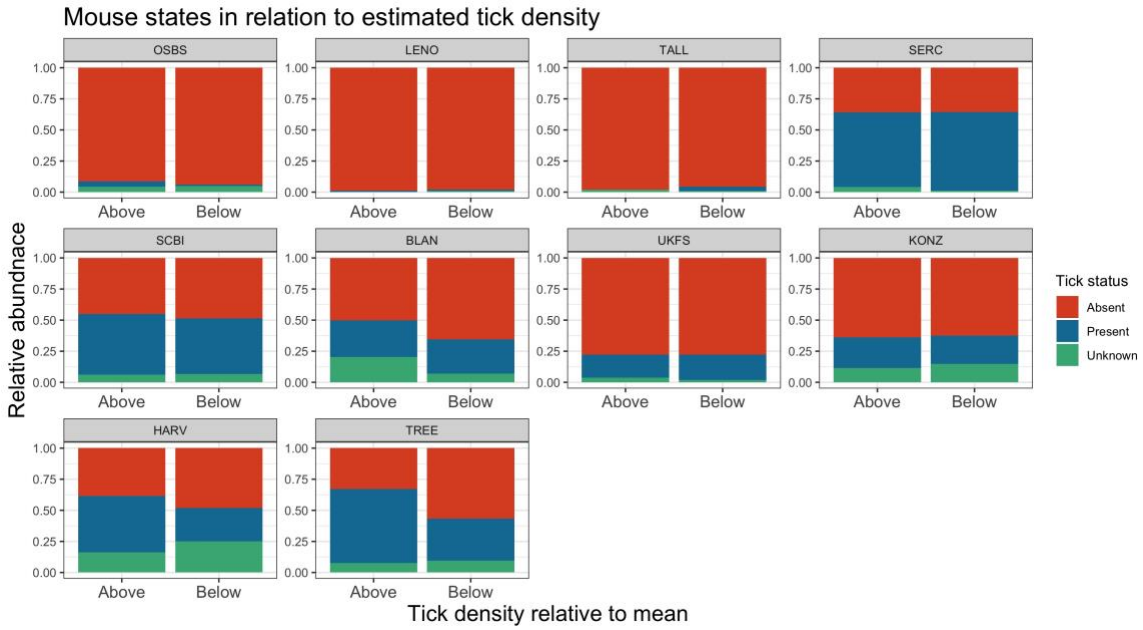

Figure 4.6 – The relative proportion of mice captured in each parasitism state, broken into the time of year during above average tick density and below average tick density at each site. Red are mice with ticks absent, blue with ticks present, and green are mice captured with unknown tick status. Each facet is a NEON site, and they are arranged by latitude with the most southern site (OSBS) in the top left, to the most northern site (TREE) on the bottom right.

Another explanation is that this trade-off could be happening because, for *A. americanum*, the environment is more favorable for survival than reproduction (Robert et al., 2015). This falls in line with (Marshall & Sinclair, 2010) who showed that repeated

stress exposure reduced reproduction in Drosophila. Furthermore, given extra resources so that individuals don't have to choose between survival and reproduction, reproduction increases in mosquitoes (Stone et al., 2011). The survival-reproduction trade-off could be due to *A. americanum's* active questing strategy, which would lead to higher fecundity (Brunner et al., 2011; Labruna et al., 2000; Wilson et al., 1990)**.**

As of 2019, NEON collection protocols changed to record the number of ticks attached to mice in discrete categories. A multievent modeling approach with a likelihood that includes mouse states for each tick-attachment category, and transitions parameters for movement into and out of each category, would shed more light on how ticks use mice across the NEON domain.

More extensions for the model include parameterizing mouse survival with weather covariates, and another constraint on parasitism status using total mice observed. Furthermore, the observation matrix (eqn. 14) could be reparametrized without the recovered dead (r) parameter because the estimate for r was essentially zero. All other demographic parameters describing the mouse population were precise, meaning removing the small number of mice recovered dead (n = 59) from the data should have little impact on posterior parameter precisions.

The outputs from the mouse model could be information used to further constrain transition parameters in stage-structured population models, such as those presented in earlier chapters. Specifically, if we know the onset and decline of host-use, the stage-structured tick models could use this information to inform either the process model (by way of questing activity) or the data model (observers, and therefore people, are less

likely to encounter ticks on drag cloth because they are attached to mice (Ostfeld, Levi, et al., 2018).

Furthermore, quantifying host-use has direct implications for the management of tick-borne diseases. Host-targeted mitigation efforts are often used to deliver acaracides to ticks (Tsao et al., 2021), meaning if we know when most mice will have ticks attached, these vehicle delivery systems would be more effective. Finally, this work represents an effort to fill a knowledge gaps outlined by Kilpatrick et al., (2017) in that we attempt to describe how hosts for larval ticks change through time, and by (Tsao et al., 2021) to describe biotic and abiotic factors affecting ticks through time and space.

CONCLUSION

This dissertation has been an exploration in building mechanistic forecasts for the main vector of Lyme disease. The first chapter started this process by building stage-structured models calibrated on daily basis for the populations at Cary. I found that including the dormant stage between questing larvae and questing nymph to be an important addition to the model, which also has biological and ecological significance. I also found that larval survival is most influenced by precipitation, and that nymphs were most influenced by mouse abundance. It also appears that the interplay between weather and mouse abundance improved model predictions. Adults were harder to predict than the other stages.

Chapter two was proof-of-concept for iteratively forecasting this population and is essentially a transfer-in-time experiment. I also showed the effectiveness of forward only data assimilation technique. This chapter showed that larval data are not necessary to forecast populations at year horizon, the caveat being larval data were used for model calibration. This has important implications for tick monitoring programs, where efforts could be moved to sample nymphs and/or adults.

Chapter three was an attempt to transfer the model in space to NEON sites along the east coast. The model calibrated at Cary overpredicted in every scenario, and models were dominated by process error. The overprediction was attributed to the spatio-temporal difference in data collection between Cary and NEON. The phenology that was built into the Cary model was evident when the model transferred, but hard to tell if this

parameterization was appropriate for the NEON sites given the magnitude of error. Encouragingly, the data assimilation updated parameters, attempting to correct for the mismatch in sampling design. Perhaps more time is needed for the model to adapt.

Lastly, in chapter four I modeled the mouse population across NEON to describe the temporal change in parasitism status in mice. This involved modeling calibrating a model to estimate the tick population, so that tick density could drive parasitism change. I found that tick density drives this change in an inverse relationship, and that most ticks use a subset of mice.

Future directions, and one thing I regret not having the opportunity to accomplish in this work, is that dissemination of forecasts to people who might use them. At the current point this would only include people at the Cary Institute, nevertheless it would have been interesting to see how folks might have used the information. Similarly, calibrating a reasonably predictive model at NEON, and transferring that information to the scientific team there is an immediate next step. These forecasts, paired with uncertainty partition, could help NEON make decisions about their sampling designs in the light of finite funding.

However, a loftier goal is to get land managers and tick-borne disease scientists to recognize the value of ecological forecasting. Almost none of the papers I've cited that relate to the management and mitigation of tick-borne disease mention predictive modeling as an avenue to increase the effectiveness of management. A paradigm shift is required before the knowledge gained from this dissertation can be productively used.

APPENDIX 1: Chapter 1 Supplementary Material

Methods

Mouse population model

$$z_{i,1} \sim Bernoulli(\gamma_1) \quad \text{[S1.1]}$$

$$z_{i,t+1} \mid z_{i,t} \ldots, z_{i,1} \sim Bernoulli(z_{i,t}\phi_t + \gamma_{t+1}\prod_{k=1}^{t}(1 - z_{i,k})) \quad \text{[S1.2]}$$

$$y_{i,t} \mid z_{i,t} \sim Bernoulli(z_{i,t}\theta) \quad \text{[S1.3]}$$

Where *z* is the state (alive or dead) of an individual *i* at time *t*. Equation four describes the state of individuals at the first observation. Then, all other states are drawn from equation five, which is governed by the survival probability between capture occasions (ϕ_t) for mice already in the population (left side of the plus sign), or by a mouse entering the population (right side of the plus sign). γ_t is the probability a mouse transitions into the population and is a nuisance parameter needed in this parameterization. The observation model, conditional on the state at time *t*, is given by equation six, where θ is the capture probability.

Tick population model

Parameters in the daily transition matrix were modelled as follows:

φ_1, φ_2, and φ_3, are the daily survival rates of larvae, nymph, and adult ticks, respectively. Survival rates for life stage *j* at time *t* were modeled as:

$$\phi_{j,t} = logit(\beta X_t) \quad [S1.4]$$

Where X_t are time-varying covariates (daily weather), and β is a vector of coefficients. We used a regularizing prior on slope parameters β. The transition probabilities are $\boldsymbol{\theta}_1$, $\boldsymbol{\theta}_2$, and $\boldsymbol{\theta}_3$, which are the daily transition rates from questing larvae to dormant nymph, dormant nymph to questing nymphs, and questing nymph to questing adult, respectively. Transition probabilities $\boldsymbol{\theta}_1$, and $\boldsymbol{\theta}_3$ are modeled as

$$\theta_t = \begin{cases} \text{logit}(\beta X_t), & \text{if } \rho_{start} < cdd_t < \rho_{end} \\ 0, & \text{otherwise} \end{cases} \quad [S1.5]$$

$$X_t \sim N(\widehat{mice}_t, sd_t) \quad [S1.6]$$

Which is to say that if the cumulative growing degrees are within the correct window ($\boldsymbol{\rho}$), then the transition is a logit-link generalized linear model. Outside this phenological window, the transition does not occur. We considered three linear models each for $\theta_1$and θ_3; intercept only, one where θ is driven by the minimum number of mice alive (MNA, i.e. mouse data without uncertainty), and one with the mean daily estimated mouse population ($\widehat{mice}_t$) with uncertainty (sd_t) from the level two model (described above) using an errors-in-variables approach (eq. S1.6).

Likewise, fecundity was modeled as:

$$\lambda_t = \begin{cases} \lambda_t, & \rho_{start} > cdd_t > \rho_{end} \\ 0, & otherwise \end{cases} \quad [S1.7]$$

The cumulative growing degree day thresholds for all transition parameters, ρ, were not estimated as part of the model but were set manually to match the phenology of the questing life stage being transitioned into. These thresholds were based on tick observations. The cumulative growing degree windows were set to [400, 2500], [0, 1000] or [2500,] and [1000, 2500] for the larvae-to-nymph transition, nymph-to-adult transition, and fecundity, respectively.

Supplementary Figures

Figure S1.1 Across-site larvae one-step-ahead predictions

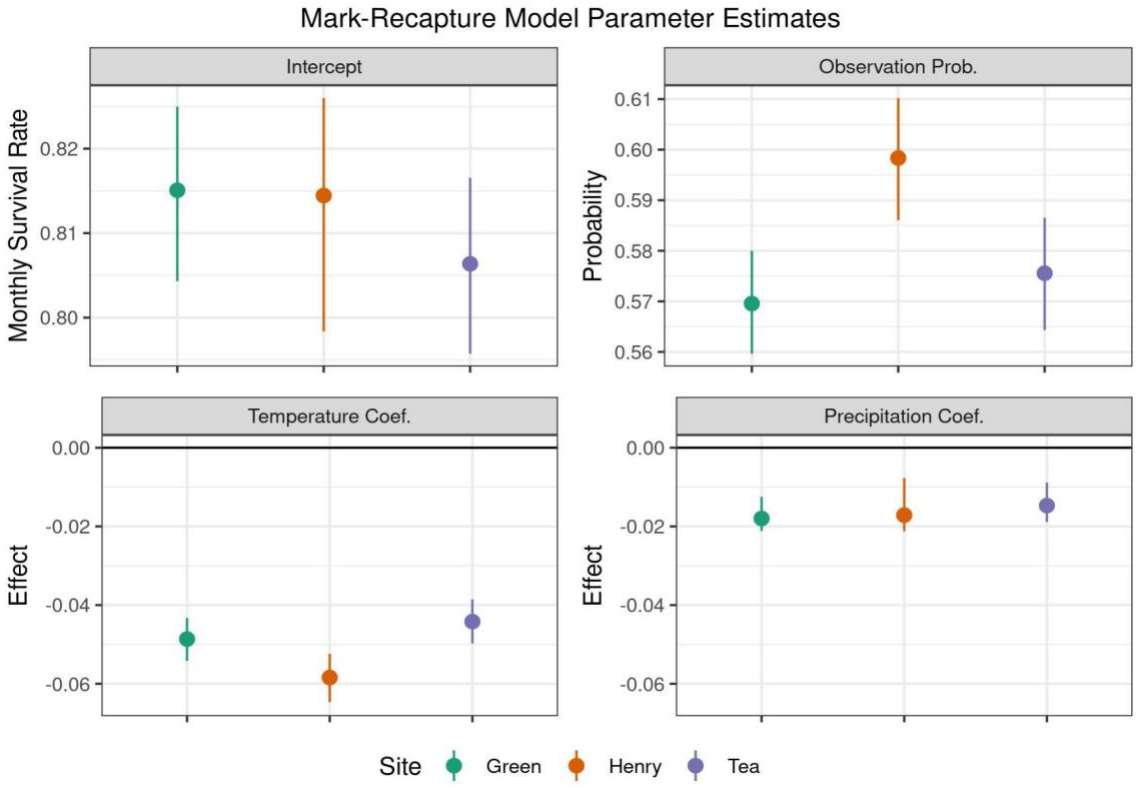

Figure S1.1: Demographic and observation parameter posterior for the mouse mark-recapture sub model. Top left: intercept for mouse survival, presented as monthly survival rate. Top right: observation probability. Bottom left: the effect of temperature on daily mouse survival. Bottom right: the effect of precipitation on daily mouse survival.

Figure S1.2 Across-site larvae one-step-ahead predictions

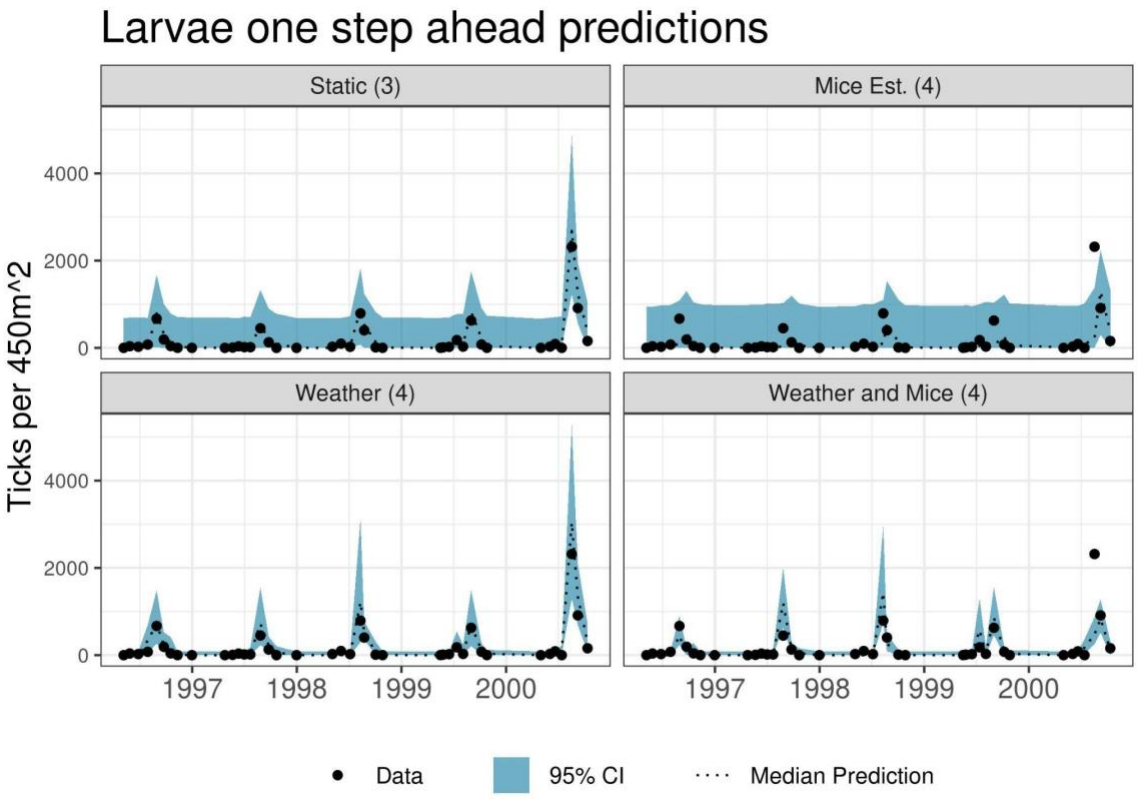

Figure S1.2: One-step ahead predictions from an across-site simulation for larvae. The model was calibrated at Henry, and run at Tea. Showing 1996 - 2000 because 1996 and 2000 were years with the peak nymph counts. Displaying output from for models: Static (3) (top left), Mice Est. (4) (top right), Weather (4) (bottom left), and Weather and Mice (4) (bottom right). Models not displayed (Static (4) and Mice MNA (4)) were excluded because they have very similar predictions to the Mice Est. (4) model.

Figure S1.3 Across-site adult one-step-ahead predictions

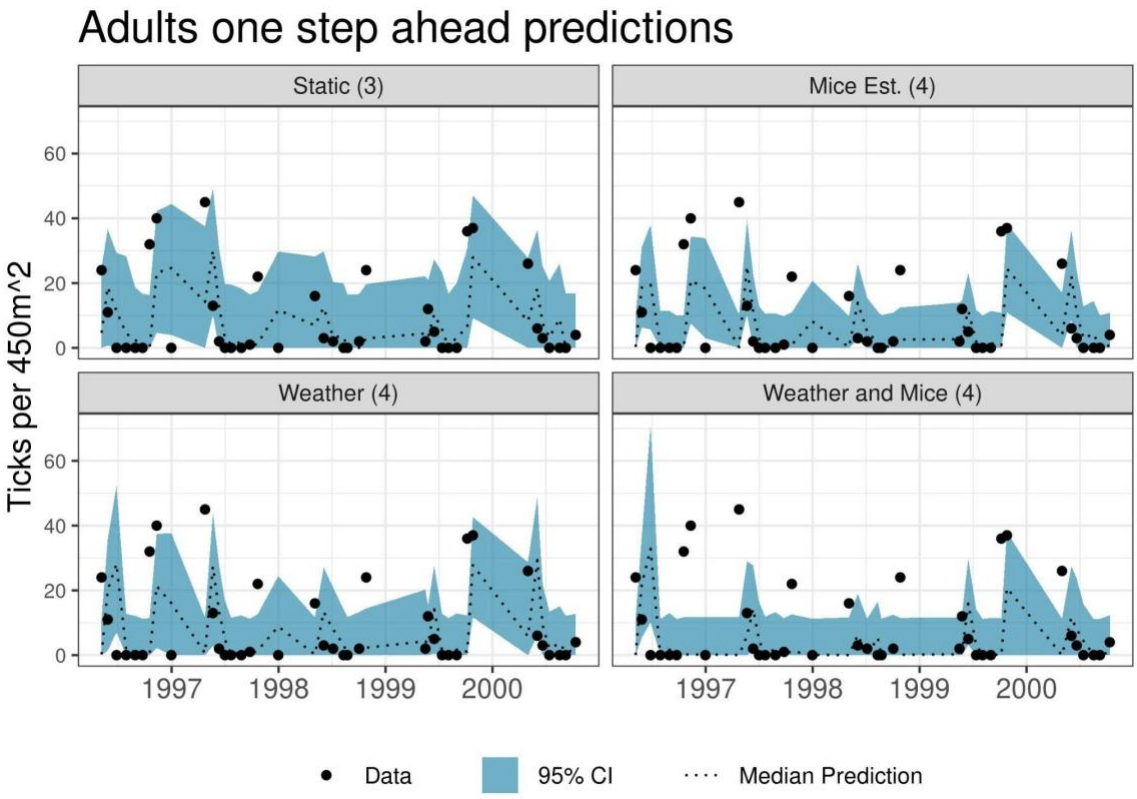

Figure S1.3: One-step ahead predictions from an across-site simulation for adults. The model was calibrated at Henry, and run at Tea. Showing 1996 - 2000 because 1996 and 2000 were years with the peak nymph counts. Displaying output from for models: Static (3) (top left), Mice Est. (4) (top right), Weather (4) (bottom left), and Weather and Mice (4) (bottom right). Models not displayed (Static (4) and Mice MNA (4)) were excluded because they have very similar predictions to the Mice Est. (4) model.

Figure S1.4 The effect of mice on tick transition rates

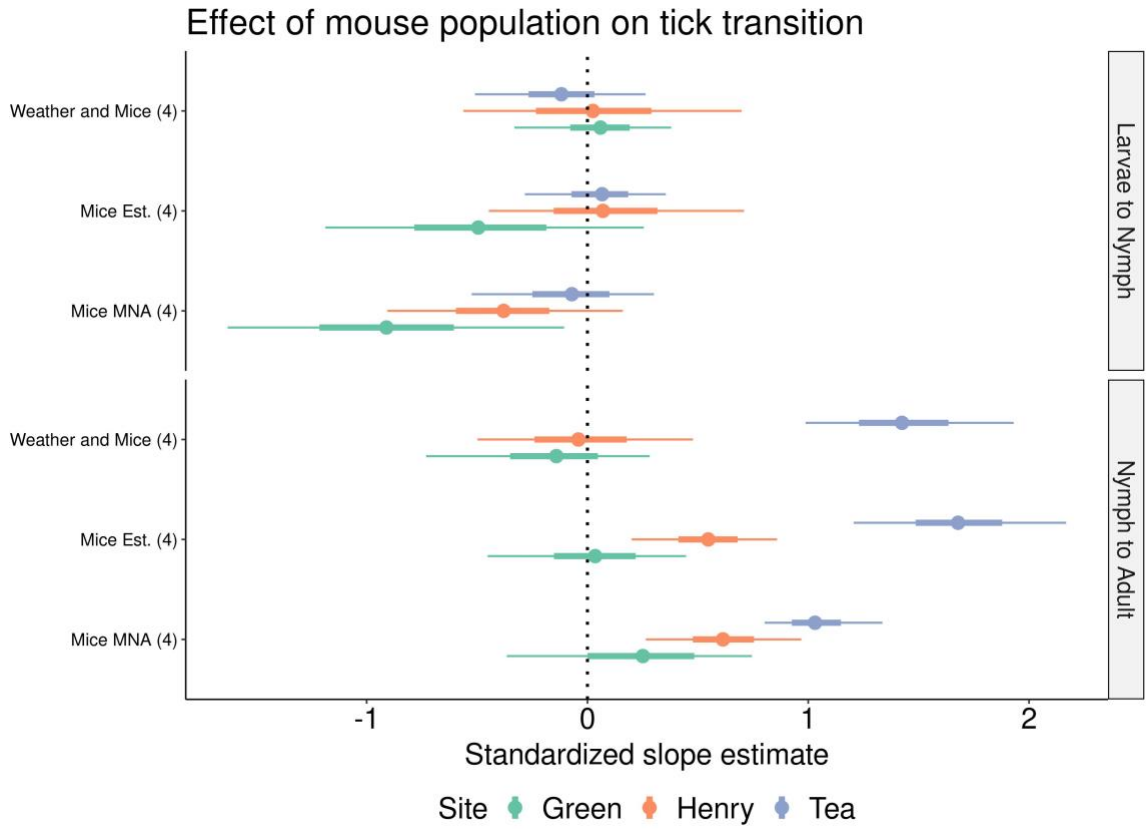

Figure S1.4: The effect the mouse population has on larvae-to-nymph transition (top row) and the nymph-to-adult transition (bottom row). The models that use mice are on the x-axis, showing the 90% CI for all posteriors. The Mice MNA (4) model uses the minimum number alive of mice (mouse data), while the Weather and Mice (4) and Mice Est. (4) use the estimated abundance from the level 2 mouse population model.

Figure S1.5 Reproduction parameter posteriors

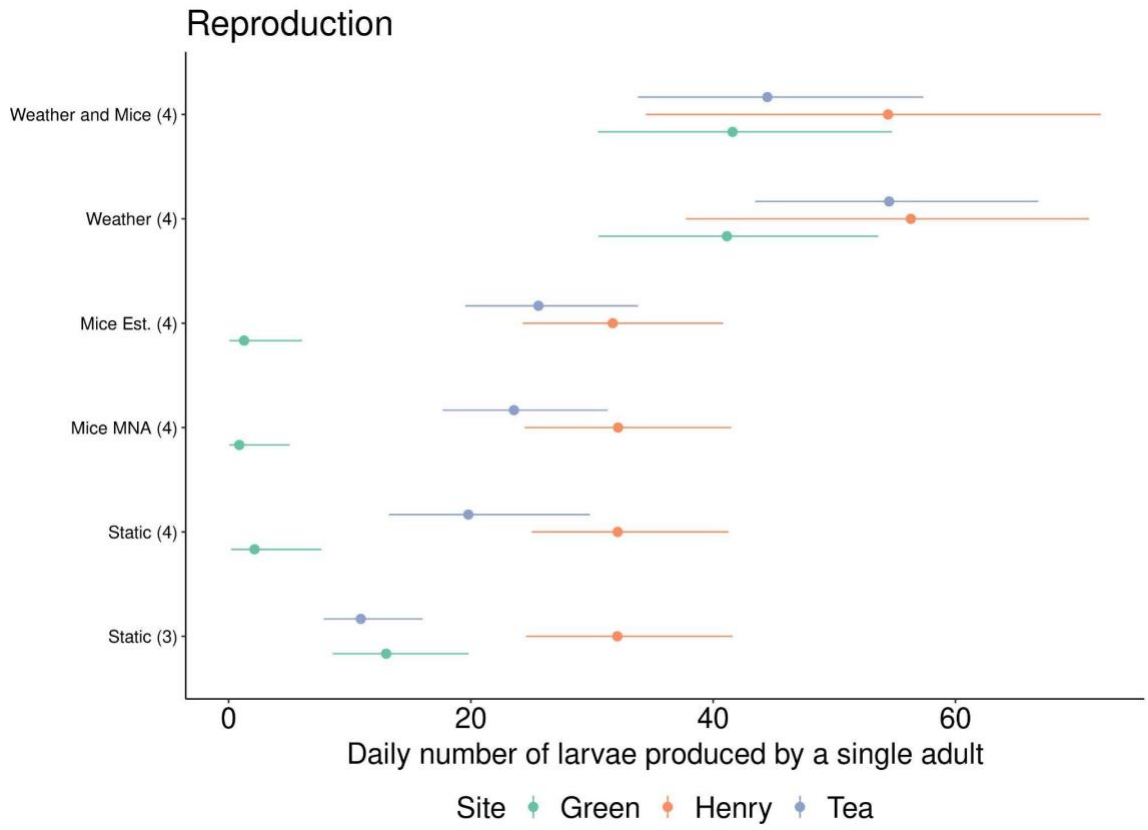

Figure S1.5: 90% CI for the reproduction parameter. Model is on the y-axis, colors correspond to the site the model was fit. Points are the median value.

Figure S1.6 Larval prediction skill

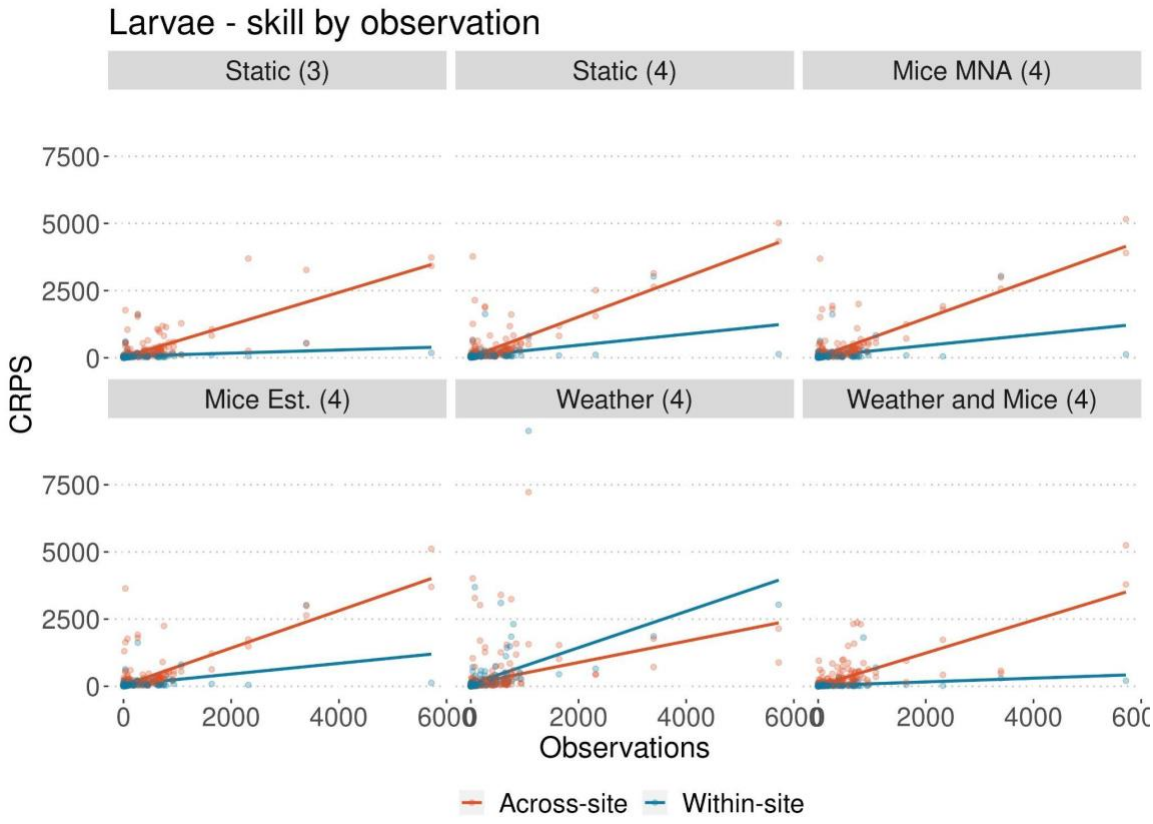

Figure S1.6: Prediction skill (CRPS, lower is better) for larvae with respect to the number of larvae observed. Each facet shows the scores for each model. Blue dots represent scores from the within-site simulations, red dots represent scores from the across-site simulations. Lines are linear trends.

Figure S1.7 Adult prediction skill

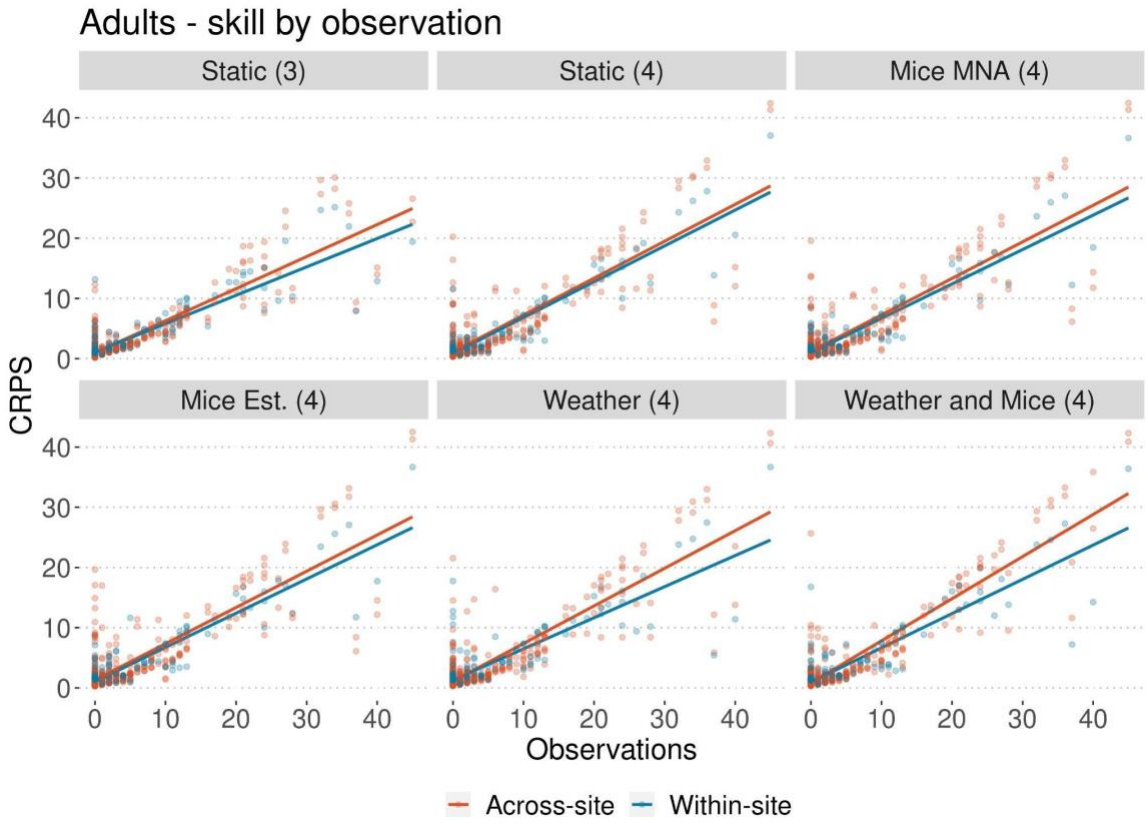

Figure S1.7: Prediction skill (CRPS, lower is better) for adults with respect to the number of adults observed. Each facet shows the scores for each model. Blue dots represent scores from the within-site simulations, red dots represent scores from the across-site simulations. Lines are linear trends.

Figure S1.8 Larval predication variance partitioning

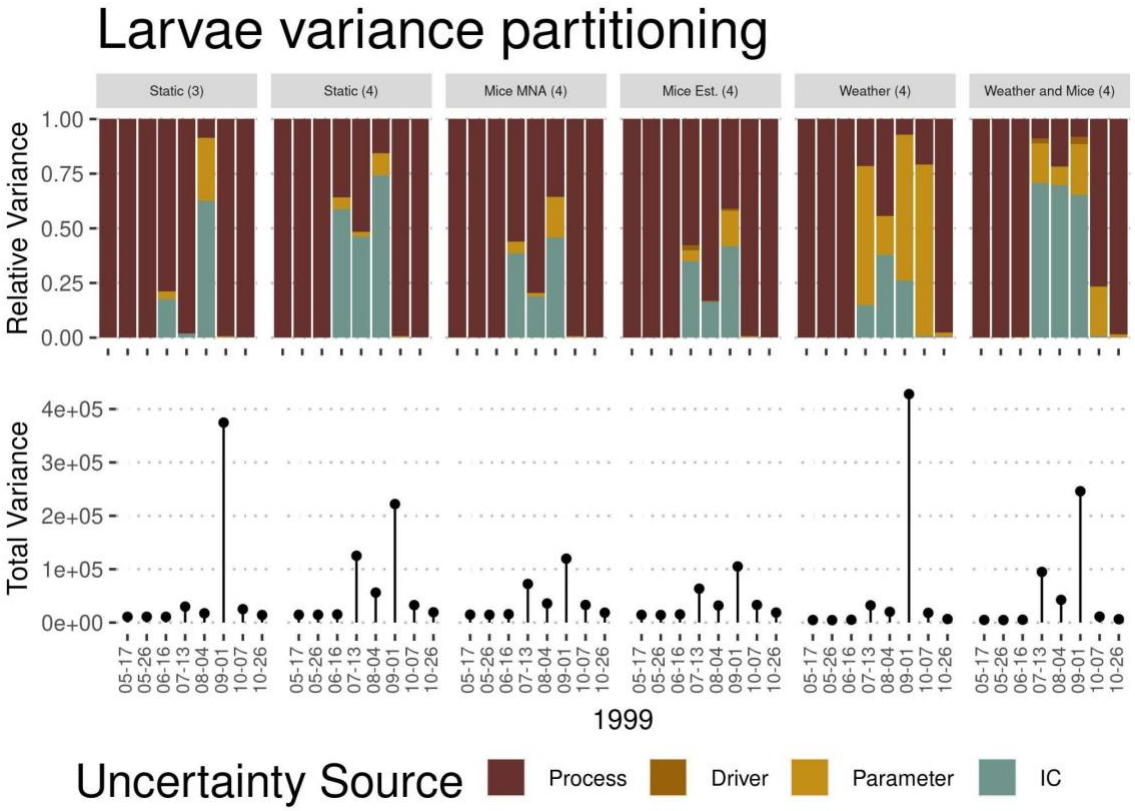

Figure S1.8: Variance partitioning for larval predictions at Tea in 1999. The top row shows the relative proportion of the total variance that is made up of either process error (model structural uncertainty), driver error (from level 2 mouse population model, only present in Mice Est. (4) and Weather and Mice (4) models), parameter uncertainty (from parameter distributions), and initial condition uncertainty (errors in the latent state). The bottom row shows the total amount of variance in the prediction.

Figure S1.9 Adult predication variance partitioning

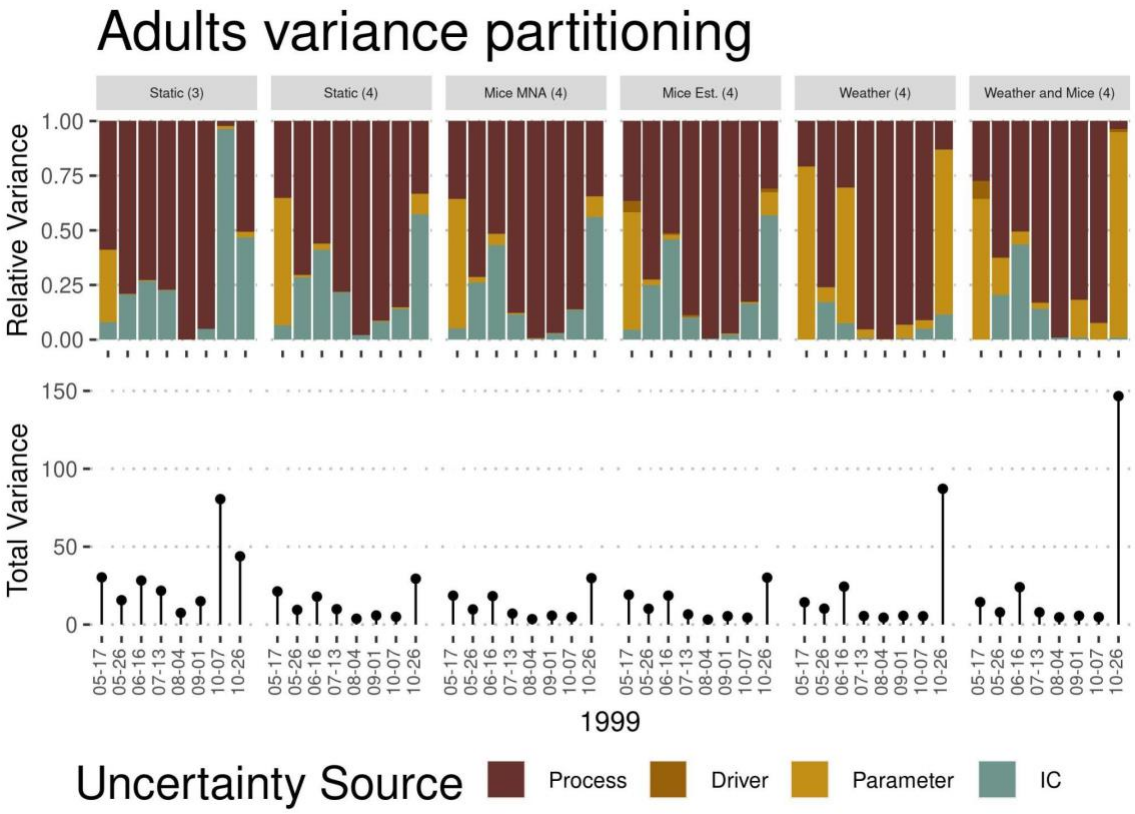

Figure S1.9: Variance partitioning for adult predictions at Tea in 1999. The top row shows the relative proportion of the total variance that is made up of either process error (model structural uncertainty), driver error (from level 2 mouse population model, only present in Mice Est. (4) and Weather and Mice (4) models), parameter uncertainty (from parameter distributions), and initial condition uncertainty (errors in the latent state). The bottom row shows the total amount of variance in the prediction.

Supplementary Tables

Table S1.1 Survival intercepts as monthly rates

		Larvae			Nymphs			Adults		
Model	**Site**	**Median**	**10% CI**	**90% CI**	**Median**	**10% CI**	**90% CI**	**Median**	**10% CI**	**90% CI**
Static (3)	Green	0.43	0.41	0.46	0.51	0.49	0.53	0.77	0.64	0.87
	Henry	0.41	0.39	0.43	0.51	0.49	0.53	0.86	0.79	0.92
	Tea	0.36	0.34	0.39	0.51	0.49	0.53	0.86	0.73	0.92
Static (4)	Green	0.44	0.42	0.47	0.49	0.47	0.50	0.68	0.48	0.81
	Henry	0.41	0.39	0.44	0.48	0.46	0.50	0.82	0.71	0.91
	Tea	0.43	0.40	0.45	0.48	0.46	0.50	0.37	0.26	0.52
Mice MNA (4)	Green	0.44	0.42	0.47	0.49	0.47	0.50	0.69	0.49	0.83
	Henry	0.41	0.39	0.44	0.48	0.46	0.50	0.80	0.68	0.89
	Tea	0.39	0.36	0.42	0.48	0.46	0.50	0.42	0.32	0.53
Mice Est. (4)	Green	0.44	0.42	0.47	0.49	0.47	0.50	0.68	0.48	0.81
	Henry	0.41	0.39	0.44	0.48	0.46	0.50	0.80	0.68	0.89
	Tea	0.38	0.35	0.41	0.48	0.46	0.50	0.43	0.34	0.53
Weather (4)	Green	0.45	0.43	0.47	0.52	0.50	0.54	0.92	0.79	0.97
	Henry	0.45	0.43	0.47	0.51	0.49	0.53	0.76	0.42	0.92
	Tea	0.45	0.43	0.47	0.51	0.49	0.53	0.89	0.80	0.96
Weather and Mice (4)	Green	0.45	0.43	0.47	0.51	0.50	0.53	0.92	0.77	0.97
	Henry	0.45	0.42	0.47	0.51	0.49	0.53	0.79	0.45	0.93
	Tea	0.45	0.42	0.47	0.51	0.49	0.53	0.86	0.71	0.94

Appendix 2: Chapter 2

Supplementary Figures

Figure S2.1 NMME bias correction

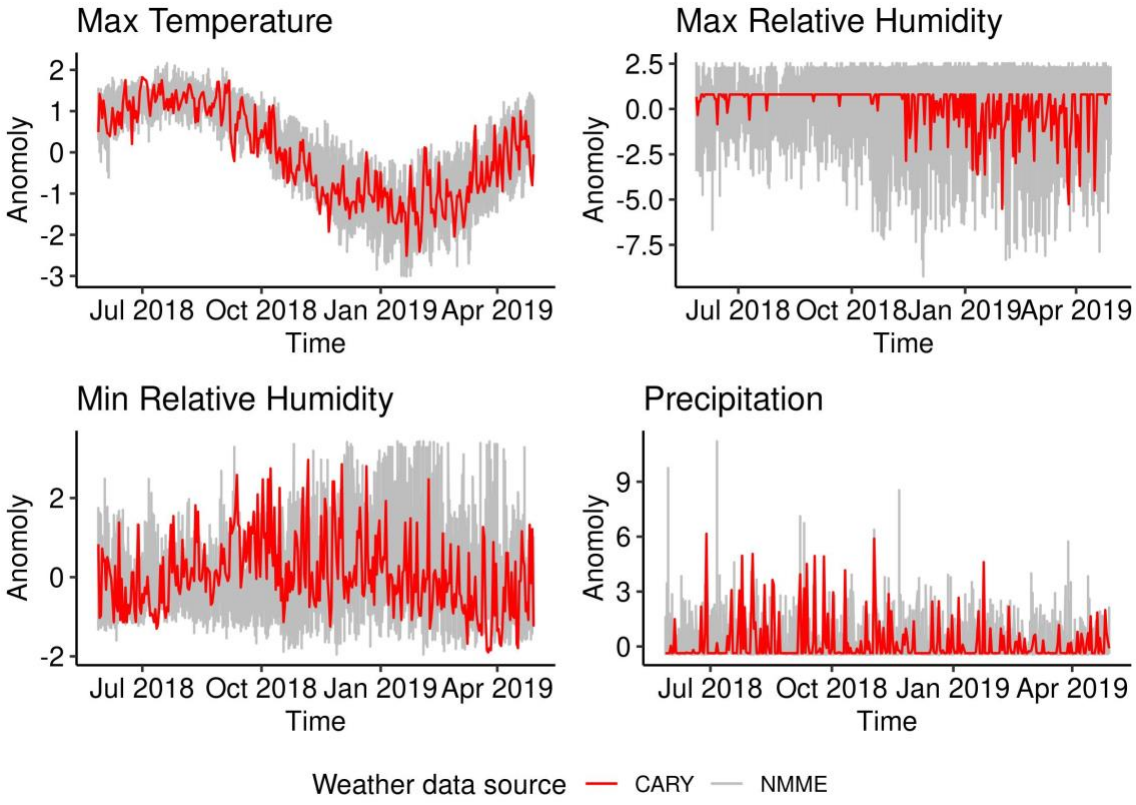

Figure S2.1 – Example of the downscaling performed to match the gridded NMME ensembles (grey), to match the observed weather at Cary (red). The NMME ensembles drawn are the downscaled product.

Figure S2.2 Larvae phenology scores

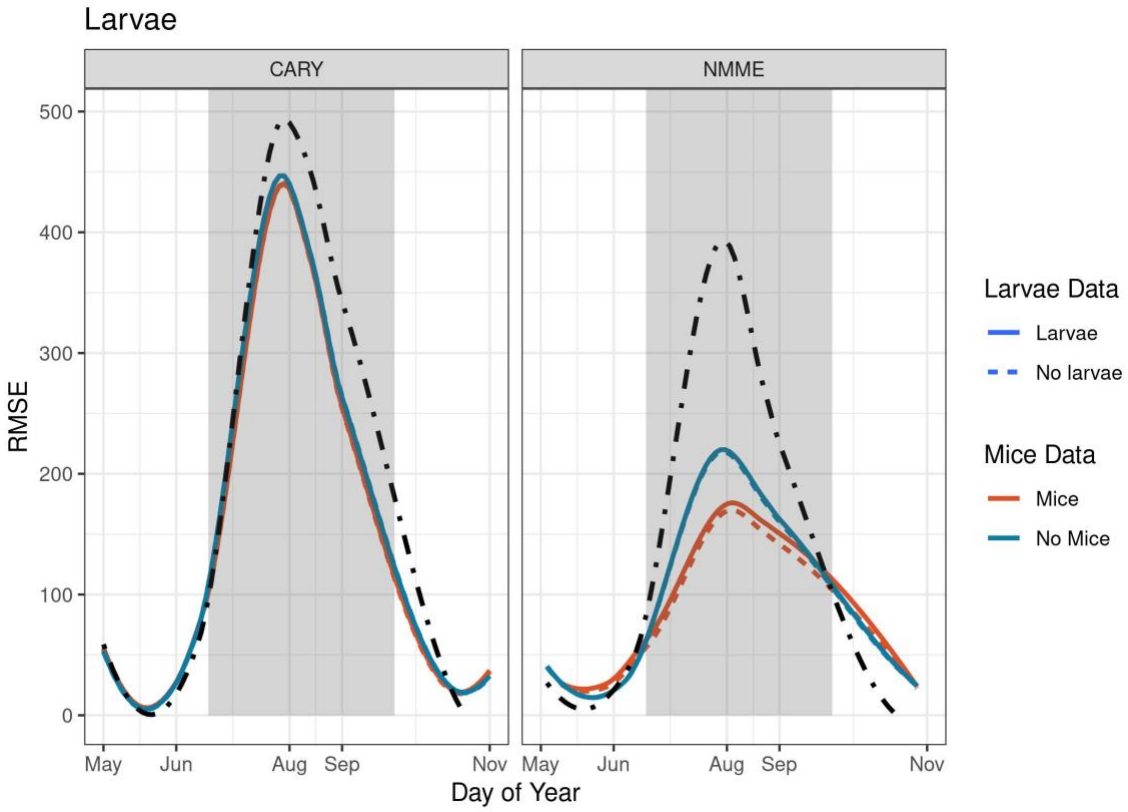

Figure S2.2 - Loess curves over the root mean square error (RMSE) for larval forecasts. The left panel shows the models that used the Cary meteorological data as weather covariates, the right showing the models that used NMME. The black dot-dash line is the RMSE from the null model. Red shows RMSE for models that used mice to constrain transition rates, blue is those without mice. Solid lines show the RMSE of models that assimilates the larvae data, dashed lines those that did not assimilated larval data. The shaded region is the expected questing period for nymphs, and when peak counts are observed.

Figure S2.3 Adult phenology scores

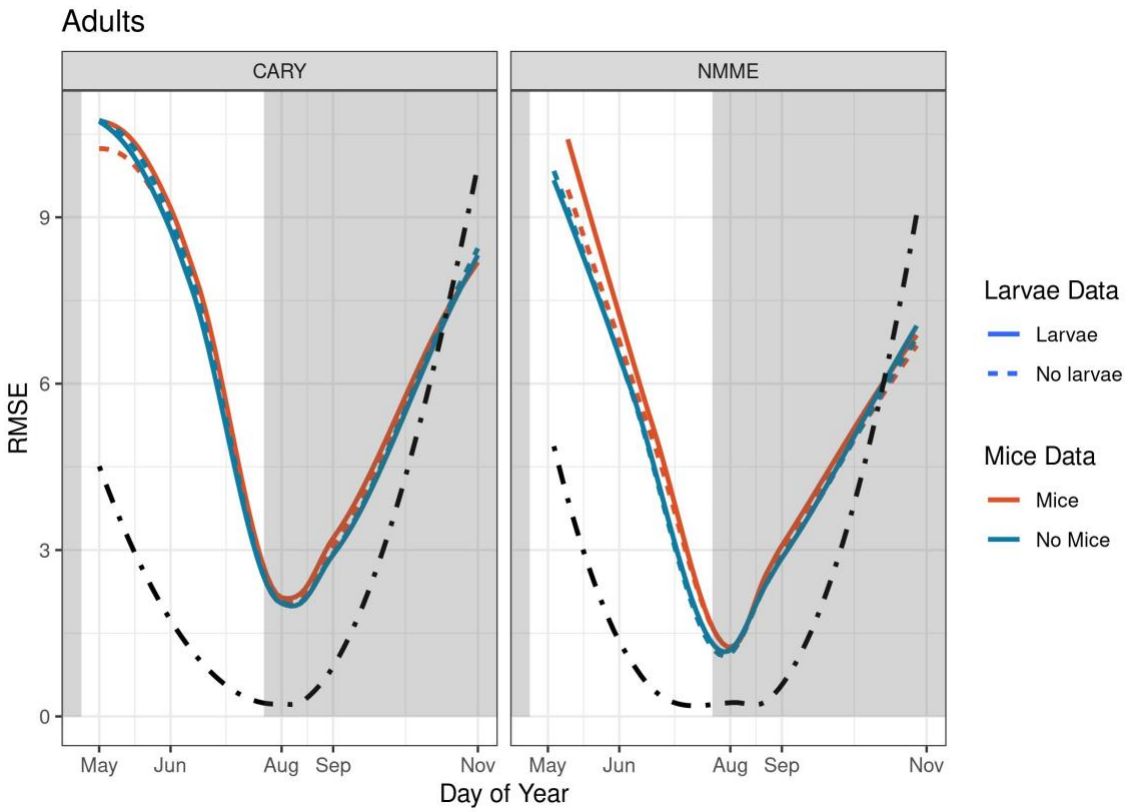

Figure S2.3 - Loess curves over the root mean square error (RMSE) for larval forecasts. The left panel shows the models that used the Cary meteorological data as weather covariates, the right showing the models that used NMME. The black dot-dash line is the RMSE from the null model. Red shows RMSE for models that used mice to constrain transition rates, blue is those without mice. Solid lines show the RMSE of models that assimilates the larvae data, dashed lines those that did not assimilated larval data. The shaded region is the expected questing period for nymphs, and when peak counts are observed.

Appendix 3: Chapter 3

Supplementary Figures

Figure S3.1 Average difference in CRPS for larval *Ixodes scapularis* forecasts relative to the null model

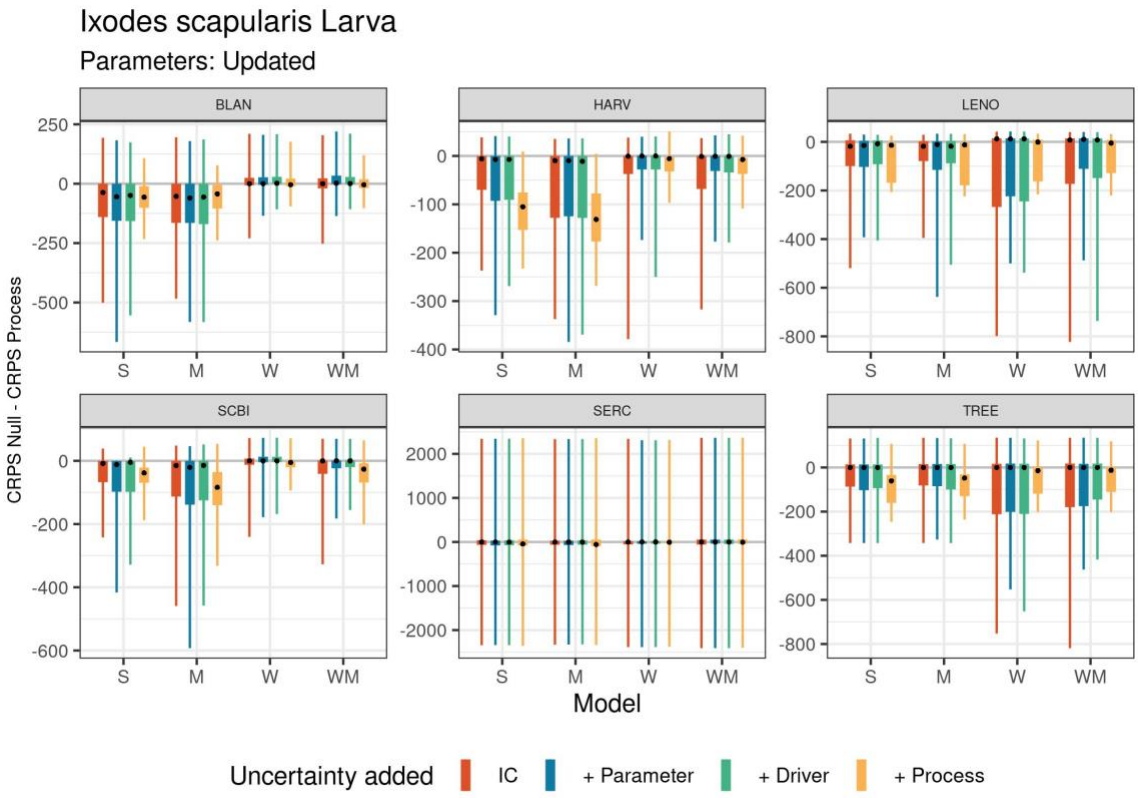

Figure S3.1 - The distribution of the difference in CRPS over the entire forecasting period for *I. scapularis* larvae. For each forecast, the difference between the null model score and the process model score was calculated, values are the average of these differences with 95% CI. Colors represent forecasts as uncertainty is added, starting with initial condition uncertainty (IC, red), then parameter uncertainty was added (blue), followed by adding driver uncertainty (green), and the forecast with all uncertainty included (Process, yellow). Models are shown on the x-axis as the Static model (S), Mouse model (M), Weather model (W), and the model with both weather and mice (WM). Negative values indicate the process model was worse than the null, positive values when the process model was better. The null model is a GAM smoothed over day of year for each life stage at each site.

Figure S3.2 Average difference in CRPS for larval *Amblyomma americanum* forecasts relative to the null model

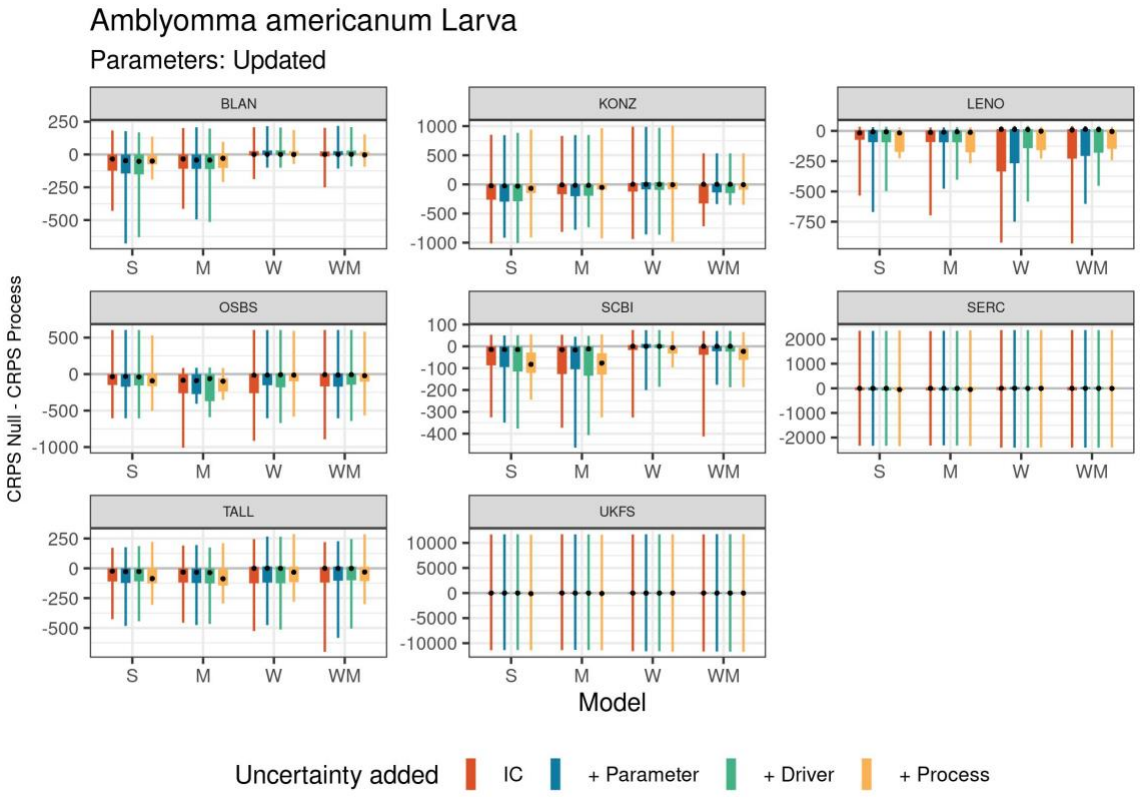

Figure S3.2 - The distribution of the difference in CRPS over the entire forecasting period for A. *americanum* larvae. For each forecast, the difference between the null model score and the process model score was calculated, values are the average of these differences with 95% CI. Colors represent forecasts as uncertainty is added, starting with initial condition uncertainty (IC, red), then parameter uncertainty was added (blue), followed by adding driver uncertainty (green), and the forecast with all uncertainty included (Process, yellow). Models are shown on the x-axis as the Static model (S), Mouse model (M), Weather model (W), and the model with both weather and mice (WM). Negative values indicate the process model was worse than the null, positive values when the process model was better. The null model is a GAM smoothed over day of year for each life stage at each site.

Figure S3.3 Average difference in CRPS for nymphal *Amblyomma americanum* forecasts relative to the null model

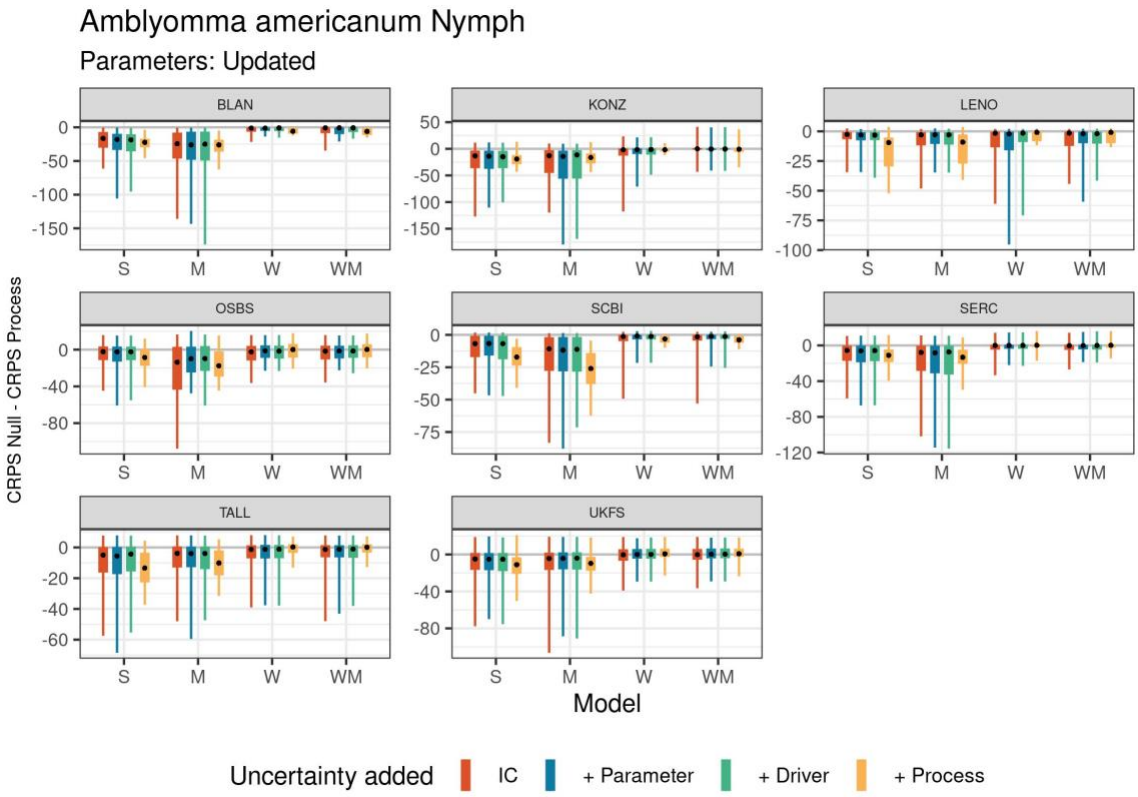

Figure S3.3 - The distribution of the difference in CRPS over the entire forecasting period for A. *americanum* nymphs. For each forecast, the difference between the null model score and the process model score was calculated, values are the average of these differences with 95% CI. Colors represent forecasts as uncertainty is added, starting with initial condition uncertainty (IC, red), then parameter uncertainty was added (blue), followed by adding driver uncertainty (green), and the forecast with all uncertainty included (Process, yellow). Models are shown on the x-axis as the Static model (S), Mouse model (M), Weather model (W), and the model with both weather and mice (WM). Negative values indicate the process model was worse than the null, positive values when the process model was better. The null model is a GAM smoothed over day of year for each life stage at each site.

Figure S3.4 Average difference in CRPS for adult *Ixodes scapularis* forecasts relative to the null model

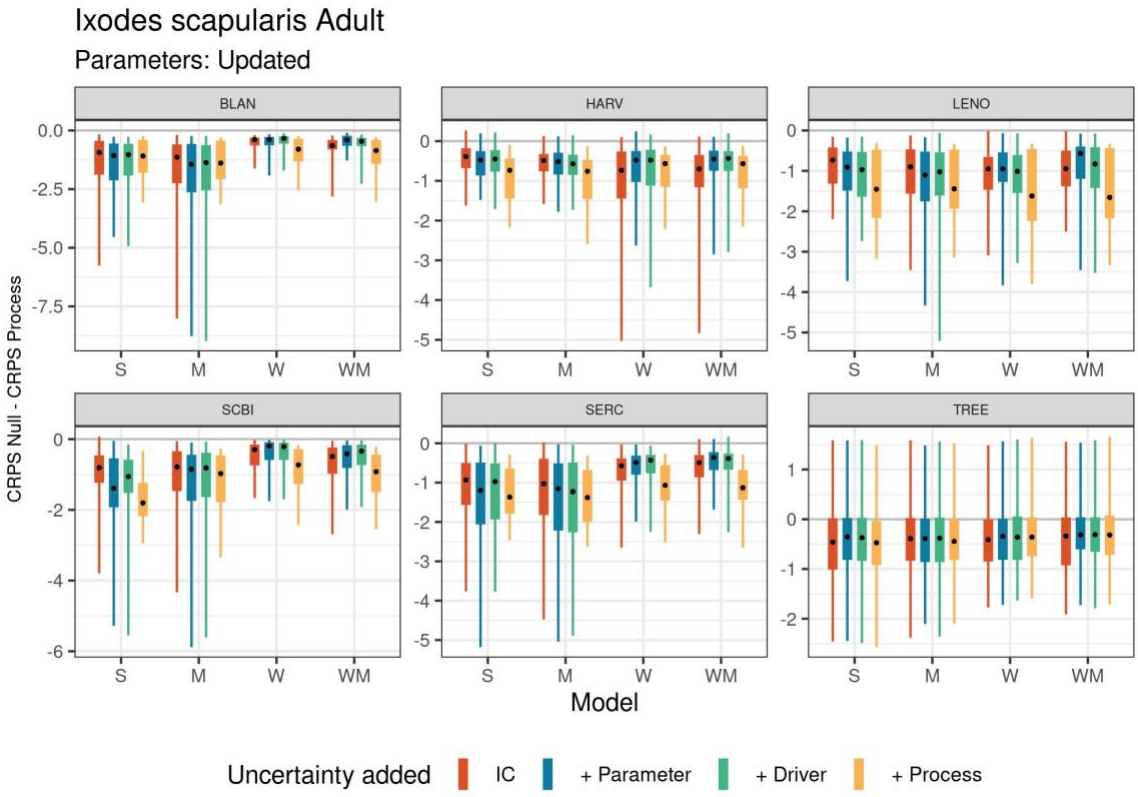

Figure S3.4 - The distribution of the difference in CRPS over the entire forecasting period for I. *scapularis* adults. For each forecast, the difference between the null model score and the process model score was calculated, values are the average of these differences with 95% CI. Colors represent forecasts as uncertainty is added, starting with initial condition uncertainty (IC, red), then parameter uncertainty was added (blue), followed by adding driver uncertainty (green), and the forecast with all uncertainty included (Process, yellow). Models are shown on the x-axis as the Static model (S), Mouse model (M), Weather model (W), and the model with both weather and mice (WM). Negative values indicate the process model was worse than the null, positive values when the process model was better. The null model is a GAM smoothed over day of year for each life stage at each site.

Figure S3.5 Average difference in CRPS for adult *Amblyomma americanum* forecasts relative to the null model

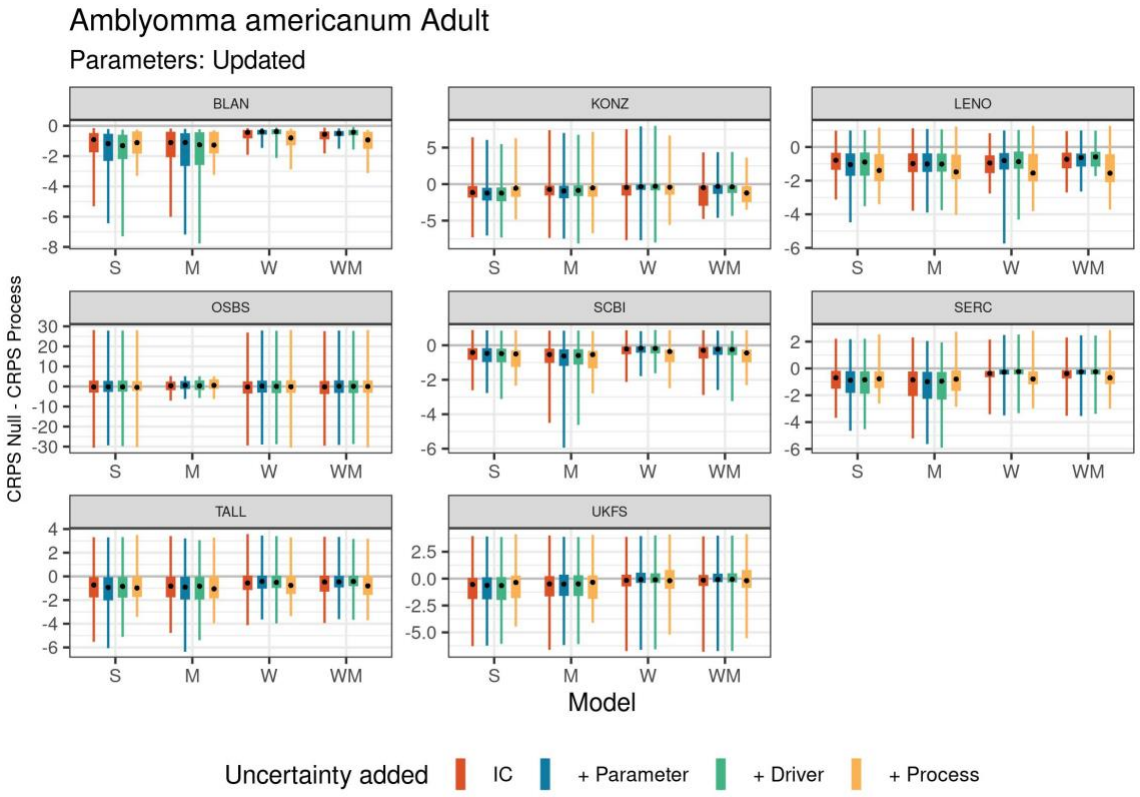

Figure S3.5 - The distribution of the difference in CRPS over the entire forecasting period for A. *americanum* adults. For each forecast, the difference between the null model score and the process model score was calculated, values are the average of these differences with 95% CI. Colors represent forecasts as uncertainty is added, starting with initial condition uncertainty (IC, red), then parameter uncertainty was added (blue), followed by adding driver uncertainty (green), and the forecast with all uncertainty included (Process, yellow). Models are shown on the x-axis as the Static model (S), Mouse model (M), Weather model (W), and the model with both weather and mice (WM). Negative values indicate the process model was worse than the null, positive values when the process model was better. The null model is a GAM smoothed over day of year for each life stage at each site.

Figure S3.6 Relative Variance

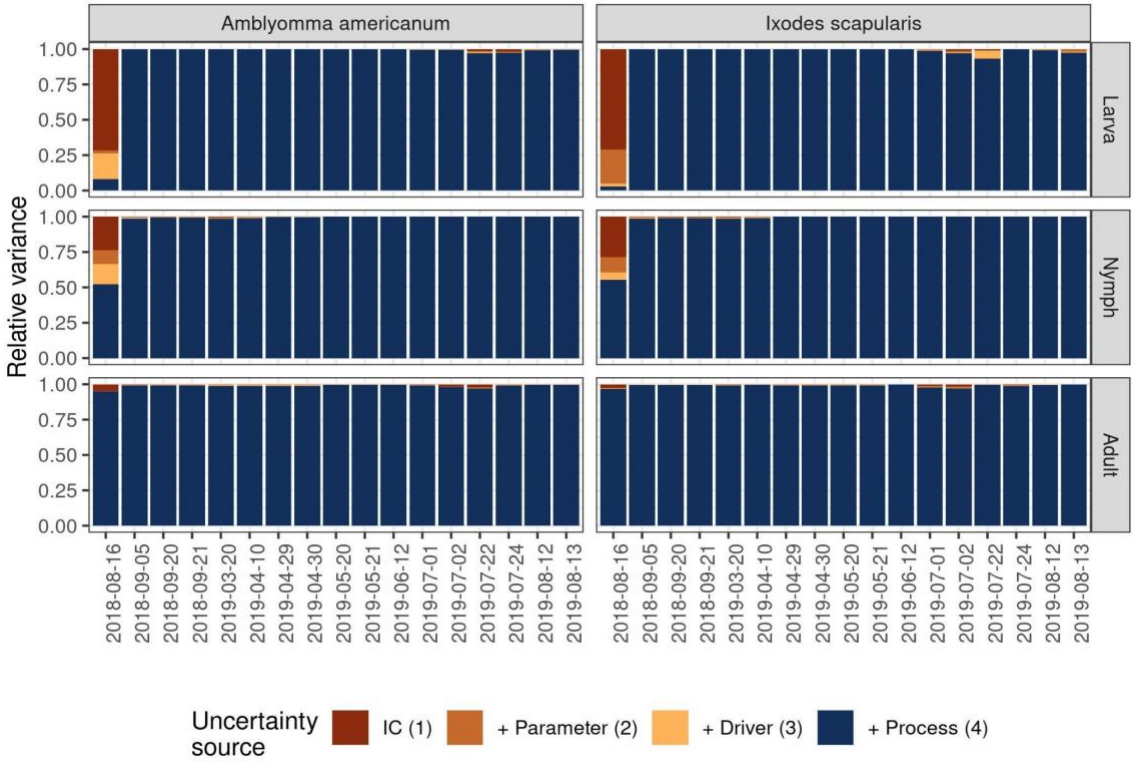

Figure 3.6 Relative variance from a forecast issued on August 15, 2018, at SERC with the Weather and Mice model. The relative variance for each observation date in the "future" is plotted on the x-axis. In general, forecasts are dominated by process uncertainty.

Figure S3.7 Larval forecast bias across land cover types

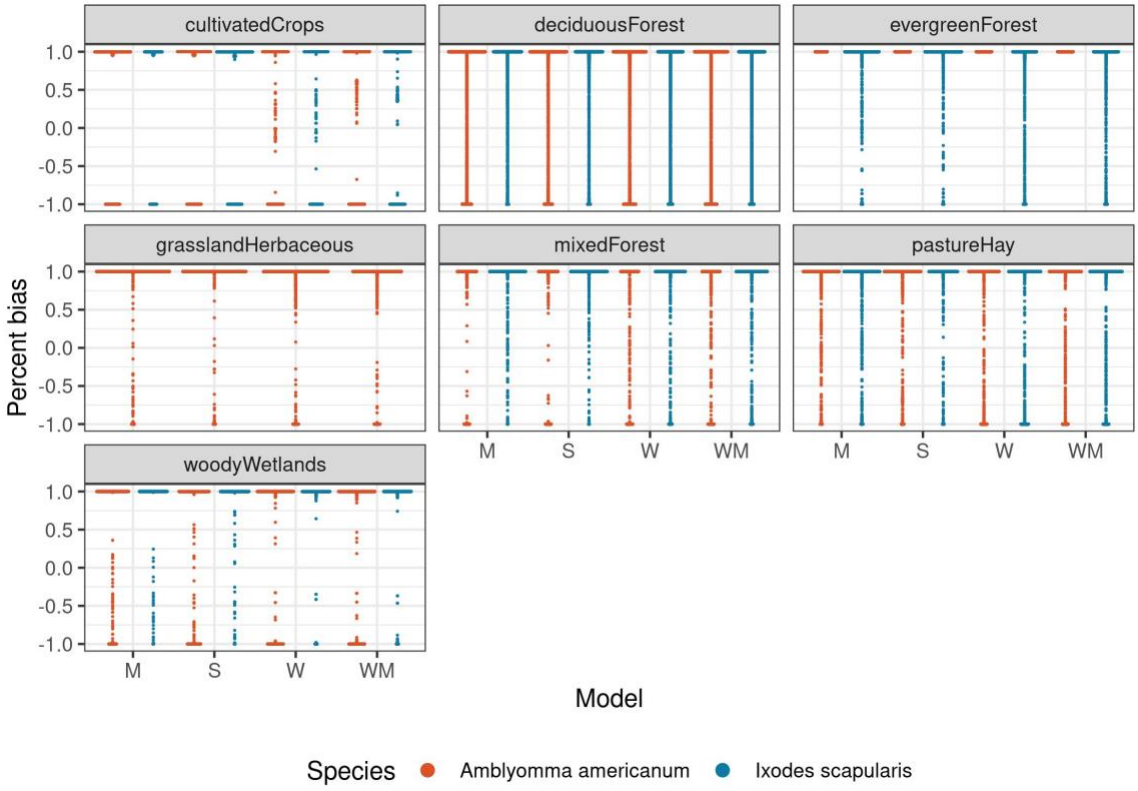

Figure S3.7 – Forecast bias (each point from a single forecast) for each model and species in each land cover type for larvae. Models are Mice (M), Static (S), Weather (W), and Weather and Mice (WM).

Figure S3.8 Nymphal forecast bias across land cover types

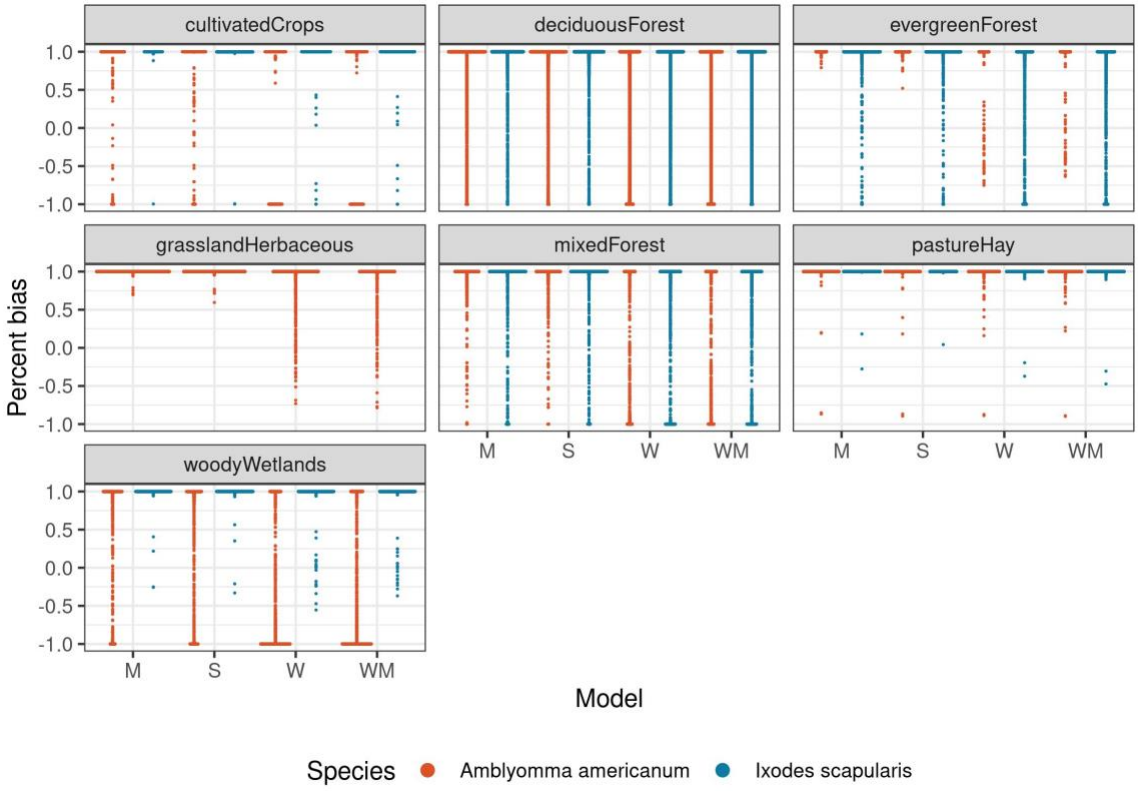

Figure S3.8 – Forecast bias (each point from a single forecast) for each model and species in each land cover type for nymphs. Models are Mice (M), Static (S), Weather (W), and Weather and Mice (WM).

Figure S3.9 Adult forecast bias across land cover types

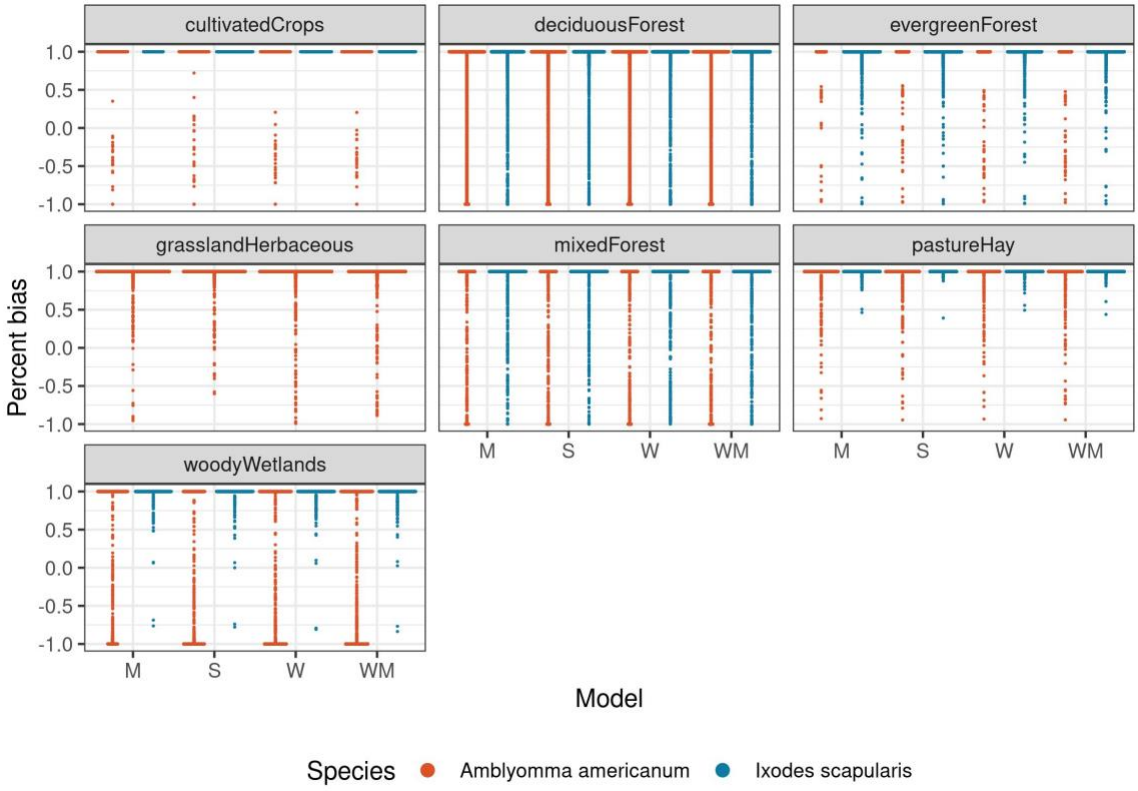

Figure S3.9 – Forecast bias (each point from a single forecast) for each model and species in each land cover type for adults. Models are Mice (M), Static (S), Weather (W), and Weather and Mice (WM).

Figure S3.10 Survival parameter updates I. scapularis

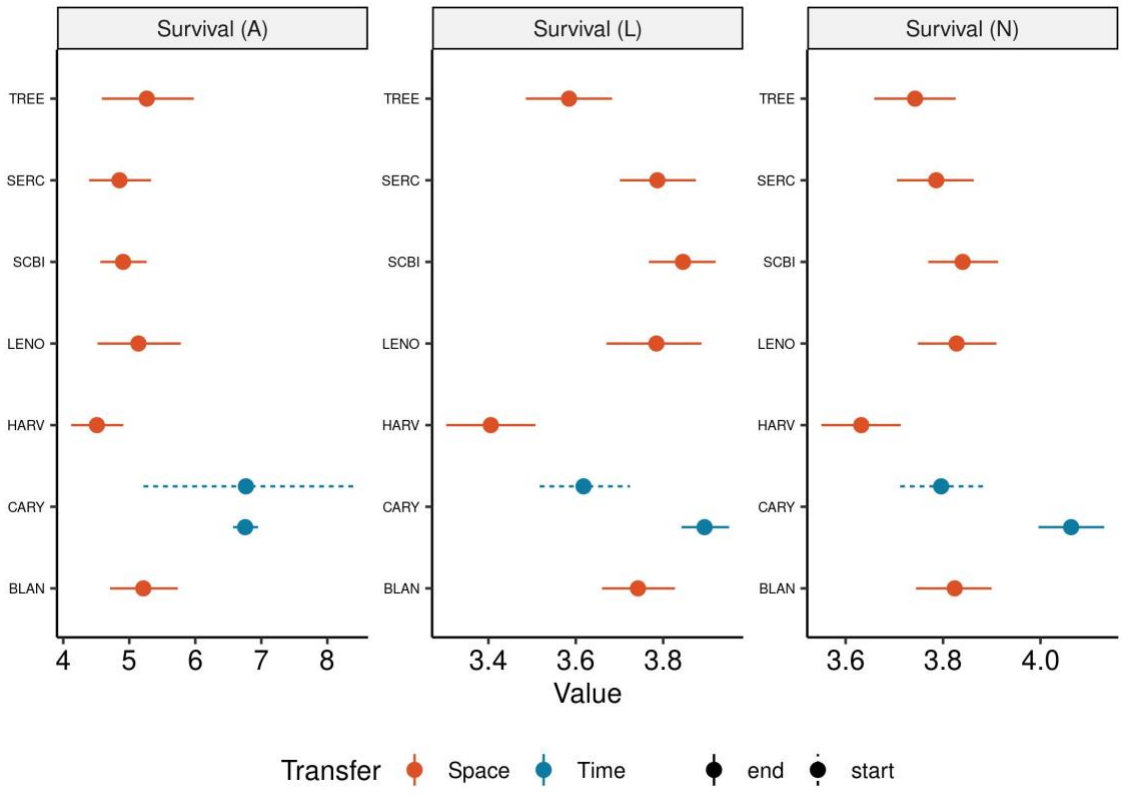

Figure S3.10 - The change survival *I. scapularis*. The forecasts started with informative priors for each effect, represented by the blue dashed 95% interval. The red intervals are posterior widths for each effect after the last forecast of 2019 at NEON sites (transfer-in-space). For comparison, the solid blue interval is the posterior after the last forecast from chapter 2 (transfer-in-time) experiments. Rates are untransformed.

Figure S3.11 Survival parameter updates I. scapularis

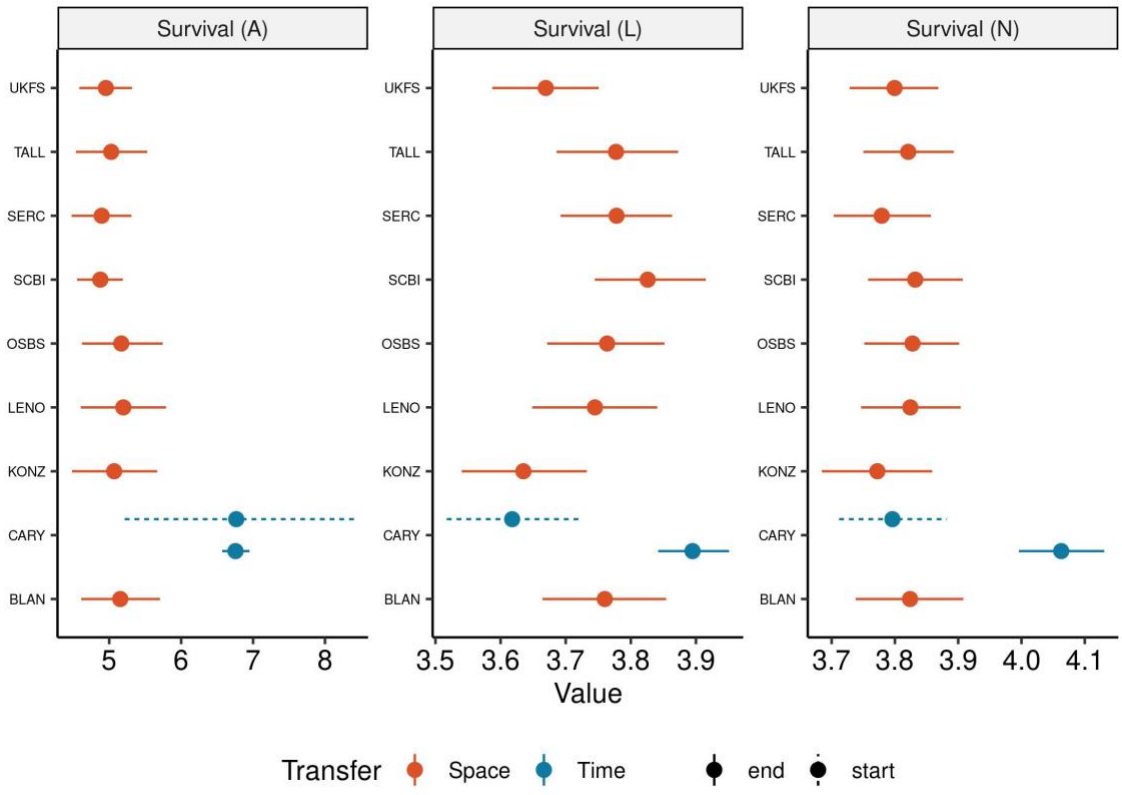

Figure S3.11 - The change survival *A. americanum*. The forecasts started with informative priors for each effect, represented by the blue dashed 95% interval. The red intervals are posterior widths for each effect after the last forecast of 2019 at NEON sites (transfer-in-space). For comparison, the solid blue interval is the posterior after the last forecast from chapter 2 (transfer-in-time) experiments. Rates are untransformed.

Figure S3.12 Transition parameter updates A. americanum

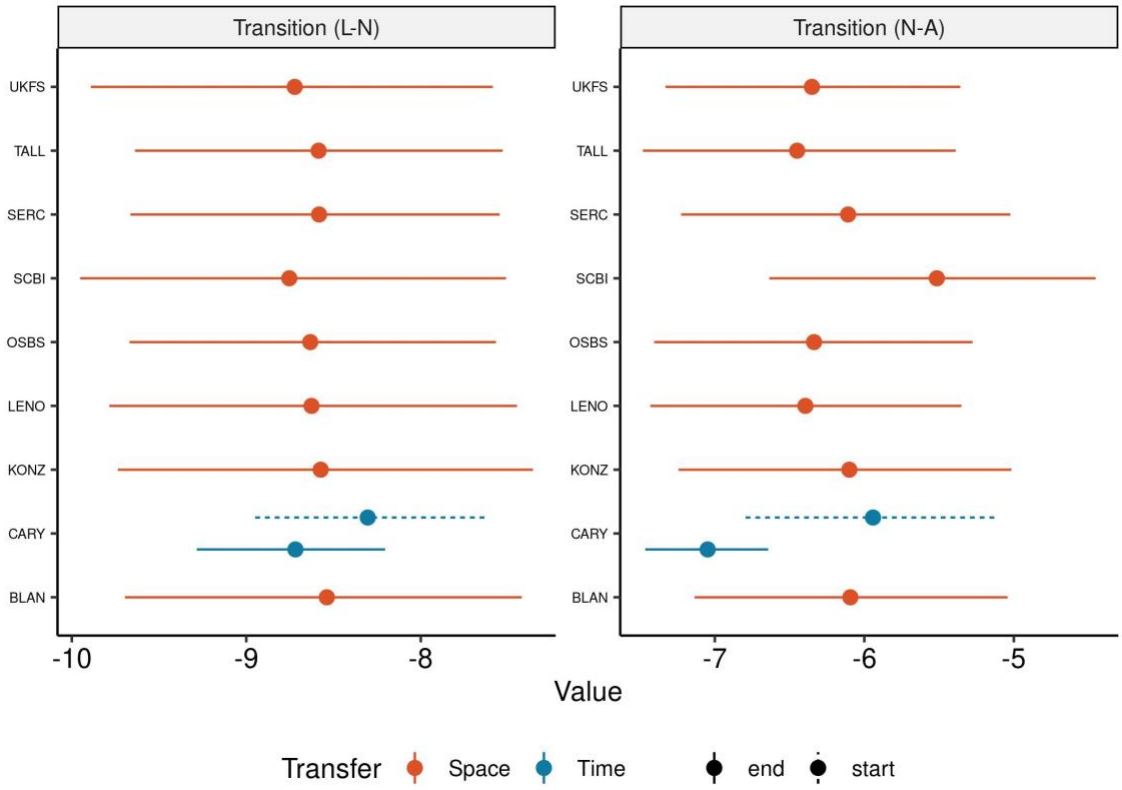

Figure S3.12 - The change transition *A. americanum*. The forecasts started with informative priors for each effect, represented by the blue dashed 95% interval. The red intervals are posterior widths for each effect after the last forecast of 2019 at NEON sites (transfer-in-space). For comparison, the solid blue interval is the posterior after the last forecast from chapter 2 (transfer-in-time) experiments. Rates are untransformed.

Figure S3.13 Transition parameter updates I. scapularis

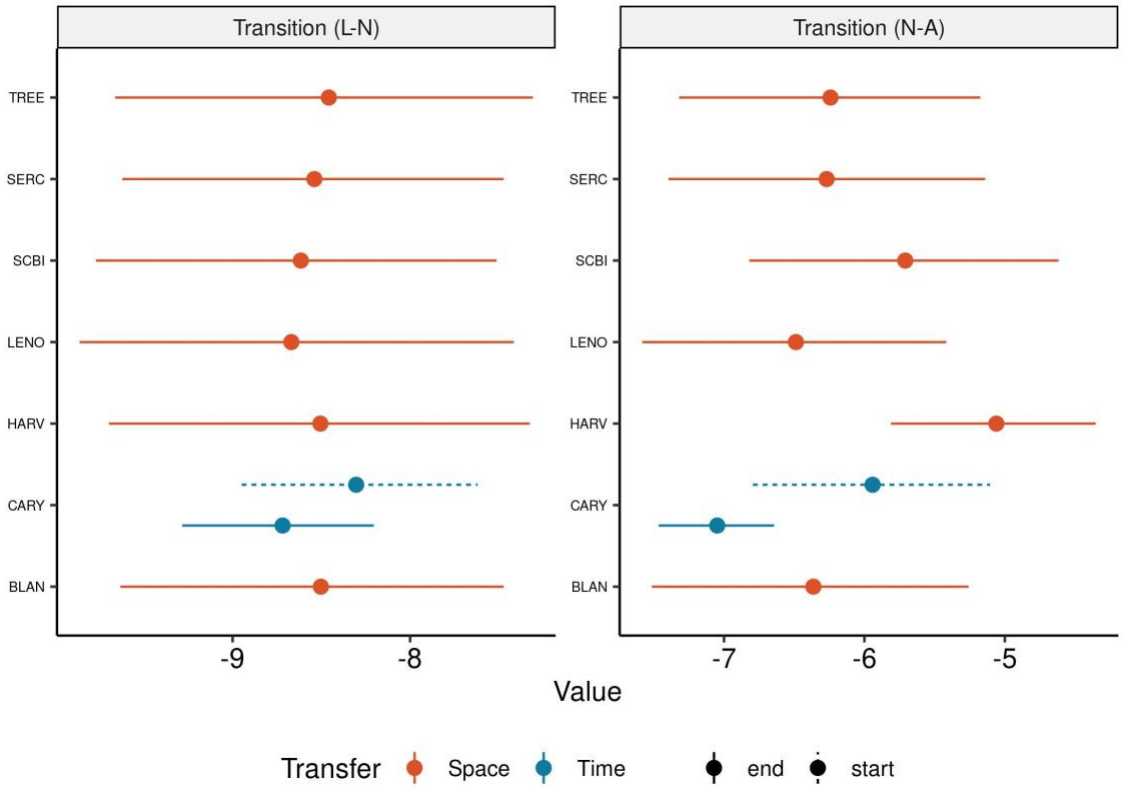

Figure S3.13 - The change survival *I. scapularis*. The forecasts started with informative priors for each effect, represented by the blue dashed 95% interval. The red intervals are posterior widths for each effect after the last forecast of 2019 at NEON sites (transfer-in-space). For comparison, the solid blue interval is the posterior after the last forecast from chapter 2 (transfer-in-time) experiments. Rates are untransformed.

Appendix 4: Chapter 4

Supplementary Figures

Figure S4.1 Monthly mouse survival estimates at each NEON site

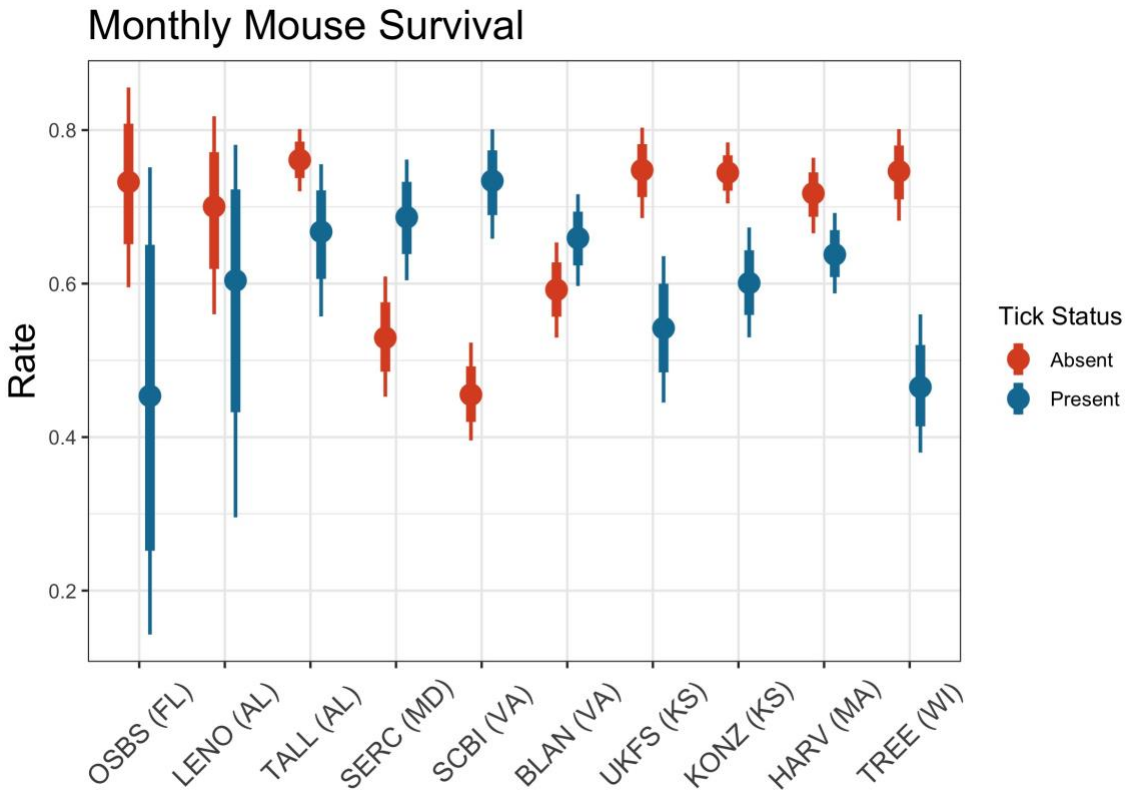

Figure S4.1 – 95% posterior credible interval (narrow lines) and 75% posterior credible interval for monthly mouse survival rate at each NEON site for each mouse state; mice with ticks attached in blue, those without ticks attached in red.

Figure S4.2 Base rate of state change for mice at NEON sites

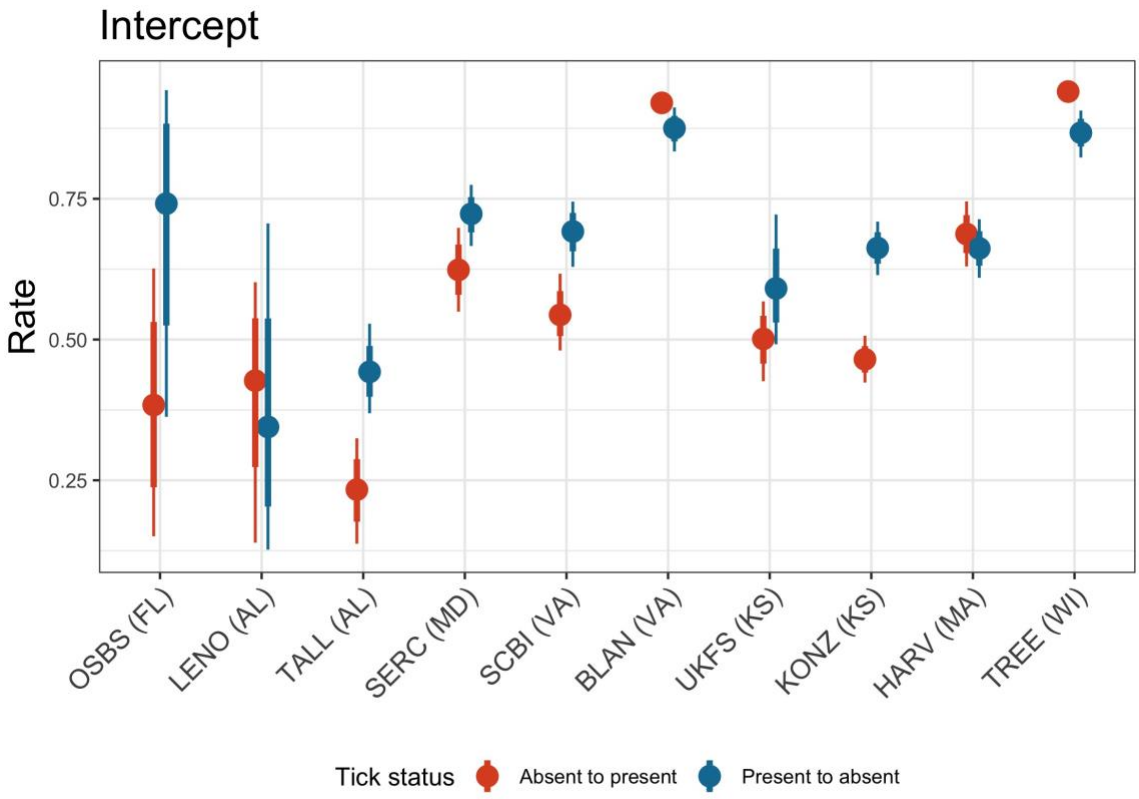

Figure S4.1 – 95% posterior credible interval (narrow lines) and 75% posterior credible interval (wide lines) for daily mouse state change at each NEON site. Transitioning from mice with ticks present to tick absent in blue, the reverse direction in red.

Figure S4.3 Survival estimates comparison to calibration

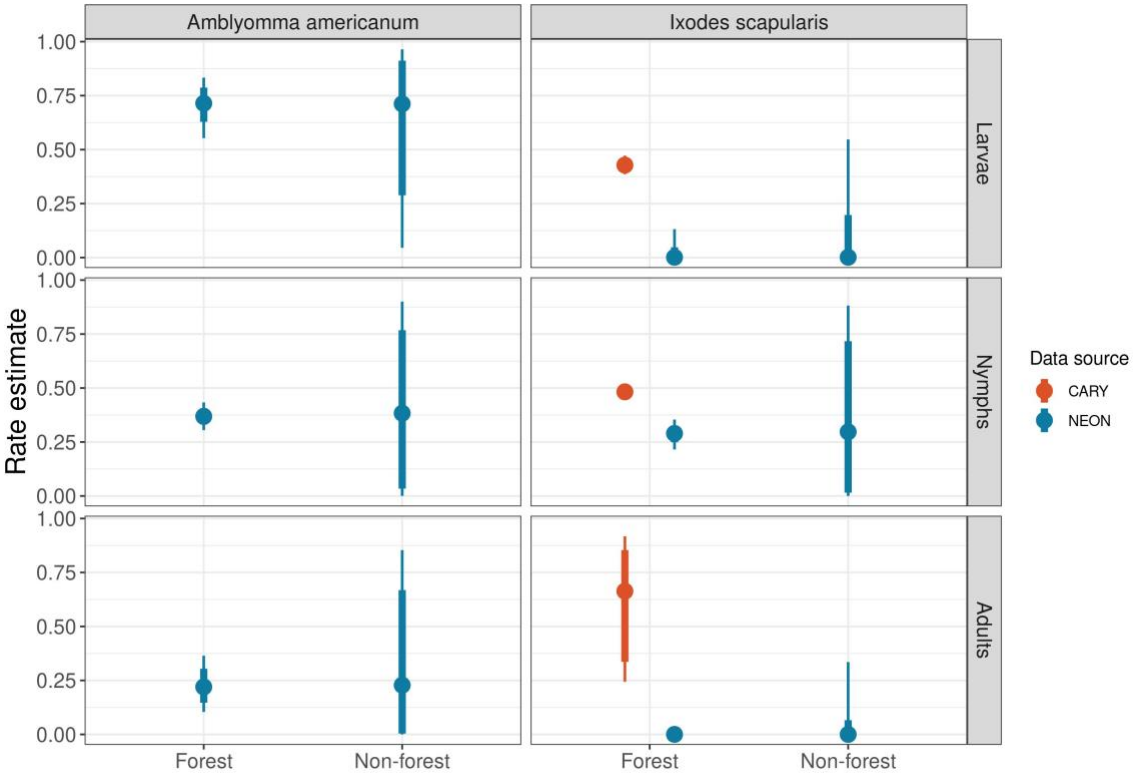

Figure S4.3 – 95% posterior credible interval (narrow lines) and 75% posterior credible interval (wide lines) for daily tick survival for both species (columns) in forest and non-forest plots (x-axis) and by data source.

Figure S4.4 Transition estimates comparison to calibration

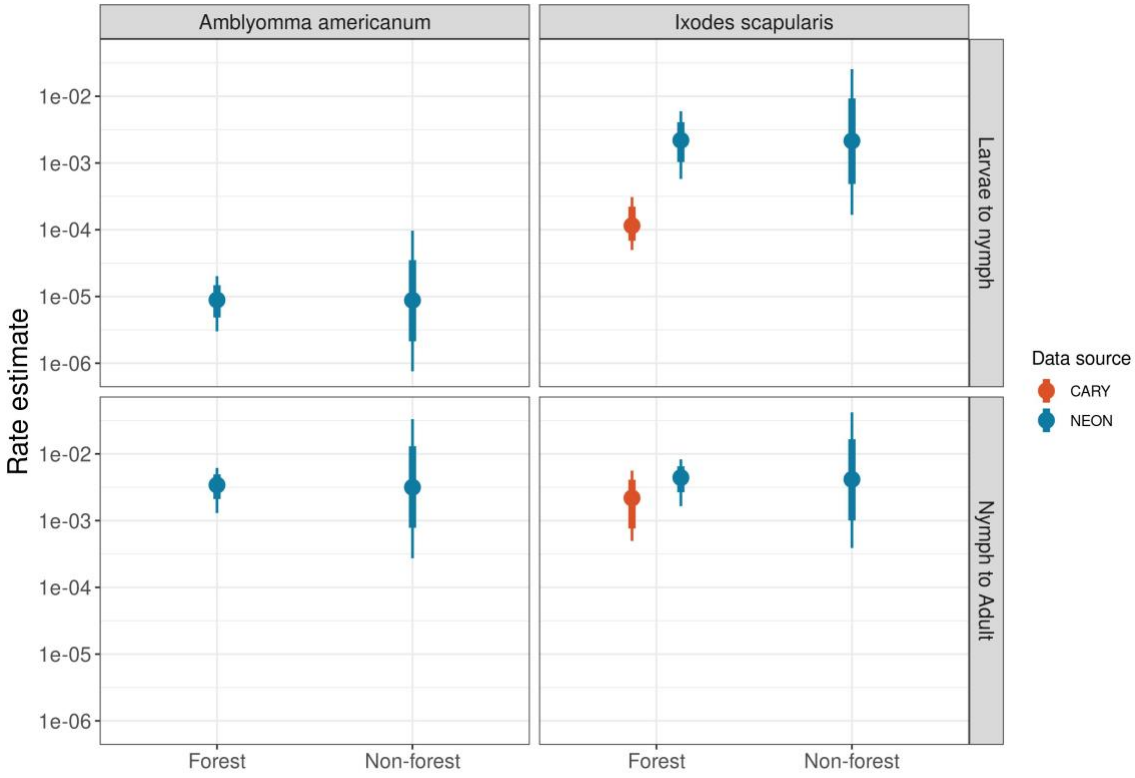

Figure S4.4 – 95% posterior credible interval (narrow lines) and 75% posterior credible interval (wide lines) for daily tick transition (rows) for each species (columns) in forest and non-forest plots (x-axis) and by data source.

Supplementary Tables

Table S4.1. Non-zero elements of the daily projection matrix A used for ticks at NEON.

Transition name (day t to t + 1)	**Position**	**Value**
Questing larvae to questing larvae	A $_{1, 1}$	$\phi_{\mathbf{1},j,k}(\mathbf{1}-\boldsymbol{\theta}_{\mathbf{1},j,k})$
Questing adults to questing larvae	A$_{1, 4}$	$\lambda_{j,k}$
Questing larvae to dormant nymphs	A $_{2, 1}$	$\phi_{\mathbf{1},j,k}\boldsymbol{\theta}_{\mathbf{1},j,k}$
Dormant nymphs to dormant nymphs	A $_{2, 2}$	$\mathbf{1}-\boldsymbol{\theta}_{\mathbf{2},j,k}$
Dormant nymphs to questing nymphs	A $_{3, 2}$	$\theta_{\mathbf{2},j,k}$
Questing nymphs to questing nymph	A $_{3, 3}$	$\phi_{\mathbf{2},j,k}(\mathbf{1}-\boldsymbol{\theta}_{\mathbf{3},j,k})$
Questing nymphs to questing adults	A $_{4, 3}$	$\phi_{\mathbf{2},j,k}\boldsymbol{\theta}_{\mathbf{3},j,k}$
Questing adults to questing adults	A $_{4, 4}$	$\phi_{\mathbf{3},j,k}$

Table S4.1: The non-zero elements of the daily transition matrix for the four-stage model. Indexes for position represent row and column.

Table S4.2 Observation parameter probabilities

Probability	Site	Tick Status	Median	Lower 95 %	Upper 95%
Capture	OSBS (FL)	Present	0.018	0.003	0.064
		Absent	0.299	0.228	0.385
	LENO (AL)	Present	0.010	0.001	0.041
		Absent	0.428	0.328	0.532
	TALL (AL)	Present	0.020	0.012	0.030
		Absent	0.330	0.302	0.359
	SERC (MD)	Present	0.520	0.459	0.588
		Absent	0.271	0.233	0.314
	SCBI (VA)	Present	0.254	0.217	0.296
		Absent	0.195	0.172	0.226
	BLAN (VA)	Present	0.430	0.384	0.478
		Absent	0.625	0.574	0.677
	UKFS (KS)	Present	0.098	0.073	0.132
		Absent	0.364	0.321	0.412
	KONZ (KS)	Present	0.308	0.269	0.348
		Absent	0.325	0.301	0.350
	HARV (MA)	Present	0.211	0.190	0.234
		Absent	0.198	0.177	0.223
	TREE (WI)	Present	0.244	0.214	0.279
		Absent	0.329	0.289	0.374
ID	-	Present	0.760	0.739	0.781
	-	Absent	0.972	0.959	0.982
Recovered Dead	-	-	0.008	0.005	0.011

Table S4.3 Demographic parameter rates

Parameter	Life Stage	Species	Cover Type	Median	Lower 95%	Upper 95%
Survival	Larvae	Amblyomma americanum	Forest	0.71	0.56	0.83
			Non-forest	0.71	0.04	0.97
		Ixodes scapularis	Forest	1.49E-03	1.95E-08	0.13
			Non-forest	1.49E-03	1.53E-18	0.56
	Nymphs	Amblyomma americanum	Forest	0.37	0.30	0.43
			Non-forest	0.37	3.38E-04	0.89
		Ixodes scapularis	Forest	0.29	0.22	0.35
			Non-forest	0.29	4.97E-05	0.87
	Adults	Amblyomma americanum	Forest	0.22	0.10	0.37
			Non-forest	0.23	6.07E-06	0.85
		Ixodes scapularis	Forest	4.61E-05	3.20E-10	0.02
			Non-forest	5.78E-05	2.00E-23	0.37
Transition	Larvae to nymph	Amblyomma americanum	Forest	8.80E-06	3.02E-06	2.07E-05
			Non-forest	8.62E-06	8.13E-07	9.68E-05
		Ixodes scapularis	Forest	2.20E-03	6.03E-04	0.01
			Non-forest	2.12E-03	1.86E-04	0.03
	Nymph to Adult	Amblyomma americanum	Forest	3.41E-03	1.27E-03	0.01
			Non-forest	3.10E-03	2.77E-04	0.03
		Ixodes scapularis	Forest	4.41E-03	1.61E-03	0.01
			Non-forest	4.08E-03	3.66E-04	0.04
Reproduction	Adult to Larvae	Amblyomma americanum	Forest	3.17	0.74	8.56
			Non-forest	2.98	0.22	34.03
		Ixodes scapularis	Forest	39.12	8.67	119.75
			Non-forest	36.96	2.93	426.40

BIBLIOGRAPHY

Addison, P. F. E., Rumpff, L., Bau, S. S., Carey, J. M., Chee, Y. E., Jarrad, F. C., McBride, M. F., & Burgman, M. A. (2013). Practical solutions for making models indispensable in conservation decision-making. *Diversity and Distributions*, *19*(5–6), 490–502. https://doi.org/10.1111/ddi.12054

Alasmari, S., & Wall, R. (2021). Metabolic rate and resource depletion in the tick Ixodes ricinus in response to temperature. *Experimental and Applied Acarology*, *83*(1), 81–93. https://doi.org/10.1007/s10493-020-00568-1

Allan, B. F., Dutra, H. P., Goessling, L. S., Barnett, K., Chase, J. M., Marquis, R. J., Pang, G., Storch, G. A., Thach, R. E., & Orrock, J. L. (2010). Invasive honeysuckle eradication reduces tick-borne disease risk by altering host dynamics. *Proceedings of the National Academy of Sciences of the United States of America*, *107*(43), 18523–18527. https://doi.org/10.1073/pnas.1008362107

Anderson, J. F., & Magnarelli, L. A. (2008). Biology of Ticks. *Infectious Disease Clinics of North America*, *22*(2), 195–215. https://doi.org/10.1016/j.idc.2007.12.006

Arsnoe, I. M., Hickling, G. J., Ginsberg, H. S., McElreath, R., & Tsao, J. I. (2015). Different Populations of Blacklegged Tick Nymphs Exhibit Differences in Questing Behavior That Have Implications for Human Lyme Disease Risk. *PLoS ONE*, *10*(5), e0127450. https://doi.org/10.1371/journal.pone.0127450

Arsnoe, I., Tsao, J. I., & Hickling, G. J. (2019). Nymphal Ixodes scapularis questing behavior explains geographic variation in Lyme borreliosis risk in the eastern

United States. *Ticks and Tick-Borne Diseases*, *10*(3), 553–563. https://doi.org/10.1016/j.ttbdis.2019.01.001

Atwood, T. B., Connolly, R. M., Ritchie, E. G., Lovelock, C. E., Heithaus, M. R., Hays, G. C., Fourqurean, J. W., & Macreadie, P. I. (2015). Predators help protect carbon stocks in blue carbon ecosystems. *Nature Climate Change*, *5*(12), Article 12. https://doi.org/10.1038/nclimate2763

Bacon, E. A., Kopsco, H., Gronemeyer, P., Mateus-Pinilla, N., & Smith, R. L. (2021). Effects of Climate on the Variation in Abundance of Three Tick Species in Illinois. *Journal of Medical Entomology*, tjab189. https://doi.org/10.1093/jme/tjab189

Barbour, A. G., Bunikis, J., Fish, D., & Hanincová, K. (2015). Association between body size and reservoir competence of mammals bearing Borrelia burgdorferi at an endemic site in the northeastern United States. *Parasites & Vectors*, *8*(1), 299. https://doi.org/10.1186/s13071-015-0903-5

Barbour, A. G., & Fish, D. (1993). The Biological and Social Phenomenon of Lyme Disease. *Science, 260*(5114), 1610–1616.

Berger, K. A., Ginsberg, H. S., Gonzalez, L., & Mather, T. N. (2014). Relative Humidity and Activity Patterns of *Ixodes scapularis* (Acari: Ixodidae). *Journal of Medical Entomology, 51*(4), 769–776. https://doi.org/10.1603/ME13186

Bertrand, M. R., & Wilson, M. L. (1996). Microclimate-dependent survival of unfed adult Ixodes scapularis (Acari:Ixodidae) in nature: Life cycle and study design

implications. *Journal of Medical Entomology*, *33*(4), 619–627. https://doi.org/10.1093/jmedent/33.4.619

Boettiger, C. (2022). The forecast trap. *Ecology Letters*, *25*(7), 1655–1664. https://doi.org/10.1111/ele.14024

Boettiger, C., Thomas, Q., Laney, C., & Lunch, C. (2021). *neonstore: NEON Data Store*. https://CRAN.R-project.org/package=neonstore

Brooks, S. P., & Gelman, A. (1998). General Methods for Monitoring Convergence of Iterative Simulations. *Journal of Computational and Graphical Statistics*, *7*(4), 434–455. https://doi.org/10.1080/10618600.1998.10474787

Brunner, J. L., Cheney, L., Keesing, F., Killilea, M., Logiudice, K., Previtali, A., & Ostfeld, R. S. (2011). Molting Success of Ixodes scapularis Varies Among Individual Blood Meal Hosts and Species. *Journal of Medical Entomology*, *48*(4), 860–866. https://doi.org/10.1603/ME10256

Brunner, J. L., Killilea, M., & Ostfeld, R. S. (2012). Overwintering Survival of Nymphal *Ixodes scapularis* (Acari: Ixodidae) Under Natural Conditions. *Journal of Medical Entomology*, *49*(5), 981–987. https://doi.org/10.1603/ME12060

Brunner, J. L., & Ostfeld, R. S. (2008). Multiple Causes of Variable Tick Burdens on Small-Mammal Hosts. *Ecology*, *89*(8), 2259–2272. https://doi.org/10.1890/07-0665.1

Burgdorfer, W., Barbour, A. G., Hayes, S. F., Benach, J. L., Grunwaldt, E., & Davis, J. P. (1982). Lyme Disease—A Tick-Borne Spirochetosis? *Science*, *216*(4552), 1317–1319. https://doi.org/10.1126/science.7043737

Buzdugan, S. N., Vergne, T., Grosbois, V., Delahay, R. J., & Drewe, J. A. (2017). Inference of the infection status of individuals using longitudinal testing data from cryptic populations: Towards a probabilistic approach to diagnosis. *Scientific Reports*, *7*(1), Article 1. https://doi.org/10.1038/s41598-017-00806-4

Caswell, H. (2000). *Matrix population models* (Vol. 1). Sinauer Sunderland.

CDC. (2021, May 17). *Lyme Disease Charts and Figures: Historical Data | Lyme Disease | CDC*. https://www.cdc.gov/lyme/stats/graphs.html

Childs, J. E., & Paddock, C. D. (2003). The Ascendancy of Amblyomma americanum as a Vector of Pathogens Affecting Humans in the United States. *Annual Review of Entomology*, *48*(1), 307–337. https://doi.org/10.1146/annurev.ento.48.091801.112728

Choquet, R., Carrié, C., Chambert, T., & Boulinier, T. (2013). Estimating transitions between states using measurements with imperfect detection: Application to serological data. *Ecology*, *94*(10), 2160–2165. https://doi.org/10.1890/12-1849.1

Collins, C. R., & Kays, R. W. (2014). Patterns of Mortality in a Wild Population of White-Footed Mice. *Northeastern Naturalist*, *21*(2), 323–336. https://doi.org/10.1656/045.021.0213

Conn, P. B., & Cooch, E. G. (2009). Multistate capture–recapture analysis under imperfect state observation: An application to disease models. *Journal of Applied Ecology*, *46*(2), 486–492. https://doi.org/10.1111/j.1365-2664.2008.01597.x

Couet, P., Gally, F., Canonne, C., & Besnard, A. (2019). Joint estimation of survival and breeding probability in female dolphins and calves with uncertainty in state

assignment. *Ecology and Evolution*, *9*(23), 13043–13055. https://doi.org/10.1002/ece3.5693

Cox, R. M., Parker, E. U., Cheney, D. M., Liebl, A. L., Martin, L. B., & Calsbeek, R. (2010). Experimental evidence for physiological costs underlying the trade-off between reproduction and survival. *Functional Ecology*, *24*(6), 1262–1269. https://doi.org/10.1111/j.1365-2435.2010.01756.x

Davis, A. J., Farrar, R., Jump, B., Hall, P., Guerrant, T., & Pepin, K. M. (2022). An efficient method of evaluating multiple concurrent management actions on invasive populations. *Ecological Applications*, *32*(6), e2623. https://doi.org/10.1002/eap.2623

de Valpine, P., Paciorek, C., Turek, D., Michaud, N., Anderson-Bergman, C., Obermeyer, F., Cortes, C. W., Rodrìguez, A., Lang, D. T., & Paganin, S. (2022). *NIMBLE: MCMC, Particle Filtering, and Programmable Hierarchical Modeling* (0.12.2) [Computer software]. https://doi.org/10.5281/zenodo.1211190

de Valpine, P., Turek, D., Paciorek, C. J., Anderson-Bergman, C., Lang, D. T., & Bodik, R. (2017). Programming With Models: Writing Statistical Algorithms for General Model Structures With NIMBLE. *Journal of Computational and Graphical Statistics*, *26*(2), 403–413. https://doi.org/10.1080/10618600.2016.1172487

Desprez, M., McMahon, C. R., Hindell, M. A., Harcourt, R., & Gimenez, O. (2013). Known unknowns in an imperfect world: Incorporating uncertainty in recruitment estimates using multi-event capture–recapture models. *Ecology and Evolution*, *3*(14), 4658–4668. https://doi.org/10.1002/ece3.846

Dhawan, R., Fischhoff, I. R., & Ostfeld, R. S. (2018). Effects of weather variability on population dynamics of white-footed mice (Peromyscus leucopus) and eastern chipmunks (Tamias striatus). *Journal of Mammalogy*, *99*(6), 1436–1443. https://doi.org/10.1093/jmammal/gyy126

Dietze, M. (2017). *Ecological Forecasting*. Princeton University Press. https://doi.org/doi:10.1515/9781400885459

Dietze, M. C. (2017). Prediction in ecology: A first-principles framework. *Ecological Applications*, *27*(7), 2048–2060. https://doi.org/10.1002/eap.1589

Dietze, M. C., Fox, A., Beck-Johnson, L. M., Betancourt, J. L., Hooten, M. B., Jarnevich, C. S., Keitt, T. H., Kenney, M. A., Laney, C. M., Larsen, L. G., Loescher, H. W., Lunch, C. K., Pijanowski, B. C., Randerson, J. T., Read, E. K., Tredennick, A. T., Vargas, R., Weathers, K. C., & White, E. P. (2018). Iterative near-term ecological forecasting: Needs, opportunities, and challenges. *Proceedings of the National Academy of Sciences of the United States of America*, *115*(7), 1424–1432. https://doi.org/10.1073/pnas.1710231115

Diuk-Wasser, M. A., Gatewood, A. G., Cortinas, M. R., Yaremych-Hamer, S., Tsao, J., Kitron, U., Hickling, G., Brownstein, J. S., Walker, E., Piesman, J., & Fish, D. (2006). Spatiotemporal Patterns of Host-Seeking Ixodes scapularis Nymphs (Acari: Ixodidae) in the United States. *Journal of Medical Entomology*, *43*(2), 166–176. https://doi.org/10.1603/0022-2585(2006)043[0166:spohis]2.0.co;2

Diuk-Wasser, M. A., VanAcker, M. C., & Fernandez, M. P. (2020). Impact of Land Use Changes and Habitat Fragmentation on the Eco-epidemiology of Tick-Borne

Diseases. *Journal of Medical Entomology*, *58*(4), 1546–1564. https://doi.org/10.1093/jme/tjaa209

Dobson, A. D. M., Finnie, T. J. R., & Randolph, S. E. (2011). A modified matrix model to describe the seasonal population ecology of the European tick Ixodes ricinus: Ixodes ricinus population model. *Journal of Applied Ecology*, *48*(4), 1017–1028. https://doi.org/10.1111/j.1365-2664.2011.02003.x

Donahue, J. G., Piesman, J., & Spielman, A. (1987). Reservoir competence of white-footed mice for Lyme disease spirochetes. *The American Journal of Tropical Medicine and Hygiene*, *36*(1), 92–96. https://doi.org/10.4269/ajtmh.1987.36.92

Eisen, L. (2020). Stemming the Rising Tide of Human-Biting Ticks and Tickborne Diseases, United States. *Emerging Infectious Diseases*, *26*(4), 641–647. https://doi.org/10.3201/eid2604.191629

Eisen, L., & Eisen, R. J. (2016). Critical Evaluation of the Linkage Between Tick-Based Risk Measures and the Occurrence of Lyme Disease Cases. *Journal of Medical Entomology*, *53*(5), 1050–1062. https://doi.org/10.1093/jme/tjw092

Eisen, R. J., & Eisen, L. (2018). The Blacklegged Tick, Ixodes scapularis: An Increasing Public Health Concern. *Trends in Parasitology*, *34*(4), 295–309. https://doi.org/10.1016/j.pt.2017.12.006

Eisen, L., & Stafford, K. C., III. (2020). Barriers to Effective Tick Management and Tick-Bite Prevention in the United States (Acari: Ixodidae). *Journal of Medical Entomology*, *58*(4), 1588–1600. https://doi.org/10.1093/jme/tjaa079

Eisen, R. J., Eisen, L., & Beard, C. B. (2016). County-Scale Distribution of *Ixodes scapularis* and *Ixodes pacificus* (Acari: Ixodidae) in the Continental United States. *Journal of Medical Entomology*, *53*(2), 349–386. https://doi.org/10.1093/jme/tjv237

Estrada, A., & Arroyo, B. (2012). Occurrence vs abundance models: Differences between species with varying aggregation patterns. *Biological Conservation*, *152*, 37–45. https://doi.org/10.1016/j.biocon.2012.03.031

Evans, M. E. K., Holsinger, K. E., & Menges, E. S. (2010). Fire, vital rates, and population viability: A hierarchical Bayesian analysis of the endangered Florida scrub mint. *Ecological Monographs*, *80*(4), 627–649. https://doi.org/10.1890/09-1758.1

Galloway, N. L., Monello, R. J., Brimeyer, D., Cole, E. K., & Hobbs, N. T. (2021). Supporting adaptive management with ecological forecasting: Chronic wasting disease in the Jackson Elk Herd. *Ecosphere*, *12*(10), e03776. https://doi.org/10.1002/ecs2.3776

Geier, A. R., & Best, L. B. (1980). Habitat Selection by Small Mammals of Riparian Communities: Evaluating Effects of Habitat Alterations. *The Journal of Wildlife Management*, *44*(1), 16–24. https://doi.org/10.2307/3808346

Gelman, A., & Rubin, D. B. (1992). Inference from Iterative Simulation Using Multiple Sequences. *Statistical Science*, *7*(4), 457–472. https://doi.org/10.1214/ss/1177011136

Genovart, M., Pradel, R., & Oro, D. (2012). Exploiting uncertain ecological fieldwork data with multi-event capture–recapture modelling: An example with bird sex assignment. *Journal of Animal Ecology*, *81*(5), 970–977. https://doi.org/10.1111/j.1365-2656.2012.01991.x

Ginsberg, H. S., Albert, M., Acevedo, L., Dyer, M. C., Arsnoe, I. M., Tsao, J. I., Mather, T. N., & LeBrun, R. A. (2017). Environmental Factors Affecting Survival of Immature Ixodes scapularis and Implications for Geographical Distribution of Lyme Disease: The Climate/Behavior Hypothesis. *PLoS ONE*, *12*(1), e0168723. https://doi.org/10.1371/journal.pone.0168723

Ginsberg, H. S., Hickling, G. J., Burke, R. L., Ogden, N. H., Beati, L., LeBrun, R. A., Arsnoe, I. M., Gerhold, R., Han, S., Jackson, K., Maestas, L., Moody, T., Pang, G., Ross, B., Rulison, E. L., & Tsao, J. I. (2021). Why Lyme disease is common in the northern US, but rare in the south: The roles of host choice, host-seeking behavior, and tick density. *PLoS Biology*, *19*(1), e3001066. https://doi.org/10.1371/journal.pbio.3001066

Ginsberg, H. S., Rulison, E. L., Azevedo, A., Pang, G. C., Kuczaj, I. M., Tsao, J. I., & LeBrun, R. A. (2014). Comparison of survival patterns of northern and southern genotypes of the North American tick Ixodes scapularis (Acari: Ixodidae) under northern and southern conditions. *Parasites & Vectors*, *7*(1), 394. https://doi.org/10.1186/1756-3305-7-394

Ginsberg, H. S., Rulison, E. L., Miller, J. L., Pang, G., Arsnoe, I. M., Hickling, G. J., Ogden, N. H., LeBrun, R. A., & Tsao, J. I. (2020). Local abundance of Ixodes

scapularis in forests: Effects of environmental moisture, vegetation characteristics, and host abundance. *Ticks and Tick-Borne Diseases*, *11*(1), 101271. https://doi.org/10.1016/j.ttbdis.2019.101271

Gleim, E. R., Conner, L. M., Berghaus, R. D., Levin, M. L., Zemtsova, G. E., & Yabsley, M. J. (2014). The Phenology of Ticks and the Effects of Long-Term Prescribed Burning on Tick Population Dynamics in Southwestern Georgia and Northwestern Florida. *PLoS ONE*, *9*(11), e112174. https://doi.org/10.1371/journal.pone.0112174

Gneiting, T., & Raftery, A. E. (2007). Strictly Proper Scoring Rules, Prediction, and Estimation. *Journal of the American Statistical Association*, *102*(477), 359–378. https://doi.org/10.1198/016214506000001437

Goodwin, B. J., Ostfeld, R. S., & Schauber, E. M. (2001). Spatiotemporal Variation in a Lyme Disease Host and Vector: Black-Legged Ticks on White-Footed Mice. *Vector-Borne and Zoonotic Diseases*, *1*(2), 129–138. https://doi.org/10.1089/153036601316977732

Gray, J., Kahl, O., Lane, R. S., & Stanek, G. (2002). *Lyme borreliosis: Biology, epidemiology, and control*. CABI.

Gray, J.S. (1998). The ecology of ticks transmitting Lyme borreliosis. *Experimental & Applied Acarology*, *22*, 10.

Gross, K., Craig, B. A., & Hutchison, W. D. (2002). Bayesian Estimation of a Demographic Matrix Model from Stage-Frequency Data. *Ecology*, *83*(12), 3285–3298.

Hamer, S. A., Tsao, J. I., Walker, E. D., & Hickling, G. J. (2010). Invasion of the Lyme Disease Vector Ixodes scapularis: Implications for Borrelia burgdorferi Endemicity. *EcoHealth*, *7*(1), 47–63. https://doi.org/10.1007/s10393-010-0287-0

Hayes, L. E., Scott, J. A., & Stafford, K. C. (2015). Influences of weather on Ixodes scapularis nymphal densities at long-term study sites in Connecticut. *Ticks and Tick-Borne Diseases*, *6*(3), 258–266. https://doi.org/10.1016/j.ttbdis.2015.01.006

Hernández-Camacho, C. J., Bakker, V. J., Aurioles-Gamboa, D., Laake, J., & Gerber, L. R. (2015). The Use of Surrogate Data in Demographic Population Viability Analysis: A Case Study of California Sea Lions. *PLoS ONE*, *10*(9), e0139158. https://doi.org/10.1371/journal.pone.0139158

Hersh, M. H., LaDeau, S. L., Previtali, M. A., & Ostfeld, R. S. (2014). When is a parasite not a parasite? Effects of larval tick burdens on white-footed mouse survival. *Ecology*, *95*(5), 1360–1369. https://doi.org/10.1890/12-2156.1

Hertz, J. C., Ferree Clemons, B. C., Lord, C. C., Allan, S. A., & Kaufman, P. E. (2017). Distribution and host associations of ixodid ticks collected from wildlife in Florida, USA. *Experimental and Applied Acarology*, *73*(2), 223–236. https://doi.org/10.1007/s10493-017-0183-1

Hinckley, A. F., Meek, J. I., Ray, J. A. E., Niesobecki, S. A., Connally, N. P., Feldman, K. A., Jones, E. H., Backenson, P. B., White, J. L., Lukacik, G., Kay, A. B., Miranda, W. P., & Mead, P. S. (2016). Effectiveness of Residential Acaricides to Prevent Lyme and Other Tick-borne Diseases in Humans. *The Journal of Infectious Diseases*, *214*(2), 182–188. https://doi.org/10.1093/infdis/jiv775

Howard, C., Stephens, P. A., Pearce-Higgins, J. W., Gregory, R. D., & Willis, S. G. (2014). Improving species distribution models: The value of data on abundance. *Methods in Ecology and Evolution*, *5*(6), 506–513. https://doi.org/10.1111/2041-210X.12184

Hroobi, A., Boorgula, G. D., Gordon, D., Bai, J., Goodin, D., Anderson, G., Wilson, S., Staggs, A., & Raghavan, R. K. (2021). Diversity and seasonality of host-seeking ticks in a periurban environment in the Central Midwest (USA). *PLoS ONE*, *16*(4), e0250272. https://doi.org/10.1371/journal.pone.0250272

Hufkens, K., Basler, D., Milliman, T., Melaas, E. K., & Richardson, A. D. (2018). An integrated phenology modelling framework in R: modelling vegetation phenology with phenor. *Methods in Ecology & Evolution*, *9*, 1–10. https://doi.org/10.1111/2041-210X.12970

Jennelle, C. S., Cooch, E. G., Conroy, M. J., & Senar, J. C. (2007). State-Specific Detection Probabilities and Disease Prevalence. *Ecological Applications*, *17*(1), 154–167. https://doi.org/10.1890/1051-0761(2007)017[0154:SDPADP]2.0.CO;2

Johnson-Bice, S. M., Ferguson, J. M., Erb, J. D., Gable, T. D., & Windels, S. K. (2021). Ecological forecasts reveal limitations of common model selection methods: Predicting changes in beaver colony densities. *Ecological Applications*, *31*(1). https://doi.org/10.1002/eap.2198

Jones, C. J., & Kitron, U. D. (2000). Populations of Ixodes scapularis (Acari: Ixodidae) Are Modulated by Drought at a Lyme Disease Focus in Illinois. *Journal of Medical Entomology*, *37*(3), 8.

Jordan, R. A., & Schulze, T. L. (2019). Ability of Two Commercially Available Host-Targeted Technologies to Reduce Abundance of Ixodes scapularis (Acari: Ixodidae) in a Residential Landscape. *Journal of Medical Entomology*, *56*(4), 1095–1101. https://doi.org/10.1093/jme/tjz046

Keesing, F., Brunner, J., Duerr, S., Killilea, M., LoGiudice, K., Schmidt, K., Vuong, H., & Ostfeld, R. S. (2009). Hosts as ecological traps for the vector of Lyme disease. *Proceedings of the Royal Society B: Biological Sciences*, *276*(1675), 3911–3919. https://doi.org/10.1098/rspb.2009.1159

Kelly, V. (2020). *Cary Environmental Monitoring Program Daily Meteorological and Solar Radiation Data: 1988-2021* [Data set]. Cary Institute. https://doi.org/10.25390/caryinstitute.11553219.v3

Kéry, M., & Schaub, M. (2011). *Bayesian population analysis using WinBUGS: a hierarchical perspective*. Academic Press.

Kéry, M., & Schaub, M. (2012). Estimation of Survival, Recruitment, and Population Size from Capture–Recapture Data Using the Jolly–Seber Model. In *Bayesian Population Analysis using WinBUGS* (pp. 315–346). Elsevier. https://doi.org/10.1016/B978-0-12-387020-9.00010-9

Kessler, W. H., Ganser, C., & Glass, G. E. (2019). Modeling the Distribution of Medically Important Tick Species in Florida. *Insects*, *10*(7), 190. https://doi.org/10.3390/insects10070190

Khatchikian, C. E., Prusinski, M. A., Stone, M., Backenson, P. B., Wang, I.-N., Foley, E., Seifert, S. N., Levy, M. Z., & Brisson, D. (2015). Recent and rapid population

growth and range expansion of the Lyme disease tick vector, *Ixodes scapularis* , in North America: Population and Range Expansion of Ticks. *Evolution*, *69*(7), 1678–1689. https://doi.org/10.1111/evo.12690

Kilpatrick, A. M., Dobson, A. D. M., Levi, T., Salkeld, D. J., Swei, A., Ginsberg, H. S., Kjemtrup, A., Padgett, K. A., Jensen, P. M., Fish, D., Ogden, N. H., & Diuk-Wasser, M. A. (2017). Lyme disease ecology in a changing world: Consensus, uncertainty and critical gaps for improving control. *Philosophical Transactions of the Royal Society B: Biological Sciences*, *372*(1722), 15. http://dx.doi.org/10.1098/rstb.2016.0117

Kirtman, B. P., Min, D., Infanti, J. M., Kinter, J. L., Paolino, D. A., Zhang, Q., Dool, H. van den, Saha, S., Mendez, M. P., Becker, E., Peng, P., Tripp, P., Huang, J., DeWitt, D. G., Tippett, M. K., Barnston, A. G., Li, S., Rosati, A., Schubert, S. D., … Wood, E. F. (2014). The North American Multimodel Ensemble: Phase-1 Seasonal-to-Interannual Prediction; Phase-2 toward Developing Intraseasonal Prediction. *Bulletin of the American Meteorological Society*, *95*(4), 585–601. https://doi.org/10.1175/BAMS-D-12-00050.1

Kleiven, E. F., Henden, J.-A., Ims, R. A., & Yoccoz, N. G. (2018). Seasonal difference in temporal transferability of an ecological model: Near-term predictions of lemming outbreak abundances. *Scientific Reports*, *8*(1), Article 1. https://doi.org/10.1038/s41598-018-33443-6

Kollars, T. M., Jr., Oliver, J. H., Jr., Kollars, P. G., & Durden, L. A. (1999). Seasonal Activity and Host Associations of Ixodes scapularis (Acari: Ixodidae) in

Southeastern Missouri. *Journal of Medical Entomology*, *36*(6), 720–726. https://doi.org/10.1093/jmedent/36.6.720

Kollars, T. M., Oliver, J. H., Durden, L. A., & Kollars, P. G. (2000). Host association and seasonal activity of Amblyomma americanum (Acari: Ixodidae) in Missouri. *The Journal of Parasitology*, *86*(5), 1156–1159. https://doi.org/10.1645/0022-3395(2000)086[1156:HAASAO]2.0.CO;2

Labruna, M. B., Leite, R. C., Faccini, J. L., & Ferreira, F. (2000). Life cycle of the tick Haemaphysalis leporis-palustris (Acari: Ixodidae) under laboratory conditions. *Experimental & Applied Acarology*, *24*(9), 683–694. https://doi.org/10.1023/a:1010768511790

LaDeau, S. L., Glass, G. E., Hobbs, N. T., Latimer, A., & Ostfeld, R. S. (2011). Data–model fusion to better understand emerging pathogens and improve infectious disease forecasting. *Ecological Applications*, *21*(5), 1443–1460. https://doi.org/10.1890/09-1409.1

Lantos, P. M., Tsao, J., Janko, M., Arab, A., von Fricken, M. E., Auwaerter, P. G., Nigrovic, L. E., Fowler, V., Ruffin, F., Gaines, D., Broyhill, J., & Swenson, J. (2021). Environmental Correlates of Lyme Disease Emergence in Southwest Virginia, 2005–2014. *Journal of Medical Entomology*, *58*(5), 1680–1685. https://doi.org/10.1093/jme/tjab038

Lebreton, J., Nichols, J. D., Barker, R. J., Pradel, R., & Spendelow, J. A. (2009). Chapter 3 Modeling Individual Animal Histories with Multistate Capture–Recapture

Models. In *Advances in Ecological Research* (Vol. 41, pp. 87–173). Academic Press. https://doi.org/10.1016/S0065-2504(09)00403-6

Levi, T., Keesing, F., Holt, R. D., Barfield, M., & Ostfeld, R. S. (2016). Quantifying dilution and amplification in a community of hosts for tick-borne pathogens. *Ecological Applications*, *26*(2), 484–498. https://doi.org/10.1890/15-0122

Levi, T., Keesing, F., Oggenfuss, K., & Ostfeld, R. S. (2015). Accelerated phenology of blacklegged ticks under climate warming. *Philosophical Transactions of the Royal Society B: Biological Sciences*, *370*(1665), 20130556. https://doi.org/10.1098/rstb.2013.0556

Lewis, A. S. L., Woelmer, W. M., Wander, H. L., Howard, D. W., Smith, J. W., McClure, R. P., Lofton, M. E., Hammond, N. W., Corrigan, R. S., Thomas, R. Q., & Carey, C. C. (2022). Increased adoption of best practices in ecological forecasting enables comparisons of forecastability. *Ecological Applications*, *32*(2), e2500. https://doi.org/10.1002/eap.2500

Lindsay, L. R., Barker, I. K., Surgeoner, G. A., Mcewen, S. A., Gillespie, T. J., & Addison, E. M. (1998). Survival and Development of the Different Life Stages of Ixodes scapularis (Acari: Ixodidae) Held within Four Habitats on Long Point, Ontario, Canada. *Journal of Medical Entomology*, *35*(3), 189–199. https://doi.org/10.1093/jmedent/35.3.189

Lindsay, L. R., Mathison, S. W., Barker, I. K., McEwen, S. A., Gillespie, T. J., & Surgeoner, G. A. (1999). Microclimate and Habitat in Relation to *Ixodes*

scapularis (Acari: Ixodidae) Populations on Long Point, Ontario, Canada. *Journal of Medical Entomology*, *36*(3), 255–262. https://doi.org/10.1093/jmedent/36.3.255

Linske, M. A., Williams, S. C., Stafford, K. C., & Ortega, I. M. (2018). Ixodes scapularis (Acari: Ixodidae) Reservoir Host Diversity and Abundance Impacts on Dilution of Borrelia burgdorferi (Spirochaetales: Spirochaetaceae) in Residential and Woodland Habitats in Connecticut, United States. *Journal of Medical Entomology*, *55*(3), 681–690. https://doi.org/10.1093/jme/tjx237

Little, E. A. H., Anderson, J. F., Stafford, K. C., Eisen, L., Eisen, R. J., & Molaei, G. (2019). Predicting spatiotemporal patterns of Lyme disease incidence from passively collected surveillance data for Borrelia burgdorferi sensu lato-infected Ixodes scapularis ticks. *Ticks and Tick-Borne Diseases*, *10*(5), 970–980. https://doi.org/10.1016/j.ttbdis.2019.04.010

Llera, A., & Beckmann, C. (2016). Estimating an Inverse Gamma distribution. *arXiv* https://doi.org/10.48550/arXiv.1605.01019

LoGiudice, K., Ostfeld, R. S., Schmidt, K. A., & Keesing, F. (2003). The Ecology of Infectious Disease: Effects of Host Diversity and Community Composition on Lyme Disease Risk. *Proceedings of the National Academy of Sciences of the United States of America*, *100*(2), 567–571.

Mader, E. M., Ganser, C., Geiger, A., Harrington, L. C., Foley, J., Smith, R. L., Mateus-Pinilla, N., Teel, P. D., & Eisen, R. J. (2020). A Survey of Tick Surveillance and Control Practices in the United States. *Journal of Medical Entomology*, *58*(4), 1503–1512. https://doi.org/10.1093/jme/tjaa094

Maguire, K. C., Nieto-Lugilde, D., Blois, J. L., Fitzpatrick, M. C., Williams, J. W., Ferrier, S., & Lorenz, D. J. (2016). Controlled comparison of species- and community-level models across novel climates and communities. *Proceedings of the Royal Society B: Biological Sciences*, *283*(1826), 20152817. https://doi.org/10.1098/rspb.2015.2817

Marshall, K. E., & Sinclair, B. J. (2010). Repeated stress exposure results in a survival–reproduction trade-off in Drosophila melanogaster. *Proceedings of the Royal Society B: Biological Sciences*, *277*(1683), 963–969. https://doi.org/10.1098/rspb.2009.1807

Mather, T. N., Nicholson, M. C., Donnelly, E. F., & Matyas, B. T. (1996). Entomologic Index for Human Risk of Lyme Disease. *American Journal of Epidemiology, 144*(11), 1066–1069. https://doi.org/10.1093/oxfordjournals.aje.a008879

Mathisson, D. C., Kross, S. M., Palmer, M. I., & Diuk-Wasser, M. A. (2021). Effect of Vegetation on the Abundance of Tick Vectors in the Northeastern United States: A Review of the Literature. *Journal of Medical Entomology, 58*(6), 2030–2037. https://doi.org/10.1093/jme/tjab098

Matthiopoulos, J., Fieberg, J., Aarts, G., Beyer, H. L., Morales, J. M., & Haydon, D. T. (2015). Establishing the link between habitat selection and animal population dynamics. *Ecological Monographs*, *85*(3), 413–436. https://doi.org/10.1890/14-2244.1

Mays, S. E., Houston, A. E., & Trout Fryxell, R. T. (2016). Comparison of novel and conventional methods of trapping ixodid ticks in the southeastern U.S.A. *Medical and Veterinary Entomology*, *30*(2), 123–134. https://doi.org/10.1111/mve.12160

McNab, B. K. (1963). Bioenergetics and the Determination of Home Range Size. *The American Naturalist*, *97*(894), 133–140. https://doi.org/10.1086/282264

Michielsens, C. G. J., McAllister, M. K., Kuikka, S., Mäntyniemi, S., Romakkaniemi, A., Pakarinen, T., Karlsson, L., & Uusitalo, L. (2008). Combining multiple Bayesian data analyses in a sequential framework for quantitative fisheries stock assessment. *Canadian Journal of Fisheries and Aquatic Sciences*, *65*(5), 962–974. https://doi.org/10.1139/f08-015

Monzón, J. D., Atkinson, E. G., Henn, B. M., & Benach, J. L. (2016). Population and Evolutionary Genomics of Amblyomma americanum, an Expanding Arthropod Disease Vector. *Genome Biology and Evolution*, *8*(5), 1351–1360. https://doi.org/10.1093/gbe/evw080

Mount, G. A., Haile, D. G., Barnard, D. R., & Daniels, E. (1993). New Version of LSTSIM for Computer Simulation of Amblyomma americanum (Acari: Ixodidae) Population Dynamics. *Journal of Medical Entomology*, *30*(5), 843–857. https://doi.org/10.1093/jmedent/30.5.843

Murray, K. A., Skerratt, L. F., Speare, R., & McCallum, H. (2009). Impact and Dynamics of Disease in Species Threatened by the Amphibian Chytrid Fungus, Batrachochytrium dendrobatidis. *Conservation Biology*, *23*(5), 1242–1252. https://doi.org/10.1111/j.1523-1739.2009.01211.x

National Ecological Observatory Network (NEON). (2022a). *Small mammal box trapping (DP1.10072.001)*. National Ecological Observatory Network (NEON). https://doi.org/10.48443/H3DK-3A71

National Ecological Observatory Network (NEON). (2022b). *Ticks sampled using drag cloths (DP1.10093.001)*. National Ecological Observatory Network (NEON). https://doi.org/10.48443/7JH5-8S51

Needham, G. R. (1991). Off-Host Physiological Ecology of Ixodid Ticks. *Annual Review of Entomology*, *36*, 659–681. https://doi.org/10.1146/annurev.en.36.010191.003303

Nicholson, M. C., & Mather, T. N. (1996). Methods for evaluating Lyme disease risks using geographic information systems and geospatial analysis. *Journal of Medical Entomology*, *33*(5), 711–720. https://doi.org/10.1093/jmedent/33.5.711

Niu, S., Luo, Y., Dietze, M. C., Keenan, T. F., Shi, Z., Li, J., & Iii, F. S. C. (2014). The role of data assimilation in predictive ecology. *Ecosphere*, *5*(5), art65. https://doi.org/10.1890/ES13-00273.1

Nupp, T. E., & Swihart, R. K. (1996). Effect of forest patch area on population attributes of white-footed mice (*Peromyscus leucopus*) in fragmented landscapes. *Canadian Journal of Zoology*, *74*(3), 467–472. https://doi.org/10.1139/z96-054

Nupp, T. E., & Swihart, R. K. (2000). Landscape-Level Correlates for Small-Mammal Assemblages in Forest Fragments of Farmland. *Journal of Mammalogy*, *81*(2), 512–526. https://doi.org/10.1644/1545-1542(2000)081%3C0512:LLCOSM%3E2.0.CO;2

Ogden, N. H., Ben Beard, C., Ginsberg, H. S., & Tsao, J. I. (2020). Possible Effects of Climate Change on Ixodid Ticks and the Pathogens They Transmit: Predictions and Observations. *Journal of Medical Entomology, 58*(4), 1536–1545. https://doi.org/10.1093/jme/tjaa220

Ogden, N. H., Bigras-Poulin, M., Hanincová, K., Maarouf, A., O'Callaghan, C. J., & Kurtenbach, K. (2008). Projected effects of climate change on tick phenology and fitness of pathogens transmitted by the North American tick Ixodes scapularis. *Journal of Theoretical Biology*, *254*(3), 621–632. https://doi.org/10.1016/j.jtbi.2008.06.020

Ogden, N. H., Bigras-Poulin, M., O'Callaghan, C. J., Barker, I. K., Lindsay, L. R., Maarouf, A., Smoyer-Tomic, K. E., Waltner-Toews, D., & Charron, D. (2005). A dynamic population model to investigate effects of climate on geographic range and seasonality of the tick Ixodes scapularis. *International Journal for Parasitology*, *35*(4), 375–389. https://doi.org/10.1016/j.ijpara.2004.12.013

Ogden, N. H., Pang, G., Ginsberg, H. S., Hickling, G. J., Burke, R. L., Beati, L., & Tsao, J. I. (2018). Evidence for Geographic Variation in Life-Cycle Processes Affecting Phenology of the Lyme Disease Vector Ixodes scapularis (Acari: Ixodidae) in the United States. *Journal of Medical Entomology*, *55*(6), 1386–1401. https://doi.org/10.1093/jme/tjy104

Ogden, N. H., Radojevic, ´ Milka, Wu, X., Duvvuri, V. R., Leighton, P. A., & Wu, J. (2014). Estimated Effects of Projected Climate Change on the Basic Reproductive

Number of the Lyme Disease Vector Ixodes scapularis. *Environmental Health Perspectives*, *122*(6), 631–638. https://doi.org/10.1289/ehp.1307799

Oliver, J. D., Bennett, S. W., Beati, L., & Bartholomay, L. C. (2017). Range Expansion and Increasing Borrelia burgdorferi Infection of the Tick Ixodes scapularis (Acari: Ixodidae) in Iowa, 1990–2013. *Journal of Medical Entomology*, *54*(6), 1727–1734. https://doi.org/10.1093/jme/tjx121

Ostfeld, R. S., Brisson, D., Oggenfuss, K., Devine, J., Levy, M. Z., & Keesing, F. (2018). Effects of a zoonotic pathogen, *Borrelia burgdorferi* , on the behavior of a key reservoir host. *Ecology and Evolution*, *8*(8), 4074–4083. https://doi.org/10.1002/ece3.3961

Ostfeld, R. S., & Brunner, J. L. (2015). Climate change and *Ixodes* tick-borne diseases of humans. *Philosophical Transactions of the Royal Society B: Biological Sciences*, *370*(1665), 20140051. https://doi.org/10.1098/rstb.2014.0051

Ostfeld, R. S., Canham, C. D., Oggenfuss, K., Winchcombe, R. J., & Keesing, F. (2006). Climate, Deer, Rodents, and Acorns as Determinants of Variation in Lyme-Disease Risk. *PLoS Biology*, *4*(6), e145. https://doi.org/10.1371/journal.pbio.0040145

Ostfeld, R. S., Hazler, K. R., & Cepeda, O. M. (1996). Temporal and Spatial Dynamics of Ixodes scapularis (Acari: Ixodidae) in a Rural Landscape. *Journal of Medical Entomology*, *33*(1), 90–95. https://doi.org/10.1093/jmedent/33.1.90

Ostfeld, R. S., Jones, C. G., & Wolff, J. O. (1996). Of Mice and Mast. *BioScience*, *46*(5), 323–330. https://doi.org/10.2307/1312946

Ostfeld, R. S., Levi, T., Keesing, F., Oggenfuss, K., & Canham, C. D. (2018). Tick-borne disease risk in a forest food web. *Ecology*, *99*(7), 1562–1573. https://doi.org/10.1002/ecy.2386

Ostfeld, R. S., Schauber, E. M., Canham, C. D., Keesing, F., Jones, C. G., & Wolff, J. O. (2001). Effects of Acorn Production and Mouse Abundance on Abundance and *Borrelia burgdorferi* Infection Prevalence of Nymphal *Ixodes scapularis* Ticks. *Vector-Borne and Zoonotic Diseases*, *1*(1), 55–63. https://doi.org/10.1089/153036601750137688

Paddock, C. D., & Yabsley, M. J. (2007). Ecological Havoc, the Rise of White-Tailed Deer, and the Emergence of Amblyomma americanum-Associated Zoonoses in the United States. In J. E. Childs, J. S. Mackenzie, & J. A. Richt (Eds.), *Wildlife and Emerging Zoonotic Diseases: The Biology, Circumstances and Consequences of Cross-Species Transmission* (pp. 289–324). Springer. https://doi.org/10.1007/978-3-540-70962-6_12

Paton, R. S., & Matthiopoulos, J. (2016). Defining the scale of habitat availability for models of habitat selection. *Ecology*, *97*(5), 1113–1122. https://doi.org/10.1890/14-2241.1

Paull, S. H., Thibault, K. M., Benson, A. L., Thibault, K. M., & Benson, A. L. (2022). Tick abundance, diversity and pathogen data collected by the National Ecological Observatory Network. *Gigabyte*, *2022*, 1–11. https://doi.org/10.46471/gigabyte.56

Peñalver-Alcázar, M., Aragón, P., Breedveld, M. C., & Fitze, P. S. (2016). Microhabitat selection in the common lizard: Implications of biotic interactions, age, sex, local

processes, and model transferability among populations. *Ecology and Evolution*, *6*(11), 3594–3607. https://doi.org/10.1002/ece3.2138

Pennekamp, F., Iles, A. C., Garland, J., Brennan, G., Brose, U., Gaedke, U., Jacob, U., Kratina, P., Matthews, B., Munch, S., Novak, M., Palamara, G. M., Rall, B. C., Rosenbaum, B., Tabi, A., Ward, C., Williams, R., Ye, H., & Petchey, O. L. (2019). The intrinsic predictability of ecological time series and its potential to guide forecasting. *Ecological Monographs*, *89*(2). https://doi.org/10.1002/ecm.1359

Pepin, K. M., Eisen, R. J., Mead, P. S., Piesman, J., Fish, D., Hoen, A. G., Barbour, A. G., Hamer, S., & Diuk-Wasser, M. A. (2012). Geographic Variation in the Relationship between Human Lyme Disease Incidence and Density of Infected Host-Seeking Ixodes scapularis Nymphs in the Eastern United States. *The American Journal of Tropical Medicine and Hygiene*, *86*(6), 1062–1071. https://doi.org/10.4269/ajtmh.2012.11-0630

Perret, J.-L., Rais, O., & Gern, L. (2004). Influence of Climate on the Proportion of Ixodes ricinus Nymphs and Adults Questing in a Tick Population. *Journal of Medical Entomology*, *41*(3), 361–365. https://doi.org/10.1603/0022-2585-41.3.361

Piesman, J., & Eisen, L. (2008). Prevention of Tick-Borne Diseases. *Annual Review of Entomology*, *53*(1), 323–343. https://doi.org/10.1146/annurev.ento.53.103106.093429

Piesman, J., Maupin, G. O., Campos, E. G., & Happ, C. M. (1991). Duration of adult female Ixodes dammini attachment and transmission of Borrelia burgdorferi, with description of a needle aspiration isolation method. *The Journal of Infectious Diseases, 163*(4), 895–897. https://doi.org/10.1093/infdis/163.4.895

Plummer, M., Best, N., Cowles, K., & Vines, K. (2006). CODA: Convergence Diagnosis and Output Analysis for MCMC. *R News, 6*(1), 7–11.

Pradel, R. (2005). Multievent: An Extension of Multistate Capture–Recapture Models to Uncertain States. *Biometrics, 61*(2), 442–447. https://doi.org/10.1111/j.1541-0420.2005.00318.x

R Core Team. (2020). *R: A Language and Environment for Statistical Computing*. R Foundation for Statistical Computing. https://www.R-project.org/

Randolph, S. E. (2004). Tick ecology: Processes and patterns behind the epidemiological risk posed by ixodid ticks as vectors. *Parasitology, 129*(S1), S37–S65. https://doi.org/10.1017/S0031182004004925

Randon, M., Dowd, M., & Joy, R. (2022). A real-time data assimilative forecasting system for animal tracking. *Ecology, 103*(8), e3718. https://doi.org/10.1002/ecy.3718

Richter, D., Debski, A., Hubalek, Z., & Matuschka, F.-R. (2012). Absence of Lyme Disease Spirochetes in Larval Ixodes ricinus Ticks. *Vector-Borne and Zoonotic Diseases, 12*(1), 21–27. https://doi.org/10.1089/vbz.2011.0668

Ripoche, M., Lindsay, L., Ludwig, A., Ogden, N., Thivierge, K., & Leighton, P. (2018). Multi-Scale Clustering of Lyme Disease Risk at the Expanding Leading Edge of

the Range of Ixodes scapularis in Canada. *International Journal of Environmental Research and Public Health*, *15*(4), 603. https://doi.org/10.3390/ijerph15040603

Robert, A., Bolton, M., Jiguet, F., & Bried, J. (2015). The survival–reproduction association becomes stronger when conditions are good. *Proceedings of the Royal Society B: Biological Sciences*, *282*(1818), 20151529. https://doi.org/10.1098/rspb.2015.1529

Rollend, L., Fish, D., & Childs, J. E. (2013). Transovarial transmission of Borrelia spirochetes by Ixodes scapularis: A summary of the literature and recent observations. *Ticks and Tick-Borne Diseases*, *4*(1), 46–51. https://doi.org/10.1016/j.ttbdis.2012.06.008

Ruette, S., Vandel, J.-M., Albaret, M., & Devillard, S. (2015). Comparative survival pattern of the syntopic pine and stone martens in a trapped rural area in France. *Journal of Zoology*, *295*(3), 214–222. https://doi.org/10.1111/jzo.12201

Santoro, S., Pacios, I., Moreno, S., Bertó-Moran, A., & Rouco, C. (2014). Multi-event capture–recapture modeling of host–pathogen dynamics among European rabbit populations exposed to myxoma and Rabbit Hemorrhagic Disease Viruses: Common and heterogeneous patterns. *Veterinary Research*, *45*(1), 39. https://doi.org/10.1186/1297-9716-45-39

Schauber, E. M., Ostfeld, R. S., & Evans, Jr, A. S. (2005). What is the Best Predictor of Annual Lyme Disease Incidence: Weather, Mice, or Acorns? *Ecological Applications*, *15*(2), 575–586. https://doi.org/10.1890/03-5370

Schmidt, K. A., & Ostfeld, R. S. (2001). Biodiversity and the Dilution Effect in Disease Ecology. *Ecology*, *82*(3), 609–619. https://doi.org/10.1890/0012-9658(2001)082[0609:BATDEI]2.0.CO;2

Schulze, T. L., Jordan, R. A., & Hung, R. W. (2001). Effects of Selected Meteorological Factors on Diurnal Questing of *Ixodes scapularis* and *Amblyomma americanum* (Acari: Ixodidae). *Journal of Medical Entomology*, *38*(2), 318–324. https://doi.org/10.1603/0022-2585-38.2.318

Schulze, T. L., Jordan, R. A., & Hung, R. W. (2002). Effects of Microscale Habitat Physiognomy on the Focal Distribution of Ixodes scapularis and Amblyomma americanum (Acari: Ixodidae) Nymphs. *Environmental Entomology*, *31*(6), 1085–1090. https://doi.org/10.1603/0046-225X-31.6.1085

Schulze, T. L., Jordan, R. A., Schulze, C. J., Mixson, T., & Papero, M. (2005). Relative Encounter Frequencies and Prevalence of Selected Borrelia, Ehrlichia, and Anaplasma Infections in Amblyomma americanum and Ixodes scapularis (Acari: Ixodidae) Ticks from Central New Jersey. *Journal of Medical Entomology, 42*(3), 450–456. https://doi.org/10.1093/jmedent/42.3.450

Sequeira, A. M. M., Bouchet, P. J., Yates, K. L., Mengersen, K., & Caley, M. J. (2018). Transferring biodiversity models for conservation: Opportunities and challenges. *Methods in Ecology and Evolution*, *9*(5), 1250–1264. https://doi.org/10.1111/2041-210X.12998

Sequeira, A. M. M., Mellin, C., Lozano-Montes, H. M., Meeuwig, J. J., Vanderklift, M. A., Haywood, M. D. E., Babcock, R. C., & Caley, M. J. (2018). Challenges of

transferring models of fish abundance between coral reefs. *PeerJ*, *6*, e4566. https://doi.org/10.7717/peerj.4566

Sequeira, A. M. M., Mellin, C., Lozano-Montes, H. M., Vanderklift, M. A., Babcock, R. C., Haywood, M. D. E., Meeuwig, J. J., & Caley, M. J. (2016). Transferability of predictive models of coral reef fish species richness. *Journal of Applied Ecology*, *53*(1), 64–72. https://doi.org/10.1111/1365-2664.12578

Sharareh, N., Behler, R. P., Roome, A. B., Shepherd, J., Garruto, R. M., & Sabounchi, N. S. (2019). Risk Factors of Lyme Disease: An Intersection of Environmental Ecology and Systems Science. *Healthcare*, *7*(2), 66. https://doi.org/10.3390/healthcare7020066

Simonis, J. L., White, E. P., & Ernest, S. K. M. (2021). Evaluating probabilistic ecological forecasts. *Ecology*, *102*(8), e03431. https://doi.org/10.1002/ecy.3431

Soininen, E. M., Henden, J., Ravolainen, V. T., Yoccoz, N. G., Bråthen, K. A., Killengreen, S. T., & Ims, R. A. (2018). Transferability of biotic interactions: Temporal consistency of arctic plant–rodent relationships is poor. *Ecology and Evolution*, *8*(19), 9697–9711. https://doi.org/10.1002/ece3.4399

Sonenshine, D. (2018). Range Expansion of Tick Disease Vectors in North America: Implications for Spread of Tick-Borne Disease. *International Journal of Environmental Research and Public Health*, *15*(3), 478. https://doi.org/10.3390/ijerph15030478

Springer, Y. P., Jarnevich, C. S., Monaghan, A. J., Eisen, R. J., & Barnett, D. T. (2015). Modeling the Present and Future Geographic Distribution of the Lone Star Tick,

Amblyomma americanum (Ixodida: Ixodidae), in the Continental United States. *The American Journal of Tropical Medicine and Hygiene*, *93*(4), 875–890. https://doi.org/10.4269/ajtmh.15-0330

Stafford, K. C., Cartter, M. L., Magnarelli, L. A., Ertel, S.-H., & Mshar, P. A. (1998). Temporal Correlations between Tick Abundance and Prevalence of Ticks Infected with Borrelia burgdorferi and Increasing Incidence of Lyme Disease. *Journal of Clinical Microbiology*, *36*(5), 1240–1244. https://doi.org/10.1128/JCM.36.5.1240-1244.1998

Stanek, G., Wormser, G. P., Gray, J., & Strle, F. (2012). Lyme borreliosis. *The Lancet*, *379*(9814), 461–473. https://doi.org/10.1016/S0140-6736(11)60103-7

Stone, C. M., Hamilton, I. M., & Foster, W. A. (2011). A survival and reproduction trade-off is resolved in accordance with resource availability by virgin female mosquitoes. *Animal Behaviour*, *81*(4), 765–774. https://doi.org/10.1016/j.anbehav.2011.01.008

Stuart-Smith, R. D., Bates, A. E., Lefcheck, J. S., Duffy, J. E., Baker, S. C., Thomson, R. J., Stuart-Smith, J. F., Hill, N. A., Kininmonth, S. J., Airoldi, L., Becerro, M. A., Campbell, S. J., Dawson, T. P., Navarrete, S. A., Soler, G. A., Strain, E. M. A., Willis, T. J., & Edgar, G. J. (2013). Integrating abundance and functional traits reveals new global hotspots of fish diversity. *Nature*, *501*(7468), Article 7468. https://doi.org/10.1038/nature12529

Taylor, S. D., & White, E. P. (2020). *Influence of climate forecasts, data assimilation, and uncertainty propagation on the performance of near-term phenology forecasts* [Preprint]. Ecology. https://doi.org/10.1101/2020.08.18.256057

Thornton, M. M., Shrestha, R., Wei, Y., Thornton, P. E., Kao, S., & Wilson, B. E. (2020). *Daymet: Daily Surface Weather Data on a 1-km Grid for North America, Version 4*. ORNL Distributed Active Archive Center. https://doi.org/10.3334/ORNLDAAC/1840

Tilly, K., Rosa, P. A., & Stewart, P. E. (2008). Biology of Infection with Borrelia burgdorferi. *Infectious Disease Clinics of North America*, *22*(2), 217–234. https://doi.org/10.1016/j.idc.2007.12.013

Tsao, J. I., Hamer, S. A., Han, S., Sidge, J. L., & Hickling, G. J. (2021). The Contribution of Wildlife Hosts to the Rise of Ticks and Tick-Borne Diseases in North America. *Journal of Medical Entomology*, *58*(4), 1565–1587. https://doi.org/10.1093/jme/tjab047

Van der Putten, W. H., Macel, M., & Visser, M. E. (2010). Predicting species distribution and abundance responses to climate change: Why it is essential to include biotic interactions across trophic levels. *Philosophical Transactions of the Royal Society B: Biological Sciences*, *365*(1549), 2025–2034. https://doi.org/10.1098/rstb.2010.0037

White, E. P., Yenni, G. M., Taylor, S. D., Christensen, E. M., Bledsoe, E. K., Simonis, J. L., & Ernest, S. K. M. (2018). *Developing an automated iterative near-term*

forecasting system for an ecological study [Preprint]. Ecology. https://doi.org/10.1101/268623

Wilson, M. L., Litwin, T. S., Gavin, T. A., Capkanis, M. C., Maclean, D. C., & Spielman, A. (1990). Host-Dependent Differences in Feeding and Reproduction of Ixodes dammini (Acari: Ixodidae). *Journal of Medical Entomology*, *27*(6), 945–954. https://doi.org/10.1093/jmedent/27.6.945

Yates, K. L., Bouchet, P. J., Caley, M. J., Mengersen, K., Randin, C. F., Parnell, S., Fielding, A. H., Bamford, A. J., Ban, S., Barbosa, A. M., Dormann, C. F., Elith, J., Embling, C. B., Ervin, G. N., Fisher, R., Gould, S., Graf, R. F., Gregr, E. J., Halpin, P. N., … Sequeira, A. M. M. (2018). Outstanding Challenges in the Transferability of Ecological Models. *Trends in Ecology & Evolution*, *33*(10), 790–802. https://doi.org/10.1016/j.tree.2018.08.001

CURRICULUM VITAE